

AD-A259 500



(1)

Performance of the Monopole
Antenna Element for the
96-Element Receiving Array
of the High-Frequency, High-
Resolution Experimental Site:
Volume 1 — Theory and
Numerical Results

MTR11291

Volume 1

December 1991

R. L. Lagace

S DTIC
ELECTE
DEC 31 1992 **D**
A

Contract Sponsor MSR

Contract No. N/A

Project No. 91030

Dept. D085

Approved for public release:
distribution unlimited.

MITRE

Bedford, Massachusetts

92-33090



12905

92 12 29 060

Department Approval:

J. Daniel Moylan

MITRE Project Approval:

Edward A. Palo

REPORT DOCUMENTATION PAGE

Form Approved
OMB No. 0704-0188

Public reporting burden for this collection of information is estimated to average 1 hour per response, including the time for reviewing instructions, searching existing data sources, gathering and maintaining the data needed, and completing and reviewing the collection of information. Send comments regarding this burden estimate or any other aspect of this collection of information, including suggestions for reducing this burden, to Washington Headquarters Services, Directorate for Information Operations and Reports, 1215 Jefferson Davis Highway, Suite 1204, Arlington, VA 22202-4302, and to the Office of Management and Budget, Paperwork Reduction Project (0704-0188), Washington, DC 20503.

1. AGENCY USE ONLY (Leave blank)	2. REPORT DATE December 1991	3. REPORT TYPE AND DATES COVERED	
4. TITLE AND SUBTITLE Performance of the Monopole Antenna Element for the 96-Element Receiving Array of the High-Frequency, High-Resolution Experimental Site: Volume 1 - Theory and Numerical Results		5. FUNDING NUMBERS	
6. AUTHOR(S) R. L. Lagace			
7. PERFORMING ORGANIZATION NAME(S) AND ADDRESS(ES) The MITRE Corporation 202 Burlington Road Bedford, MA 01730-1420		8. PERFORMING ORGANIZATION REPORT NUMBER MTR 11291 Volume 1	
9. SPONSORING/MONITORING AGENCY NAME(S) AND ADDRESS(ES) Same as above		10. SPONSORING/MONITORING AGENCY REPORT NUMBER Same as above	
11. SUPPLEMENTARY NOTES			
12a. DISTRIBUTION / AVAILABILITY STATEMENT Approved for public release; distribution unlimited		12b. DISTRIBUTION CODE	
13. ABSTRACT (Maximum 200 words) See attached.			
14. SUBJECT TERMS Antenna Element, Numerical Electromagnetics Code-Ground Screen (NEC-GS)		15. NUMBER OF PAGES 115	
		16. PRICE CODE	
17. SECURITY CLASSIFICATION OF REPORT Unclassified	18. SECURITY CLASSIFICATION OF THIS PAGE Unclassified	19. SECURITY CLASSIFICATION OF ABSTRACT Unclassified	20. LIMITATION OF ABSTRACT Unlimited

ABSTRACT

The theoretical performance of the antenna element for the 96-element receiving array of MITRE's High-Frequency, High-Resolution Experimental Site is analyzed. The antenna element consists of a monopole tower with a buried radial-wire ground screen of modest diameter. Each element is connected by a long buried coaxial cable to an associated receiver in one of three electronics shelters within the array. The analysis forms the basis for selecting the final design configuration of the monopole antenna element, its associated ground screen, and the buried feed cable. System internal noise figure and antenna directivity serve as the principal measures of performance. The contributions of antenna efficiency, cable mismatch loss, cable attenuation loss, and receiver noise figure to system internal noise figure are treated.

The monopole antenna element and an alternative dipole antenna element are modeled and analyzed using the Numerical Electromagnetics Code-Ground Screen (NEC-GS) version of the NEC Method-of-Moments software. NEC-GS, which is particularly well-suited for modeling azimuthally symmetric structures, is used to calculate the antenna input impedance, efficiency, and power gain pattern. The antenna efficiency, cable mismatch loss, and antenna directivity pattern are determined as a function of frequency, earth electrical properties, and antenna element/ground-screen geometry. Asymmetric radiation pattern effects caused by a long, buried or unburied, coaxial feed cable, and by a nearby electronics shelter, are also evaluated. This is accomplished by using NEC software versions NEC-3I and NEC-3 to model the monopole with ground screen in the presence of a jacketed feed cable and a shelter, respectively. Included are brief descriptions of NEC-GS, NEC-3, and NEC-3I versions of NEC, and some associated modeling constraints.

ABSTRACT

The theoretical performance of the antenna element for the 96-element receiving array of MITRE's High-Frequency, High-Resolution Experimental Site is analyzed. The antenna element consists of a monopole tower with a buried radial-wire ground screen of modest diameter. Each element is connected by a long buried coaxial cable to an associated receiver in one of three electronics shelters within the array. The analysis forms the basis for selecting the final design configuration of the monopole antenna element, its associated ground screen, and the buried feed cable. System internal noise figure and antenna directivity serve as the principal measures of performance. The contributions of antenna efficiency, cable mismatch loss, cable attenuation loss, and receiver noise figure to system internal noise figure are treated.

The monopole antenna element and an alternative dipole antenna element are modeled and analyzed using the Numerical Electromagnetics Code-Ground Screen (NEC-GS) version of the NEC Method-of-Moments software. NEC-GS, which is particularly well-suited for modeling azimuthally symmetric structures, is used to calculate the antenna input impedance, efficiency, and power gain pattern. The antenna efficiency, cable mismatch loss, and antenna directivity pattern are determined as a function of frequency, earth electrical properties, and antenna element/ground-screen geometry. Asymmetric radiation pattern effects caused by a long, buried or unburied, coaxial feed cable, and by a nearby electronics shelter, are also evaluated. This is accomplished by using NEC software versions NEC-3I and NEC-3 to model the monopole with ground screen in the presence of a jacketed feed cable and a shelter, respectively. Included are brief descriptions of NEC-GS, NEC-3, and NEC-3I versions of NEC, and some associated modeling constraints.

Accession For	
NTIS CRA&I	<input checked="" type="checkbox"/>
DTIC TAB	<input type="checkbox"/>
Unannounced	<input type="checkbox"/>
Justification	
By	
Distribution/	
Availability Codes	
Dist	Avail and/or Special
A-1	

ACKNOWLEDGMENTS

J. D. R. Kramer and M. M. Weiner provided constructive observations and suggestions during the course of the work and review of this report.

M. K. Eggimann and L. Giandomenico executed a large number of NEC computer runs during the course of this work.

S. Zamosciany generated the performance plots from Numerical Electromagnetic Code (NEC) computer output files.

M. H. Weeden and C. S. E. Sherman prepared the balance of the graphics and tables.

J. K. Viveiros and J. M. Tsoukalas prepared the typed manuscript.

Figures 5 and 6; and figures 7, 8, and 36 are modified versions of figures from two MITRE reports MTR-9221, March 1984 and MTR-11278, September 1991, respectively, by M. M. Weiner.

TABLE OF CONTENTS

SECTION	PAGE
1 Summary	1
1.1 The MITRE Experimental Site	1
1.2 Monopole Antenna Configuration	1
1.3 Performance Measures and Results	4
1.4 Effects of Feed Cables and Electronics Shelters	5
1.5 Organization of Report	8
2 Measures of Performance	9
2.1 System Operating Noise Figure	9
2.1.1 System Internal Noise Factor	13
2.1.2 Antenna External Noise Factor	19
2.2 Antenna Directivity	20
2.2.1 Feed Cable Effects	21
2.2.2 Electronics Shelter Effects	21
3 Applicable Numerical Electromagnetics Code (NEC) Software	23
3.1 NEC-GS Version	23
3.2 NEC-3 and NEC-3I Versions	24
3.3 Some Modeling Constraints	24
4 Numerical Results	27
4.1 Monopole Antenna with Radial Ground Screen	27
4.1.1 Geometry, Parameters, and NEC-GS Outputs	27
4.1.2 Antenna Ohmic Loss and Cable Mismatch Loss	32
4.1.3 Cable Attenuation Loss and Receiver Noise Figure	47
4.1.4 System Internal Noise Figure	50
4.1.5 Antenna Directivity	50
4.2 Final 6.3 Meter Monopole Antenna and Ground Screen Configuration	58
4.3 Alternative Dipole Antenna Configurations	65
4.3.1 Geometry and Parameters for NEC-GS Model	65
4.3.2 Antenna Ohmic Loss and Cable Mismatch Loss	77
4.4 Feed Cable Effects on Radiation Pattern	77
4.4.1 Geometry, Parameters, and NEC-3I Model	77

SECTION	PAGE
4.4.2 Radiation Patterns-Effects of Buried versus Unburied Cables and Antenna Height	81
4.4.3 Summary of Cable Effects	103
4.5 Electronics Shelter Effects on Radiation Pattern	104
4.5.1 Geometry, Parameters, and NEC-3 Model	104
4.5.2 Radiation Patterns	109
List of References	113
Glossary	115

LIST OF FIGURES

FIGURE		PAGE
1	Layout of Antennas, Feed Cables, and Nodes of the 96-Element Receive Array of the High-Frequency, High-Resolution Experimental Site	2
2	Base-Fed Monopole Antenna with Ground Screen of Radial Wires	3
3	System Internal Noise Figures versus Frequency, Soil Condition, and Maximum and Minimum Cable Lengths for 6.3 Meter High Monopole Antenna with 12 Meter Radius Ground Screen of 16 Radial Wires	6
4	Antenna Directivity versus Elevation Angle and Frequency, for 6.3 Meter High Monopole Antenna with 12 Meter Radius Ground Screen of 16 Radials, for a <i>Medium Dry Ground Condition</i>	7
5	Signal-to-Noise Equivalent Block Diagram of Radio Receiving System	10
6	Noise Equivalent Circuit of Radio Receiving System	15
7	Spherical Coordinate Geometry for General Monopole Antenna and Ground Screen of Radial Wires	28
8	NEC-GS Rotational (Cage) Model Representation of Monopole Element of Radius b and Ground Screen with M L-Shaped Radial Wires	29
9	Antenna Noise Figure (Ohmic Loss) versus Frequency and Five Soil Conditions for 5.4 Meter High Monopole with 12 Meter Radius Ground Screen of <i>16 Radials</i>	34
10	Antenna Input Resistance and Reactance versus Frequency and Five Soil Conditions for 5.4 Meter High Monopole with 12 Meter Radius Ground Screen of <i>16 Radials</i>	36
11	Cable Mismatch Loss versus Frequency and Five Soil Conditions for 75 ohm Coaxial Cable Feeding 5.4 Meter High Monopole with 12 Meter Radius Ground Screen of <i>16 Radials</i>	38
12	Antenna Noise Figure (Ohmic Loss) versus Frequency and Five Soil Conditions for 5.4 Meter High Monopole with 12 Meter Radius Ground Screen of <i>32 Radials</i>	40
13	Antenna Noise Figure (Ohmic Loss) versus Frequency and Five Soil Conditions for 5.4 Meter High Monopole with 12 Meter Radius Ground Screen Having <i>Either 16 or 32 Radials</i>	41

FIGURE	PAGE
14 Antenna Input Resistance and Reactance versus Frequency and Five Ground Conditions for 5.4 Meter High Monopole with 12 Meter Radius Ground Screen Having Either 16 or 32 Radials	42
15 Cable Mismatch Loss versus Frequency and Five Soil Conditions for 75 ohm Coaxial Cable Feeding 5.4 Meter High Monopole with 12 Meter Radius Ground Screen Having Either 16 or 32 Radials	43
16 Cable Attenuation Loss versus Frequency for Four Cable Lengths	49
17 System Internal Noise Figure Cumulative Contributions for Case of <i>Sandy Soil</i> and Maximum Length Cable for 5.4 Meter High Monopole with 12 Meter Radius Ground Screen of 16 Radials	51
18 System Internal Noise Figure versus Frequency, Soil Condition, and Maximum and Minimum Cable Lengths for 5.4 Meter High Monopole with 12 Meter Radius Ground Screen of 16 Radials	52
19 System Internal Noise Figure versus Frequency, Soil Condition, and Maximum and Minimum Cable Lengths for 5.4 Meter High Monopole with 12 Meter Radius Ground Screen of 32 Radials	53
20 Antenna Directivity versus Elevation Angle and Five Soil Conditions at Frequency of 10 MHz, for 5.4 Meter High Monopole with 12 Meter Radius Ground Screen of 16 Radials	54
21 Antenna Directivity versus Elevation Angle and Five Soil Conditions at Frequency of 10 MHz, for 5.4 Meter High Monopole with 12 Meter Radius Ground Screen of 32 Radials	55
22 Antenna Directivity versus Elevation Angle and Frequency for 5.4 Meter High Monopole with 12 Meter Radius Ground Screen of 16 Radials for a <i>Sandy Soil Condition</i>	56
23 Antenna Directivity versus Elevation Angle and Frequency for 5.4 Meter High Monopole with 12 Meter Radius Ground Screen of 32 Radials for a <i>Sandy Soil Condition</i>	57
24 Antenna Directivity versus Elevation Angle and Five Soil Conditions for 5.4 Meter High Monopole with 12 Meter Radius Ground Screen of 16 Radials at Frequency of 30 MHz	60

FIGURE	PAGE
25 Antenna Directivity versus Elevation Angle and Five Soil Conditions for <i>6.0 Meter</i> High Monopole with 12 Meter Radius Ground Screen of 16 Radials at Frequency of 30 MHz	61
26 Antenna Directivity versus Elevation Angle and Five Soil Conditions for <i>6.3 Meter</i> High Monopole with 12 Meter Radius Ground Screen of 16 Radials at Frequency of 30 MHz	62
27 Antenna Directivity versus Elevation Angle and Five Soil Conditions for <i>6.5 Meter</i> High Monopole with 12 Meter Radius Ground Screen of 16 Radials at Frequency of 30 MHz	63
28 Antenna Directivity versus Elevation Angle and Five Soil Conditions for <i>7.0 Meter</i> High Monopole with 12 Meter Radius Ground Screen of 16 Radials at Frequency of 30 MHz	64
29 Antenna Noise Figure (Ohmic Loss) versus Frequency and Five Soil Conditions for <i>6.3 Meter</i> High Monopole with 12 Meter Radius Ground Screen of 16 Radials	66
30 Antenna Input Resistance and Reactance versus Frequency for Five Soil Conditions, for <i>6.3 Meter</i> High Monopole with 12 Meter Radius Ground Screen of 16 Radials	68
31 Cable Mismatch Loss versus Frequency and Five Soil Conditions for 75 ohm Coaxial Cable Feeding <i>6.3 Meter</i> High Monopole with 12 Meter Radius Ground Screen of 16 Radials	70
32 System Internal Noise Figure Cumulative Contributions for Case of <i>Sandy Soil</i> and Maximum Length Cable for <i>6.3 Meter</i> High Monopole with 12 Meter Radius Ground Screen of 16 Radials	71
33 System Internal Noise Figures versus Frequency, Soil Condition, and Maximum and Minimum Cable Lengths for <i>6.3 Meter</i> High Monopole Antenna with 12 Meter Radius Ground Screen of 16 Radial Wires	72
34 Antenna Directivity versus Elevation Angle and Five Soil Conditions at Frequency of 10 MHz, for <i>6.3 Meter</i> High Monopole with 12 Meter Radius Ground Screen of 16 Radials	73
35 Antenna Directivity versus Elevation Angle and Frequency, for <i>6.3 Meter</i> High Monopole with 12 Meter Radius Ground Screen of 16 Radials, for <i>Sandy Soil Condition</i>	74

FIGURE	PAGE
36 Rotational (Cage) NEC-GS Model Representation of a Fat Vertical Dipole Element of Radius b in Proximity to Earth	75
37 Coordinate Geometry for Investigation of Antenna Pattern Effects Due to Presence of Long Coaxial Feed Cable	79
38 Principal Plane Elevation Plots of Cable Directivity Effects, for <i>2.4 Meter</i> Monopole on Sandy Soil	84
39 Perpendicular Plane Elevation Plots of Cable Directivity Effects, for <i>2.4 Meter</i> Monopole on Sandy Soil	85
40 Azimuthal Conical Cut Plots of Cable Directivity Effects at Two Elevation Angles, for <i>2.4 Meter</i> Monopole on Sandy Soil	86
41 Principal Plane Elevation Plots of Cable Directivity Effects, for <i>5.4 Meter</i> Monopole on Sandy Soil	87
42 Perpendicular Plane Elevation Plots of Cable Directivity Effects, for <i>5.4 Meter</i> Monopole on Sandy Soil	88
43 Azimuthal Conical Cut Plots of Cable Directivity Effects at Two Elevation Angles, for <i>5.4 Meter</i> Monopole on Sandy Soil	89
44 Azimuthal Variation of Cable Effects on Radiation Field Phase at <i>30° Elevation</i> , for <i>2.4 Meter</i> Monopole on Sandy Soil	91
45 Azimuthal Variation of Cable Effects on Radiation Field Phase at <i>10° Elevation</i> , for <i>2.4 Meter</i> Monopole on Sandy Soil	92
46 Azimuthal Variation of Cable Effects on Radiation Field Phase at <i>30° Elevation</i> , for <i>5.4 Meter</i> Monopole on Sandy Soil	93
47 Azimuthal Variation of Cable Effects on Radiation Field Phase at <i>10° Elevation</i> , for <i>5.4 Meter</i> Monopole on Sandy Soil	94
48 Cable External Current versus Distance from Antenna, for Buried and Unburied Cable Feeding <i>2.4 Meter</i> Monopole on Sandy Soil at 5 MHz	98

FIGURE		PAGE
49	Cable External Current versus Distance from Antenna, for Buried and Unburied Cable Feeding <i>5.4 Meter</i> Monopole on Sandy Soil at 5 MHz	99
50	Coordinate Geometry for Investigation of Antenna Pattern Effects Due to Presence of Electronics Shelters at Nodes	105

LIST OF TABLES

TABLE	PAGE
1 Baseline NEC-GS Rotational (Cage) Vertical Monopole Antenna Wire Model	30
2 Parameter Variations for Performance Assessment	31
3 Antenna Efficiency and Noise Figure versus Frequency for Five Soil Conditions	35
4 Antenna Input Resistance and Reactance versus Frequency for Five Soil Conditions	37
5 Change in Noise Figure Sum ($L_c + L_{nm}$) in dB as Number of Radials of 12 Meter Radius Ground Screen is Increased from 16 to 32	44
6 Change in Noise Figure Sum ($L_c + L_{nm}$) in dB as Radius of 16 Radial Ground Screen is Increased from 12 to 24 Meters	45
7 Change in Noise Figure Sum ($L_c + L_{nm}$) in dB as Radius of 32 Radial Ground Screen is Increased from 12 to 24 Meters	45
8 Change in Noise Figure Sum ($L_c + L_{nm}$) in dB as Ground Screen is Changed from 16 Radials, 12 Meters Long to 32 Radials, 24 Meters Long	45
9 Change in Noise Figure Sum ($L_c + L_{nm}$) in dB as Burial Depth of 12 Meter Radius Ground Screen of 16 Radials is Increased from 0.178m (7 inches) to 0.305m (12 inches)	46
10 Change in Noise Figure Sum ($L_c + L_{nm}$) in dB as Base of Monopole Feed Section is Raised from 0.0 to 0.2 Meter above Ground Surface	46
11 Cable Attenuation Loss (dB) versus Frequency for Four Cable Lengths (for Times Fiber TX840JBA 75 ohm Coaxial Cable)	48
12 Change in Noise Figure Sum ($L_c + L_{nm}$) in dB as Monopole Height is Increased from Reference Monopole Height of 5.4 Meters to Heights of 6.0, 6.3, 6.5, and 7.0 Meters	59
13 6.3 Meter High Monopole Antenna: Efficiency and Noise Figure versus Frequency for Five Soil Conditions	67
14 6.3 Meter High Monopole Antenna: Input Resistance and Reactance versus Frequency for Five Soil Conditions	69
15 NEC-GS Rotational (Cage) Vertical Dipole Antenna Wire Model	76

TABLE	PAGE
16 Comparison of 5 and 10 Meter Dipole Performance versus Frequency with Performance of 5 Meter Monopole with 16 Radial, 12 Meter Radius Ground Screen for a Sandy Soil Condition ($\epsilon_r = 3.5$, $\sigma = 2.3$ mS/m)	78
17 NEC-3I Wire Model and Parameters for Cable Effects Analysis	82
18 Directivity and Phase Variation for 2.4m Monopole with Buried and Unburied Feed Cable versus Frequency for <i>Sandy Soil Condition</i> ($\epsilon_r = 3.5$, $\sigma = 2.3$ millisiemens/m)	96
19 Directivity and Phase Variation for 5.4m Monopole with Buried and Unburied Feed Cable versus Frequency for <i>Sandy Soil Condition</i> ($\epsilon_r = 3.5$, $\sigma = 2.3$ millisiemens/m)	97
20 Directivity and Phase Variation for 5.4m Monopole with Buried and Unburied Feed Cable versus Frequency for <i>Very Dry Ground Condition</i> ($\epsilon_r = 4$, $\sigma = 0.15$ millisiemens/m)	101
21 Directivity and Phase Variation for 6.3m Monopole with Buried and Unburied Feed Cable versus Frequency for <i>Very Dry Ground Condition</i> ($\epsilon_r = 4$, $\sigma = 0.15$ millisiemens/m)	102
22 NEC-3 Wire Model and Parameters for Shelter Effects Analysis	107
23 Shelter Effects at 5 MHz on Radiation Pattern Power Gain and Phase, in Principal Elevation Plane Containing 5 Meter Monopole and Bisecting Shelter, versus Frequency, Distance, and Polar Angle	110
24 Shelter Effects at 15 MHz on Radiation Pattern Power Gain and Phase, in Principal Elevation Plane Containing 5 Meter Monopole and Bisecting Shelter, versus Frequency, Distance, and Polar Angle	111
25 Shelter Effects at 25 MHz on Radiation Pattern Power Gain and Phase, in Principal Elevation Plane Containing 5 Meter Monopole and Bisecting Shelter, versus Frequency, Distance, and Polar Angle	112

SECTION 1

SUMMARY

1.1 THE MITRE EXPERIMENTAL SITE

The MITRE Corporation and the University of Texas in Austin, Texas, are establishing a High-Frequency, High-Resolution Experimental Research Facility on University of Texas land in West Texas. This facility, referred to herein as the MITRE Experimental Site, will be used to support research in high frequency (HF) ionospheric propagation of signals and atmospheric noise. It will consist of a large-area sparsely filled planar array antenna, with electronics for receiving and recording signals from all the antenna elements. The site will serve as a test bed for the development and evaluation of new technology and techniques for over-the-horizon (OTH) radar, communication, and direction-finding systems at HF. This report deals with the evaluation of candidate design configurations for the individual antenna elements and associated feed cables for the initial installation of the receive antenna planar array and its electronic equipment.

The initial planar array consists of 96 vertical monopole antenna elements, pseudo-randomly placed within a 3 kilometer (km) diameter area on relatively flat land near the junction of Loving, Winkler, and Ward county lines in west Texas. Each antenna is independently connected, via a buried coaxial cable, to wide bandwidth electronics equipment located in a military shelter at one of three places called nodes. Each node services a group of 32 antennas. The nodes are interconnected by other buried cables. Figure 1 is a map showing the layout of the 96 monopole antennas and feed cables and the three nodes of the receive array. The monopole antenna locations are denoted by triangular-shaped dots and the three nodes by the numbers 100, 200, 300. The nodes are separated by approximately 1.1 km and are located at the apexes of a triangle within the 3 km diameter circle.

1.2 MONOPOLE ANTENNA CONFIGURATION

A conventional monopole antenna design that is both rugged and economical has been proposed and analyzed as the baseline candidate element for this receive array application. A conservative design approach was taken for this widely dispersed experimental array, to reduce development, capital and maintenance uncertainties, and costs.

The monopole antenna consists of a base-fed vertical tower with a small ground plane of buried radial wires, as depicted in figure 2. This basic configuration incorporates two familiar design elements. The first is a rugged, self-supporting, triangular cross-section, standard tower mounted on an insulated, base-feed section, similar to that used by the FPS-118 over-the-horizon backscatter (OTH-B) radar. The second is a relatively small and inexpensive ground plane of shallow-buried radial wires extending an appropriate distance from the tower, similar to that used in standard broadcasting applications and for making comparative antenna pattern measurements at HF. The primary purpose of the ground radials is to produce an acceptably stable antenna input impedance and low antenna noise figure (ohmic ground loss) in the face of anticipated variations in the electrical properties of the

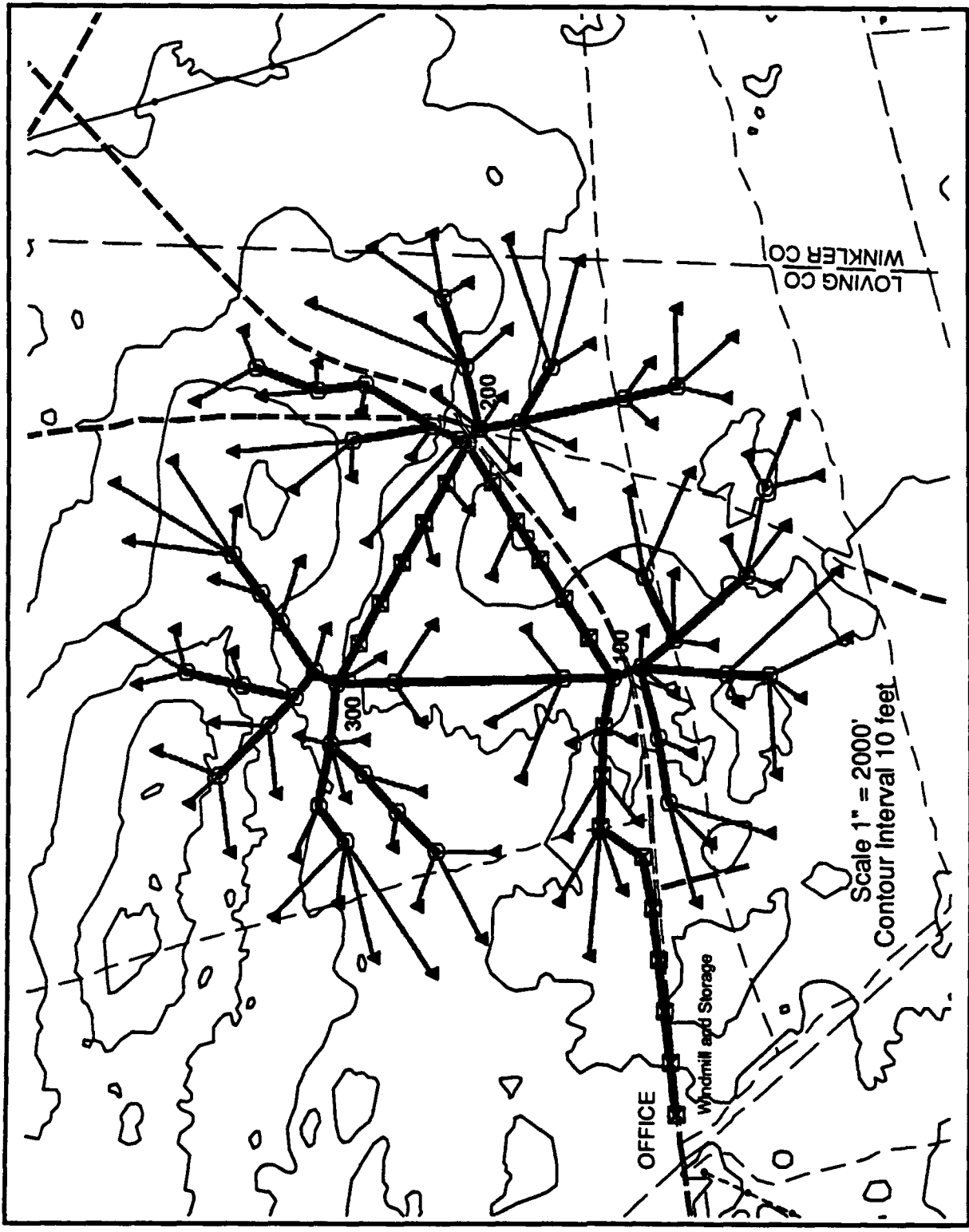


Figure 1. Layout of Antennas, Feed Cables, and Nodes of the 96-Element Receive Array of the High-Frequency, High Resolution Experimental Site

IL3061

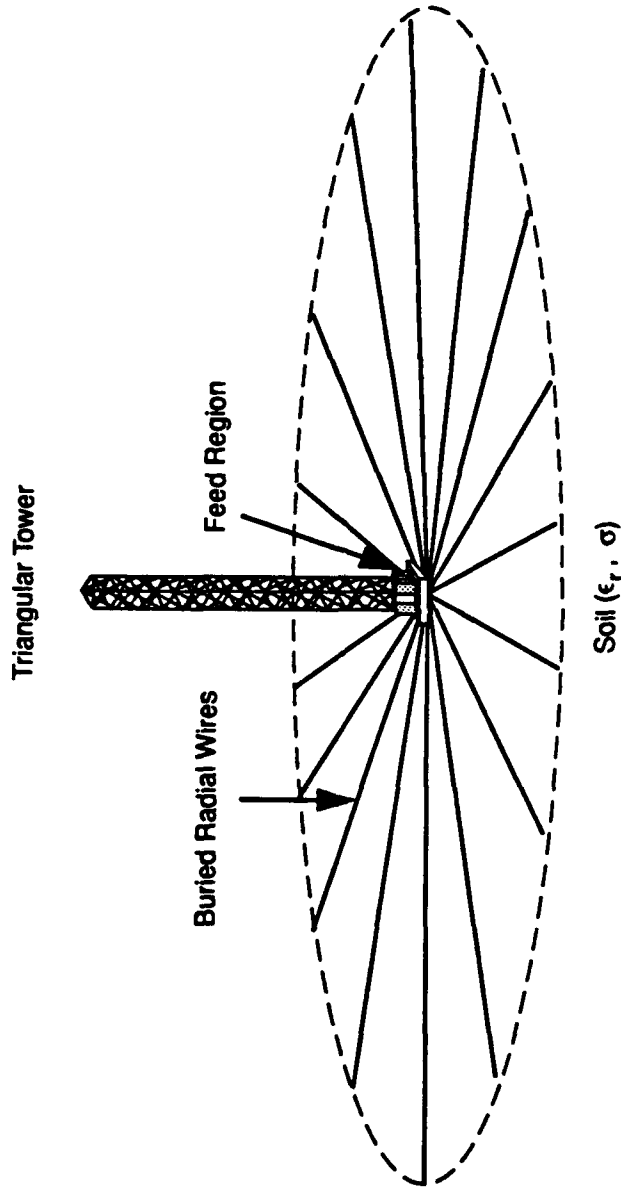


Figure 2. Base-Fed Monopole Antenna with Ground Screen of Radial Wires

underlying soil. A continuous mesh ground plane covering the 3 km diameter area of this widely dispersed array is both unnecessary and prohibitively expensive; and, therefore, was excluded from consideration.

The final specified monopole antenna design is a 6.3 meters (m) high self-supporting vertical tower, consisting of two triangular sections, each 3.05 m in length and 43 centimeter (cm) on a side, supported by a 20 cm insulated base-feed region, attached to a 2.5 cm thick by 60 cm square base plate. The base plate is secured to a buried 91 cm diameter by 1.2 m deep foundation of reinforced concrete and is connected to 16 equally spaced #10 AWG radial wires, 12 m long, buried 18 cm deep. All metal parts are of galvanized steel to minimize adverse electrochemical reactions.

1.3 PERFORMANCE MEASURES AND RESULTS

The objectives of the work described in this report were to 1) evaluate the performance of the monopole configuration as a function of frequency, tower dimensions, number and length of ground radials, and electrical properties of the surrounding earth; 2) converge on final procurement specifications for antenna and ground plane that satisfy electrical and cost requirements; and 3) generate theoretical predictions of performance as a function of frequency and earth electrical constants for the final design. All objectives were accomplished.

HF band receive systems are exposed to widely variable levels of atmospheric and manmade external noise. Therefore, the system internal noise figure and the antenna directivity (directive gain) are important measures of system performance. Comprehensive theoretical computations and sensitivity analyses of these quantities, as well as antenna efficiency and input impedance, were performed. The results were used to select and characterize the final antenna configuration. The system internal noise figure is composed of four noise figure contributions: antenna ohmic (earth and conductor) loss, matching network (when present) loss, cable (attenuation and mismatch) loss, and receiver noise figure [1-4].

Most of the Numerical Electromagnetics Code (NEC) based parametric analyses described here were conducted for a "baseline" monopole antenna 5.4 m high, which is the monopole tower structure used in the FPS-118 radar receiving array. An alternative dipole antenna candidate was also assessed. Eventually, for a set of economic and logistic reasons, a 6.3 m tower structure was selected for the monopole element at the experimental site. NEC runs were then made for the 6.3 m antenna, over a more limited range of parameter values, to predict the performance of the final design.

The NEC Method-of-Moments computer programs, NEC-3, -3I, and -GS, were independently validated at MITRE [5], and applied to modeling the vertical antenna, radial ground wires, surrounding earth, and feed cable. These programs were developed by G. Burke, et al. of Lawrence Livermore National Laboratory (LLNL) [6-12]. The Numerical Electromagnetics Code-Ground Screen (NEC-GS) version of NEC is designed to simplify the modeling and computation associated with azimuthally symmetric structures such as the antenna and ground plane configurations of interest. Therefore, NEC-GS played a key role in the calculation of antenna efficiency, input impedance, and power gain used to compute system internal noise figure contributions, as well as antenna directivity.

The selected 6.3 m high monopole configuration, with its 12 m radius ground plane of buried radial wires, provides stable, acceptable, system performance that satisfies the requirements of presently planned experiments, and is easily upgradable with a matching network as needed. Figure 3 presents summary performance results for system internal noise figure, expressed in decibels (dB), for the final 6.3 m monopole antenna design without an antenna matching network. The curves illustrate the dependence on frequency and cable length, and the desired insensitivity to earth electrical conductivity and relative dielectric constant. The marked increase in noise figure below 8 MHz is caused by the pronounced increase in cable mismatch loss as the height of the monopole antenna becomes small compared to the wavelength. A matching network has been omitted for the planned initial array experiments, because the anticipated improvement in noise figure with the network was not sufficient to overcome concerns about potential maintenance problems associated with matching network components at widely dispersed antennas exposed to frequent lightning occurrences.

The antenna directivity is relatively insensitive to both earth electrical properties and frequency over the 0° to 40° span in elevation angle of primary interest. Figure 4 illustrates the frequency dependence of directivity, in dBi, for a representative soil condition, namely, medium dry ground having a conductivity of 1.5 millisiemens/m and relative dielectric constant of 10.

1.4 EFFECTS OF FEED CABLES AND ELECTRONICS SHELTERS

As shown in figure 1, each of the monopole antennas is connected to an electronics shelter by means of a long, shallow-buried coaxial cable. The cables range in length from 200 m (660 ft) to a maximum of 1,358 m (4,454 ft), and the shelter dimensions are 2.5x2.5x6 m (8x8x20 ft). Since the size of the shelters and lengths of the cables are appreciable, the potentially adverse effects produced by each structure on the radiation patterns of the monopole antennas were estimated. Specifically, NEC-3 and -3I (I for insulated wire) programs, which are well suited to arbitrary unsymmetrical structures, were used to calculate the magnitude and phase perturbations to the radiation patterns.

NEC-3 was used to calculate pattern effects for both broadside and endfire dispositions of the shelters located at representative distances of 200 m to 400 m from a monopole antenna. The pattern effects were found to be negligibly small in all cases.

NEC-3I was used to calculate the pattern effects caused by coaxial feed cables, as a function of cable length, insulated jacketing and burial depth, frequency, earth electrical properties, and monopole height. Cable effects on antenna patterns can be significant under certain conditions, namely, when the cables are not buried and/or when the antennas are electrically very short. The MITRE receive array utilizes only buried feed cables and moderately short monopole antennas (greater than about one-tenth wavelength at the lowest operating frequency). As a result, the cable effects on the radiation patterns of these monopole antennas were found to be acceptably small and not critical to array performance.

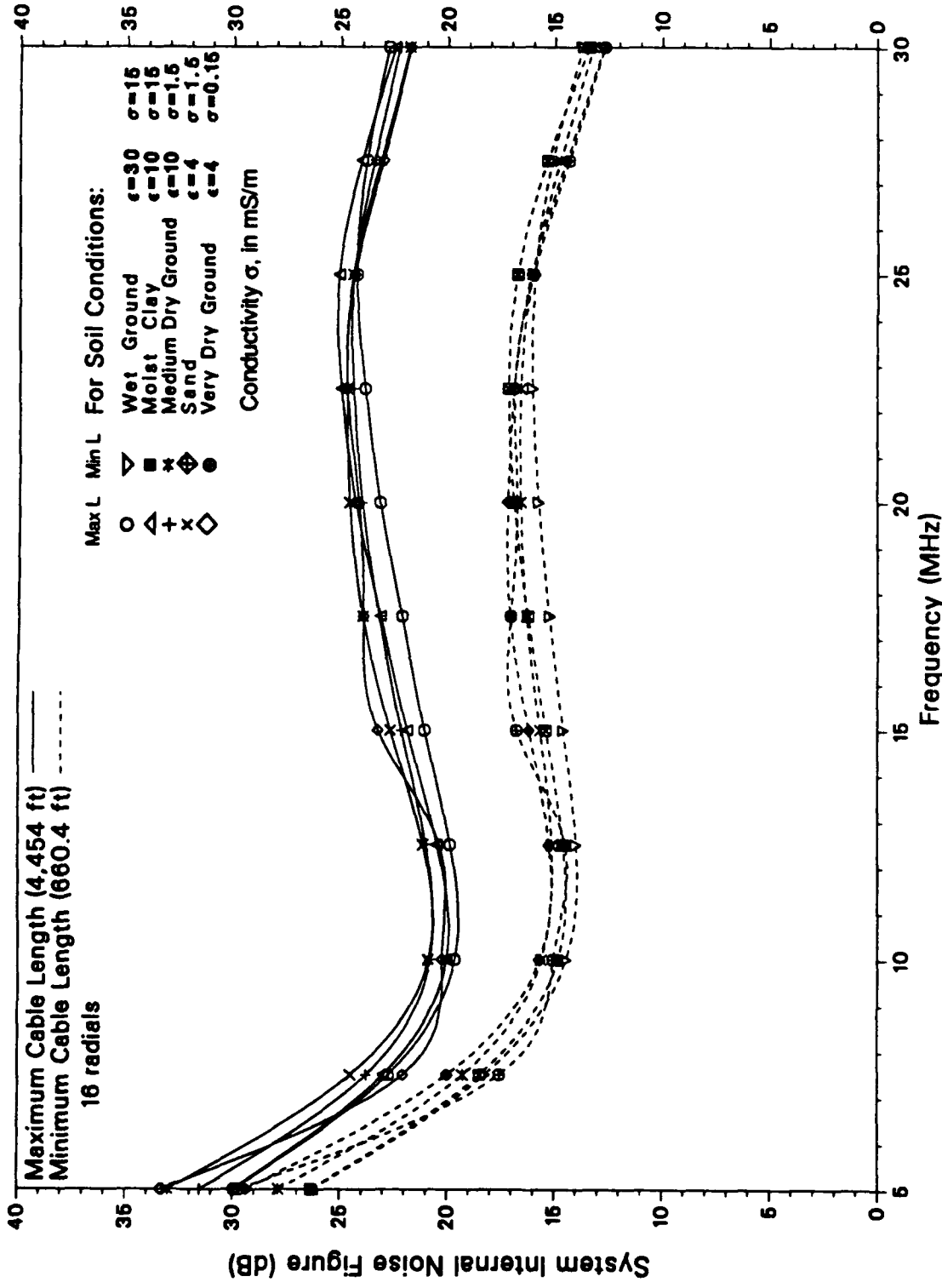


Figure 3. System Internal Noise Figures versus Frequency, Soil Condition, and Maximum and Minimum Cable Lengths for 6.3 Meter High Monopole Antenna with 12 Meter Radius Ground Screen of 16 Radial Wires

Medium Dry Ground $\epsilon=10$ $\sigma=1.5$

- 16 radials
- 5 MHz
 - △ 10 MHz
 - + 15 MHz
 - x 20 MHz
 - ◇ 25 MHz
 - ▽ 30 MHz
- Conductivity σ , in mS/m

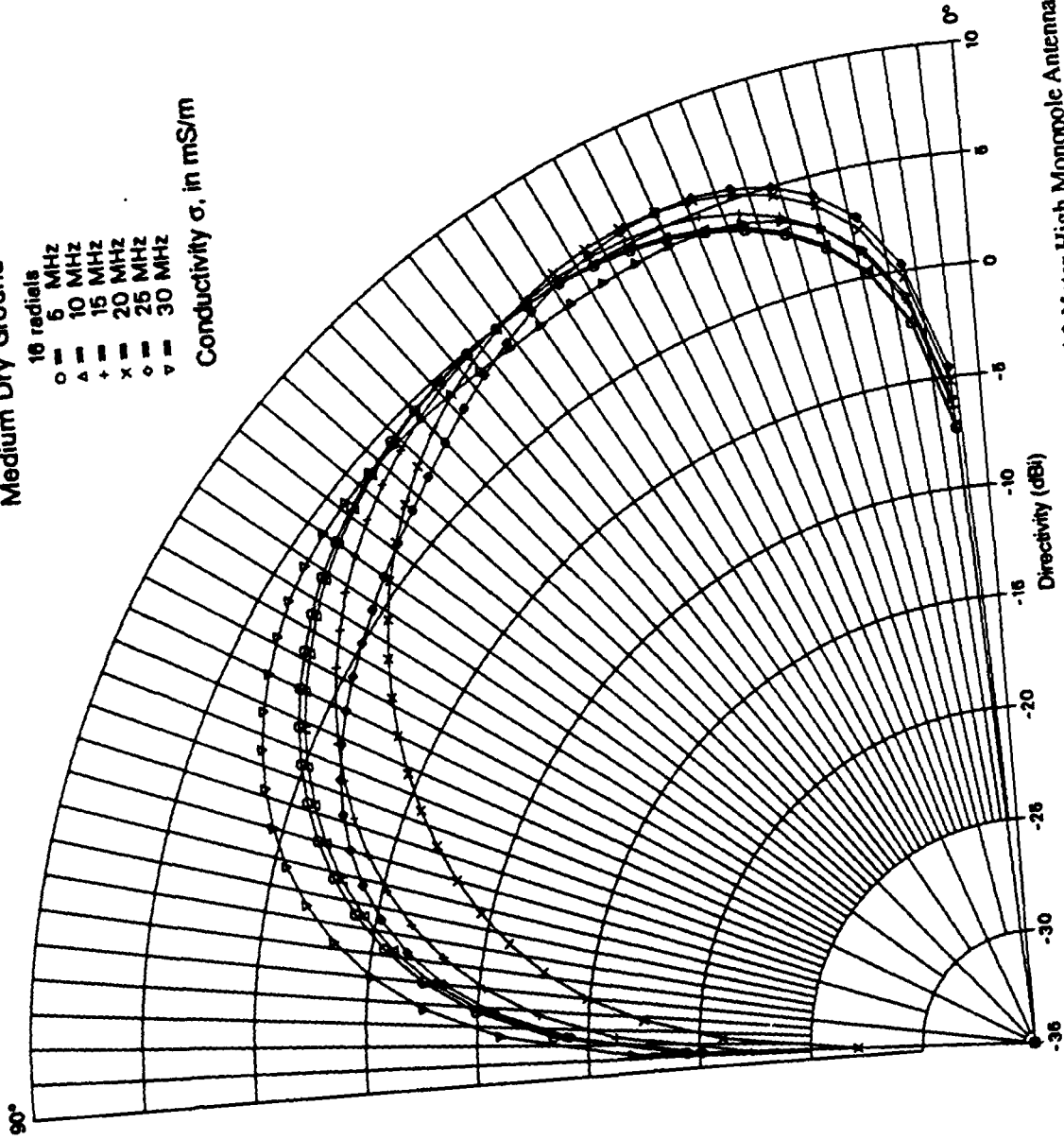


Figure 4. Antenna Directivity versus Elevation Angle and Frequency, for 6.3 Meter High Monopole Antenna with 12 Meter Radius Ground Screen of 16 Radials, for a Medium Dry Ground Condition

1.5 ORGANIZATION OF REPORT

Section 2 describes the noise figure and directivity measures of performance used to characterize the candidate and final antenna configurations. Descriptions of the applicable NEC software used for the antenna modeling and computations are presented in section 3. Section 4 presents a selection of representative results from the performance sensitivity analyses. It includes performance results for the monopole and dipole candidate antennas and for the final monopole design, as well as for the effects of the shelter and feed cable on antenna radiation patterns. A more comprehensive set of graphical and tabular results is included for convenient reference in Volume 2—Appendices.

SECTION 2

MEASURES OF PERFORMANCE

The objective of this study effort was to characterize the performance of proposed antenna designs and select a final design that met overall receive system requirements. Concentration was placed on the primary performance measures of system internal noise figure and the antenna directivity. HF band radio receive systems operate in the presence of significant levels of external atmospheric and man-made radio noise. Such systems can typically tolerate higher internal system noise levels than systems designed to operate in higher frequency bands, as long as the internal system noise levels are kept sufficiently below expected external noise levels to satisfy system performance requirements.

The experimental site will be used to conduct a diverse set of research experiments. The initial thrust of these experiments will likely be concerned with the spatial coherence of high intensity atmospheric noise bursts, which requires only moderate internal noise performance. The antenna design approach allows for evolutionary improvements in system internal noise performance to accommodate experiments that may require more stringent control of system internal noise levels. This is accomplished by providing space in the lightning arrestor enclosure at the base of the antenna so that a matching network can be easily installed if necessary.

The following sections describe the primary measures of performance used. These are the system internal noise figure and its component contributions, the antenna directivity, efficiency and input impedance, and the amplitude and phase perturbations produced in the antenna radiation pattern by the feed cables and electronics shelters.

2.1 SYSTEM OPERATING NOISE FIGURE

Only a summary presentation and explanation of key parameters and associated performance equations will be provided here, to assist understanding of the computations and their implications. Detailed and comprehensive treatments of noise performance in receiving systems can be found in reports by M. Weiner [1-4], H. Haus [13,14] and CCIR [15-17].

The performance of a radio receive system is limited by the total external and internal noise to which it is exposed. A receive system block diagram is presented in figure 5, which shows the key components and parameters used to define measures of performance. Uncapitalized performance parameters (s/n , d_r , f , l) refer to the numerical values of signal-to-noise ratio, antenna directivity, noise and available loss factors of a two-port network, respectively, and the capitalized parameters ($S-N$, D , F , L) refer to corresponding values expressed in decibels. Exceptions to these conventions are temperature T , impedance Z , and admittance Y , which are also capitalized.

The standard method of analysis is used. By definition, the predetection signal-to-noise ratio includes the time-averaged, external and internal noise powers *available* at the lossless antenna output terminals. *Available* power is defined as the power delivered by the lossless

IL3064-1

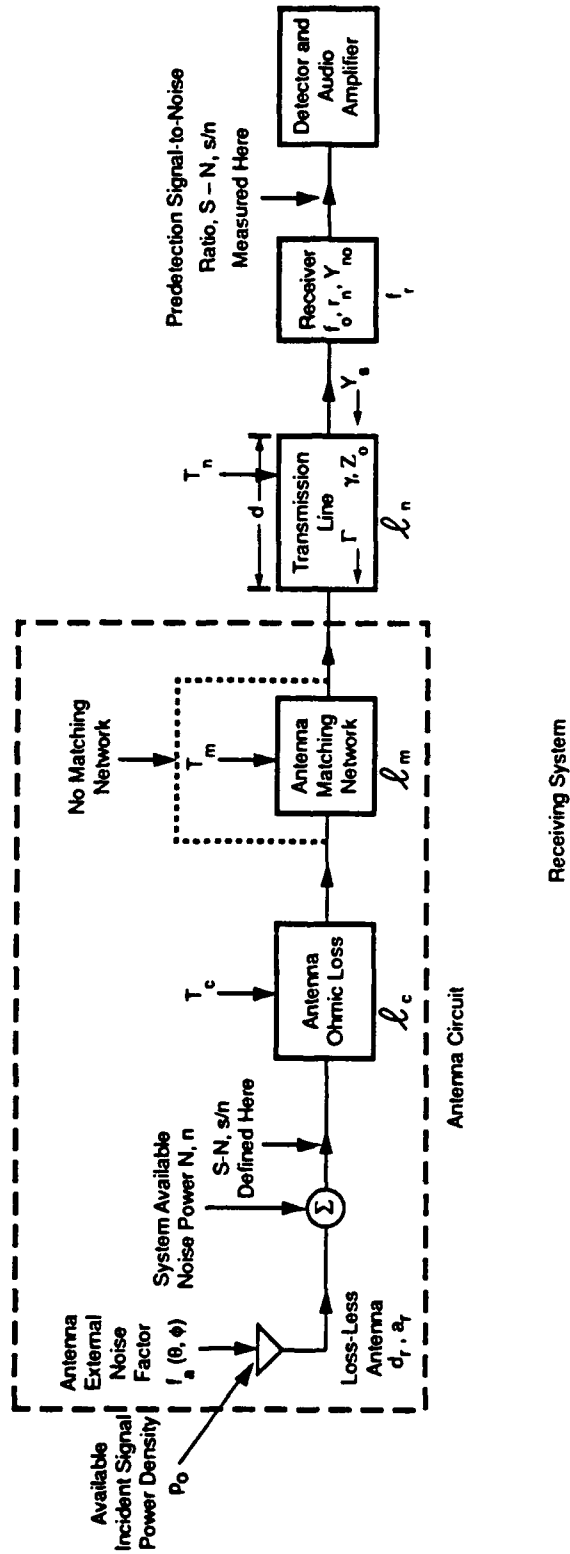


Figure 5. Signal-to-Noise Equivalent Block Diagram of Radio Receiving System

antenna (or network) to a load when the load impedance is set equal to the conjugate output impedance of the antenna (or network).

With reference to figure, 5, the system predetection signal-to-noise ratio, expressed in dB, is given by

$$S-N = (P_O + A_R) - N \text{ (dB)}, \quad (1)$$

where

- S Available signal power ($P_O + A_R$) at the output terminals of the equivalent lossless receiving antenna (dBW).
- P_O $10 \log_{10} p_O$ Available signal power density incident on receiving antenna (dBW/m²), p_O in (W/m²).
- A_R $10 \log_{10} a_R = D + 10 \log_{10} (\lambda^2/4\pi)$ Collecting area of the equivalent lossless antenna (dBm²), a_R in (m²).
- D $10 \log_{10} d_R$ Directivity of receive antenna relative to an isotropic antenna (dBi)
- N Available system operating noise power referred to the output terminals of the equivalent lossless receiving antenna (dBW)

The system available operating noise power, N, at the equivalent lossless antenna output terminals may be expressed in terms of the system *operating* noise figure, F_{Op} as

$$N = F_{Op} + N_{ref} \text{ (dBW)} \quad (2)$$

with

$$N_{ref} = 10 \log_{10} (kT_R b) \text{ (dBW)} \quad (3)$$

where

- N_{ref} Reference noise power (dBW)
- $kT_R b$ n_{ref} , Reference noise power (W)
- k Boltzmann's constant = 1.38×10^{-23} J/°K
- T_R Standard reference noise temperature = 288° K; $10 \log_{10} (kT_R) = -204$ dBJ,
- b Receiver noise power effective bandwidth (Hz),
- F_{Op} System operating noise figure (dB) referenced to N_{ref} .

N and the associated system operating noise figure, F_{Op} , incorporate noise contributions from both external sources (atmospheric, galactic, and man-made) and internal sources (receiver, transmission line, matching network, and antenna) [1].

$$F_{op} = 10 \log_{10} f_{op} \quad \text{System operating noise figure (dB)} \quad (4)$$

where

the system operating noise factor, f_{op} , for the receiving system of figure 5 can be conventionally expressed in terms of external and internal noise factors (f_a , f_s).

$$f_{op} = (f_a - 1) + f_s \quad \text{System operating noise factor} \quad (5)$$

where

f_a Antenna *external* noise factor, CCIR [15], (integrated over the antenna directive gain function)

f_s Receive system *internal* noise factor.

The "-1" in (5) in effect reduces the external noise power available from the equivalent lossless antenna by an amount equal to the reference input power level, n_{ref} , since n_{ref} has already been accounted for in the system internal noise factor, f_s . Generally, all HF receive systems are designed to be "external noise limited," namely, with the system internal noise factor significantly smaller than the expected levels of external noise ($f_s \ll f_a - 1$).

The system, subsystem, and component noise factors, f_n , are all defined in the same conventional manner, namely,

$$f_n = [s_i/n_{ref}] / [s_o/n_o] = [s_i/s_o] [n_o/n_{ref}] \quad \text{Noise factor (numeric)} \quad (6)$$

where

s_i Available signal power ($s = p_o a_T$) at input to receive system (at output terminals of the equivalent lossless receiving antenna) or any subsystem (W).

n_{ref} Available reference noise power ($kT_f b$) at input to receive system or any subsystem (W).

s_o Available signal power at output of receiver or subsystem (W)

n_o Available noise power at output of receiver or subsystem (W).

All sources of noise power, as well as the reference power, are assumed proportional to bandwidth; so noise factors are independent of bandwidth, and noise powers can be conveniently treated on a per hertz (Hz) basis, if desired.

2.1.1 System Internal Noise Factor

The receive system of interest can be represented as a cascade of linear subsystems or two-port networks. For any passive linear two-port network, or a subsystem of cascaded linear two-ports, a network *available* loss factor, $l_n (\geq 1)$ can be defined, which is given by [1, 2]

$$l_n = s_i/s_o. \quad (7)$$

$$s_i = |v_g|^2/8R_e(Z_g) \quad \text{available input signal power} \quad (8)$$

$$s_o = |v_o|^2/8R_e(Z_{out}) \quad \text{available output signal power} \quad (9)$$

where v_g and v_o are the open circuit voltages, and Z_g and Z_{out} are the output impedances of the corresponding Thevenin equivalent circuits seen by looking back toward the signal source from the network input and output terminals, respectively. The available input and output signal powers are functions of both Z_g and Z_{out} , respectively, since the *available power* from a source is defined as the power delivered by a source to a load as though the load impedance was conjugate-matched to the output impedance of the source.

Substitution of (7) into the noise factor equation (6), which is applicable to any two-port network, gives the network *available* output noise power, n_o , in the form

$$n_o = f_n n_{ref}/l_n = n_{eff}/l_n, \quad (10)$$

where n_{ref} is the available input noise power to the two-port network from a signal generator operating at the reference temperature, T_r .

Consequently, the network available output noise power, n_o , can be conveniently referred to the input terminals of an equivalent, noiseless, two-port network to give an *effective* input available noise power, n_{eff} ,

$$n_{eff} = f_n n_{ref} = n_o l_n. \quad (11)$$

This n_{eff} noise representation is a very useful one, because the noise factor, f_n , of a linear two-port is then simply the *effective* input available noise power normalized to the reference input noise power.

$$f_n = n_{eff}/n_{ref}. \quad (12)$$

These relationships also indicate that the increase in effective input available noise power, produced by the noise sources *inside* a two-port network, is given by

$$\Delta n_{eff} = n_{eff} - n_{ref} = n_{ref} (f_n - 1), \quad (13)$$

and the corresponding increase in output available power produced by the noise sources *inside* the two-port is given by

$$\Delta n_o = \Delta n_{\text{eff}}/l_n = n_{\text{ref}} (f_n - 1)/l_n \quad (14)$$

The effective available noise power, n_{effs} , referenced to the *input of a series of cascaded two-port networks*, such as the receive system shown in figure 6 (i.e., at the output of the equivalent lossless antenna), can then be expressed as

$$n_{\text{effs}} = n_{\text{ref}} f_s \quad (15)$$

where

n_{effs}	Effective system input noise power (W)
n_{ref}	Reference noise power (W)
f_s	System (cumulative) internal noise factor.

The system internal noise factor, f_s , represents the sum of the noise factor contributions from the individual two-port networks embedded in the cascade, each referred to the input of the system (i.e., to the output of the equivalent lossless antenna). When the above two-port relationships are applied [1,2] to the receive system of cascaded two-port networks represented in figure 5 and 6, the system internal noise factor can be written in the form

$$f_s = 1 + (f_c - 1) + l_c(f_m - 1) + l_c l_m(f_n - 1) + l_c l_m l_n(f_r - 1) \quad (16)$$

ref. pwr	lossy antenna	lossy matching network	lossy mismatched T-line	noisy receiver
-------------	------------------	------------------------------	-------------------------------	-------------------

where

$l_c, l_m,$ l_n	Available loss factors of the antenna, matching network, and transmission line, respectively
f_r	Noise factor of receiver.

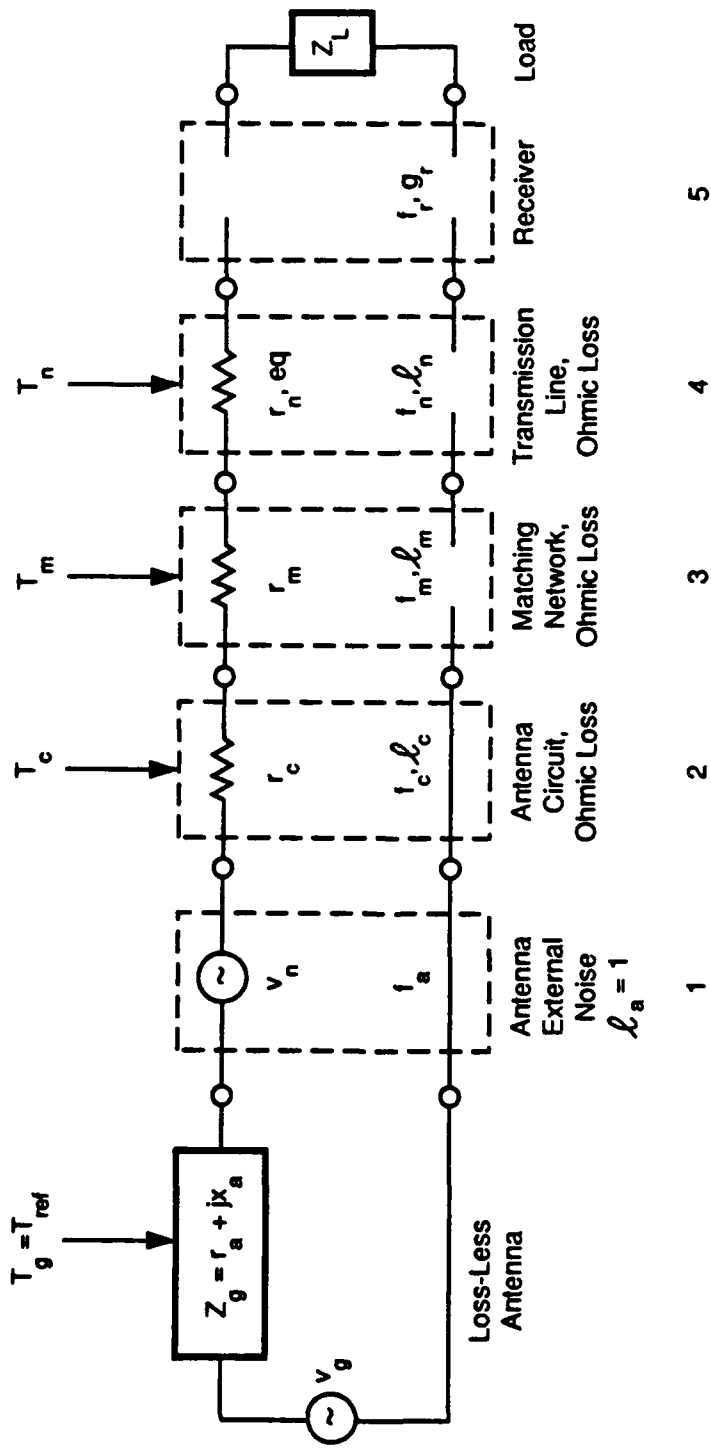
The noise factor of any linear, passive, two-port at temperature t_n can also be represented in terms of its loss factor, l_n , [1] namely,

$$f_n = 1 + (l_n - 1) T_n/T_r \quad (17)$$

which, when the temperature $T_n = T_r$, reduces to the familiar expression

$$f_n = l_n \quad (18)$$

IL3060-1



Each of Networks 1 - 5 has an Effective Bandwidth b

Figure 6. Noise Equivalent Circuit of Radio Receiving System

Substitution of (17) into (16) results in the alternative f_s expression

$$f_s = 1 + (l_c - 1) T_c / T_r + l_c (l_m - 1) T_m / T_r + l_c l_m (l_n - 1) T_n / T_r + l_c l_m l_n (f_r - 1). \quad (19)$$

When all temperatures are equal to the reference temperature, T_r , i.e., $T_r = T_c = T_m = T_n$, the condition assumed for the analyses for the MITRE experimental site, the expressions for system *internal noise factor* and *noise figure* reduce to the greatly simplified familiar equations

$$f_s = l_c l_m l_n f_r \quad (\text{numeric}) \quad (20)$$

and

$$F_s = 10 \log_{10} f_s = L_c + L_m + L_n + F_r \quad (\text{dB}) \quad (21)$$

respectively, and the system *operating noise factor* expression reduces to

$$f = (f_a - 1) + l_c l_m l_n f_r. \quad (22)$$

2.1.1.1 Available Loss Factors

The available loss factors, l_n , for the passive, two-port networks of the receive system account for the resistive losses in each of the networks embedded in the receive system cascade. The loss factors are a function of the impedance parameters and source impedances of the respective circuits. They are equal to the reciprocal of the respective circuit efficiencies, and can be derived using the definition represented by (9). Detailed derivations of these quantities can be found in [1]. Only summary results are presented here, sufficient to allow understanding and use in this application.

a) Antenna loss factor : The antenna loss factor, l_c , is given by

$$l_c = (r_a + r_c) / r_a = 1 / \eta_c \quad (23)$$

where

r_a	Antenna radiation resistance (ohms)
r_c	Antenna ohmic resistance (conductors and ground loss) (ohms)
η_c	Antenna radiation efficiency.

For the current monopole antenna and radial wire ground plane design, the ohmic resistance, r_c , consists primarily of resistive losses in the surrounding poorly conducting earth.

b) Matching network loss factor: The matching network loss factor is given by

$$l_m = [(r_a + r_c) + r_m] / (r_a + r_c) \quad (24)$$

where

r_m	Matching network equivalent resistance (ohms)
r_a	Antenna radiation resistance (ohms)
r_c	Antenna ohmic resistance (conductors and ground loss) (ohms).

The mismatch of the monopole antenna impedance to the feed cable impedance becomes inconveniently large only at the low end of the operating frequency band. Otherwise, the mismatch loss is reasonably moderate to low. Some candidate matching network designs were synthesized and analyzed by B. Rama Rao of MITRE using EESOF/ESYN and ESSOF/TOUCHSTONE software. Although significant decreases in mismatch loss were achieved, they were primarily at the most troublesome lowest frequencies, not across the HF band. Furthermore, the lossy components in the matching networks produce increases in system noise figure that partially offset the reductions generated by the mismatch loss improvements. Therefore, in view of the potentially marginal utility of matching networks and the anticipated maintenance problems associated with additional circuit components, located at widely dispersed antenna elements exposed to possibly frequent lightning occurrences, matching networks were not incorporated into the current system design. However, a provision has been made for adding a matching network at each antenna, if necessary.

c) Transmission line loss factor: The transmission line loss factor is given by

$$l_n = \frac{\exp(2\alpha d) \{1 - |\Gamma|^2 \exp(-4\alpha d) - 2[\text{Im}(Z_0) / \text{Re}(Z_0)] \text{Im}[\Gamma \exp(-2\gamma d)]\}}{1 - |\Gamma|^2 - 2[\text{Im}(Z_0) / \text{Re}(Z_0)] \text{Im}(\Gamma)} \quad (25)$$

where

$$\gamma = \alpha + j\beta \quad \text{Transmission line propagation constant} \quad (26)$$

Z_0 Transmission line characteristic impedance (ohms)

d Transmission line length (meters)

$$\Gamma = \frac{Z_1 - Z_0}{Z_1 + Z_0} \quad \text{Voltage reflection coefficient presented by the antenna and matching network at the end of transmission line. } \Gamma = \text{reflection coefficient encountered when operated as a transmitter antenna} \quad (27)$$

Z_1 Load impedance presented by the antenna and matching network to the transmission line = output impedance of antenna and matching network combination (ohms)

For this application, the characteristic impedance, Z_0 , of the coaxial cable transmission line can be approximated as being entirely real. Therefore, $\text{Im}(Z_0) = 0$, and (25) reduces to the simpler form

$$l_n = \exp(2\alpha d) \frac{[1 - |\Gamma|^2 \exp(-4\alpha d)]}{[1 - |\Gamma|^2]}, \quad \text{for } \text{Im}(Z_0)/\text{Re}(Z_0) \ll 1. \quad (28)$$

The *worst* transmission loss condition occurs when αd becomes large, making $\exp(-4\alpha d) \ll 1$, which occurs for the longest cable runs in the MITRE experimental site. Under these conditions, equation (28) reduces to:

$$l_n = \exp(2\alpha d) \frac{1}{[1 - |\Gamma|^2]} = l_{ca} l_{cm}; \quad \text{for } \text{Im}(Z_0)/\text{Re}(Z_0) \ll 1, \exp(-4\alpha d) \ll 1. \quad (29)$$

cable attenuation loss	cable mismatch loss
------------------------------	---------------------------

Equation (29) for the transmission line loss factor is separable into the conventional cable attenuation loss, l_{ca} , and cable mismatch loss, l_{cm} , factors, and has been applied to the longest cable runs to estimate worst case noise performance.

Equation (28), which accounts for the $[1 - |\Gamma|^2 \exp(-4\alpha d)]$ term in the numerator, is required to obtain the more realistic, lower estimated values for the transmission line loss factor for the shortest cable runs. The importance of this term increases as the antenna impedance presents an increasingly large mismatch to the line, which occurs below about 8 MHz in the present application. However, spot calculations for the minimum length cable condition show that the reductions in transmission line loss factor, achieved by using the more exact expression (28), are largely offset by the corresponding increases in receiver noise factor, f_r , obtained by accounting for the receiver's source impedance mismatch, through the use of the more exact semi-empirical f_r equation (30) with realistic estimated values for the r_n and Y_{on} receiver parameters.

Consequently, in the absence of the actual values for the equation (30) empirical parameters of the receiver discussed below in section 2.1.1.2, the approximate transmission loss factor equation (29) in combination with the receiver constant noise factor assumption were used throughout these analyses. This combination produced realistic upper bounds for the system internal noise factor (figure) under all cable length conditions. These bounds can be redefined, if desired, if and when the actual measured values of receiver parameters become available.

2.1.1.2 Receiver Noise Factor

The receiver noise factor, f_r , is a function of the receiver source admittance, Y_s , looking down the transmission line toward the antenna, and of the characteristic noise parameters, f_0 , r_n , Y_{no} , of the receiver, as given by [1,13, 14]

$$f_r = f_0 + [r_n/\text{Re}(Y_s)] |Y_s - Y_{no}|^2 \quad (30)$$

where

- f_0 Minimum noise factor for the optimized source admittance, $Y_s = Y_{no}$, at the reference temperature, T_r .
- Y_{no} Source admittance for which $f_r = f_0$.
- r_n Empirical noise parameter with the dimension of resistance, which is a measure of the noise factor sensitivity to a change in source admittance.

In the current analysis, the receiver noise factor, f_r , was assumed to be constant and optimized for operation into a matched 75 ohm coaxial cable transmission line, as discussed above in section 2.1.1.1c. For long cable runs, having high attenuation loss, this is a good assumption, since the source impedance $Y_s \cong Y_0$, where $Y_0 = 1/Z_0 =$ characteristic admittance of the coaxial cable. Therefore, for $Y_s \cong Y_0 = Y_{no}$, $f_r = f_0$.

Departures from this condition typically occur at the lowest operating frequencies, for receivers attached to the shortest cables, where $Y_s \neq Y_0$ and consequently $f_r \neq f_0$. Under these conditions, the source admittance and, therefore, the noise factor of such receivers given by equation (30) will be influenced by the antenna impedance and the line length. Since the receiver empirical constants r_n and Y_{no} were not available, the performance analyses were based on the $f_r = f_0$ assumption. If initial system calibration tests indicate that measurements of r_n and Y_{no} are necessary, they can be performed to determine the sensitivity of the receiver noise factor to variations in source admittance from that of a matched transmission line. Then either the associated corrections can be made to the receiver noise factor values using (30) in conjunction with the more exact calculations of the transmission line noise factor using (28), or the antenna impedance match conditions can be improved through the use of a matching network.

2.1.2 Antenna External Noise Factor

The external noise contribution to the system operating noise factor, f_{op} , in (5) is represented by f_a , the effective antenna external noise factor defined by the International Radio

Consultative Committee (CCIR) [15] in terms of the time-average, external noise power, p_n in watts, available from an equivalent lossless antenna

$$f_a = p_n/kT_a b = p_n/n_{ref} = T_a/T_r, \quad (31)$$

where T_a is the effective antenna temperature ($^{\circ}\text{K}$) in the presence of external noise. The available external noise power represents the antenna response to the incident external noise distribution, integrated over the entire sphere of the antenna directivity pattern.

Standard statistical databases of the stochastic variability of external noise (atmospheric, galactic, and man-made) are readily available from the CCIR [15-17] and other sources [18]. The CCIR assertion is that noise levels in these databases are normalized to correspond to values that would be measured with an electrically short, vertical, monopole antenna over an infinite, perfectly conducting ground plane. A recent report by M. M. Weiner [19] points out that the CCIR assertion is only partially correct. Namely, CCIR noise levels have been normalized to account for antenna ohmic losses of the ground, but not for the antenna directivity pattern of its electrically small ground plane. Therefore, these noise levels may need to be adjusted for vertical monopole antennas over finite, imperfectly conducting ground planes, such as those typically encountered at land-based sites.

2.2 ANTENNA DIRECTIVITY

Antenna directivity, $D(\theta, \phi)$, also called "directive gain," is a measure of the ability of an antenna to concentrate radiated power in a particular direction. It is defined as the ratio of the achieved radiation intensity in a particular direction to that of an isotropic antenna. Therefore, the directivity represents the response sensitivity of a receive antenna to radio waves incident upon it from different angular directions (θ, ϕ) . The gain, $G(\theta, \phi)$, of an antenna is obtained by multiplying the directivity by the antenna efficiency. The antenna directivity pattern $D(\theta, \phi)$ for an isolated, vertical, monopole antenna over uniform ground exhibits no variation with azimuthal angle ϕ . Namely, it is omnidirectional in azimuth, the desired property for an element pattern of the MITRE site circular array.

The elevation plane pattern over an imperfect ground exhibits the characteristic "doughnut-like" cross-sectional shape, with the standard monopole null at the zenith angle, a second null on the horizon due to the imperfectly conducting ground, and an amplitude variation with elevation angle that is moderately dependent on frequency and earth electrical properties. The elevation pattern response will affect the received strength of radio signals incident from particular elevation angles, and, to a lesser extent, the resultant received levels of external noise integrated over the antenna directivity pattern. Consequently, for the monopole antenna and ground plane configurations giving favorable system internal noise performance, it is important to predict directivity pattern behavior and to evaluate its elevation dependence on frequency and earth electrical properties.

Figure 1 illustrates that the array of vertical monopole elements also contains long, coaxial cables running from each element to one of three electronics shelters. Therefore, it was necessary to estimate the magnitude of potentially adverse effects that these conducting feed

cables and shelters might produce on the radiation patterns of the individual monopole antennas, particularly those effects that introduce azimuthal asymmetry.

2.2.1 Feed Cable Effects

When a coaxial cable feeding a monopole antenna is not completely shielded by a large conducting ground screen from the electromagnetic (EM) fields radiated from, or incident upon, the antenna, undesired electrical currents will be induced along the external surface of the cable. These undesired cable currents disturb the azimuthal symmetry of the antenna and contribute to the power radiated, or received, by the antenna, primarily by modifying the directivity pattern of the antenna. In a circular array application such as this one, perturbations that modify the azimuthal symmetry of the directivity pattern and its phase center are of particular concern. Large perturbations can cause unwanted variations, with azimuth scan angle, in the array's main beam directivity, and in the case of large modifications in phase center, can cause significant degradations in beam formation.

Unwanted cable currents can be suppressed by periodically loading the cable with closely spaced, ferrite toroidal cores, a method typically used on antenna pattern ranges to reduce the effects of stray cable currents. However, in this cable application, loading over long sections of cable would be required to effectively suppress these effects if the cables were left unburied, which renders this method excessively costly and logistically impractical. Therefore, primary attention was devoted to cable burial as the most practical method of suppressing unwanted cable currents.

The potential seriousness of cable effects was evaluated by modeling, with the NEC-3I computer code, a monopole antenna having a radial wire ground plane both with and without a long, radial, jacketed feed cable, and then comparing the elevation and azimuthal variations in antenna directivity and phase of the radiated fields. Comparisons were made and the implications assessed, as a function of frequency, cable length, cable unburied and buried to various depths, and electrical properties of the surrounding earth.

2.2.2 Electronics Shelter Effects

Metal objects (such as the electronics shelters located at each of the three nodes) that are placed in the vicinity of antennas, will scatter radiated or incident fields and introduce asymmetrical modifications to the directivity and phase patterns of the antennas. However, only minor effects are expected in this application because of the modest size of the shelter and the relatively large minimum distances between the antennas and the shelters.

The potential seriousness of shelter effects was evaluated by modeling with the NEC-3 computer code, a monopole antenna having a radial wire ground plane with and without the presence of an electronics shelter, and then comparing the elevation and azimuthal variations in both directivity and phase in the radiation field. Comparisons were made, and the implications assessed as a function of frequency, broadside and endfire orientations of the shelter, and distance of the shelter from the antenna.

SECTION 3

APPLICABLE NUMERICAL ELECTROMAGNETICS CODE (NEC) SOFTWARE

The Numerical Electromagnetics Code (NEC) Method-of-Moments is a powerful and widely used computer program developed by LLNL for calculating the EM interaction between conducting structures and applied voltages and/or EM fields [6-12]. The conducting structures may be driven by an input voltage or illuminated by an incident EM wave, as in the case of antennas. NEC is commonly applied to modeling antennas in VLF-to-VHF applications on ships, vehicles, and on the ground. It includes features for efficiently modeling antennas and scatterers in their environments, including antennas interacting with, or buried in, finitely conducting ground. The NEC-3 versions of the code (NEC-3, -3I, and -GS) used on this project are particularly well suited for modeling the candidate antennas, with their cables and ground screens buried in and above ground. This section presents a brief overview of NEC concepts and NEC utility to this application. Detailed treatments of NEC are available in numerous references, such as those identified in this chapter.

The methodology involves the numerical solution of the electric field integral equation for thin wires. It is applied to conducting structures that have been represented by a network of thin wires, each subdivided into segments. The code uses a moment-method model with three-term, sinusoidal-spline current expansion and point matching, and an accurate treatment of the air-ground interface based on the Sommerfeld-integral formulation, which accounts for surface wave effects. Use of the Sommerfeld-integral formulation option, i.e., subprogram SOMNTX, is particularly important and necessary for wire structures located below ground, above ground (but within about 0.1 - 0.2 wavelengths of the surface), or penetrating the ground surface, all of which occur in the antenna application for the experimental site.

Significant code validation work has been undertaken and published by the developers of NEC [10,12]. However, as an added precaution, prior to modeling and analyzing candidate antenna/ground-screen designs, the project underwrote a modest effort to validate the appropriateness and accuracy of the versions of NEC-3 installed on the MITRE Sensor Center computer system. A series of NEC runs and comparative theoretical tests were performed, and reported upon by M. M. Weiner [5], to determine the validity of numerical results for both thin dipole antennas placed close to the ground, and quarter wave monopole antennas with radial ground planes placed below the surface of the ground.

3.1 NEC-GS VERSION

NEC-GS is a specialized, reduced version of NEC-3 [8,11,12], optimized for modeling vertical monopoles on uniform radial wire ground screens. This moment-method solution involves no basic approximations, such as assumed currents or field values, which often are used in modeling radial-wire ground screens. NEC-GS can be used to model any wire structure with azimuthal (rotational) symmetry, as long as the excitation source also has rotational symmetry. For example, a thin monopole with a radial ground screen can be modeled simply by defining the monopole, one radial, and the number of radials.

By taking maximum advantage of the rotational symmetry of the screen and its currents, NEC-GS can model radial wire screens in much less time, using much less memory storage, than that required by NEC-3. More importantly, NEC-GS also provides the simplest and most accurate way to model large diameter antenna elements, such as "fat" dipoles or cylindrical tower monopoles of radius much larger than that of the thin, radial wires. Namely, a "fat" monopole with radial wire ground screen can be modeled by defining an "L"-shaped radial that has a vertical wire portion displaced a distance from the z-axis equal to the monopole radius and fed by an excitation at its base, which is, in turn, connected to the radial wire portion. This allows the fat monopole to be formed as a cage of thin wires, equal in number to the radial wires. As a result, NEC-GS played a key role in the modeling and parametric performance analyses of the monopole and dipole antenna configurations evaluated for this application.

3.2 NEC-3 AND NEC-3I VERSIONS

NEC-3 and NEC-3I are the applicable general forms of NEC when the geometry of the complete structure is not rotationally symmetric, namely, when effects caused by antenna feed cables and shelters need to be evaluated. Since pattern effects caused by feed cables and shelters will be independent of monopole tower radius, a thin wire monopole model can be used. This simpler, thin wire model allows pattern effects to be calculated without incurring excessive computation times or exceeding the present, 1500 segments, matrix limit of the Sensor Center version of NEC-3. NEC-3 was used to assess the effects of shelters, whereas NEC-3I was used to assess the effects of feed cables. The NEC-3I (insulated wire) version [9,10,12] of NEC-3 provides an option for modeling wires covered with thin insulating dielectric sheaths, which is directly applicable to modeling the jacketed, coaxial feed cables of interest to this application.

3.3 SOME MODELING CONSTRAINTS

Although NEC is a powerful and flexible computer code, a number of rules must be followed to obtain accurate, dependable results. Some of the rules particularly important to the calculations of this report are summarized below.

Segment Length vs Wavelength: Lengths of wire segments should generally be less than a maximum size of about 0.1 wavelength, but greater than a minimum size of about 10^{-4} wavelength for single precision computations, or 10^{-8} wavelength for double precision, where the wavelength refers to that in the medium containing the wire segment. However, longer segments of up to approximately 0.14 wavelength may be acceptable on long, straight wires or noncritical parts of a wire network, whereas some critical regions may even require shorter maximum lengths of 0.05 wavelength or less.

Segment Length vs Segment Diameter: Lengths of wire segments are also subject to a minimum limit relative to wire segment diameter, because of approximations used in the kernel of the electric field integral equation. Unless otherwise specified, NEC uses the thin wire kernel (TWK), which gives accurate results with length-to-diameter ratios of $l/d \geq 2$.

For smaller l/d values, the extended thin wire kernel (ETWK) option can be invoked to give accurate results to values of $l/d \geq 0.5$. Accuracy of the results also depends on the ratio of radius to wavelength being acceptably small and the excitation such that circumferential variations are avoided, which is the case in this application. However, the ETWK option can be applied only to straight sections of wire. It cannot be successfully applied to wires having bends, or step changes in radius, along themselves or at their junctions, because the ETWK option represents wire segments as thin-walled tubes, instead of solid wire cylinders. This tubular representation creates problems, at junctions with bends or radius changes, because of NEC's method of satisfying continuity conditions. Consequently, the ETWK option was not applicable to the "fat" monopole antenna with radial wire ground screen configuration.

Wire Segment Radius Changes: In the normal TWK option of NEC, radius changes can be made between adjacent solid wire segments. However, care must be taken to keep the ratio of the radii of adjacent segments to less than two, and the corresponding segment lengths as long as possible, because the capacitive effect of the step is not modeled accurately enough. In addition, the radius of a wire segment should not be changed at the point where the wire crosses an interface between two media. Furthermore, a wire crossing an interface should be segmented in such a manner that the interface is located at the junction between two segments, so that a segment does not traverse, or straddle, the interface between two media.

Wire Segment Length vs Junction Height above interface: If adequate precautions are not taken, then serious errors can occur when modeling angular junctions of conducting structures located above, but close to, the air-ground interface. The junctions between the base of a vertical monopole antenna and an unburied horizontal feed cable, junctions between the base of the antenna and its unburied radial wire ground screen, or junctions between above-ground and buried sections of a feed cable are three such examples. In these cases, the segment lengths on both sides of the junctions must be kept less than, or about equal to, the height of the junction above the air-ground interface to avoid serious errors. The segments can then be gradually increased in length, with increasing distance from the junctions, by using the tapered-length option for segments.

Corresponding results for junctions in buried wires located close to the interface are much more stable than those for wires above the surface of the ground, so stringent precautions concerning segment lengths in the vicinity of buried junctions are generally not required.

Insulated Wires: When modeling an insulated wire, such as a jacketed coaxial cable using NEC-3I, the maximum usable segment length on the insulated wire is influenced by the relative values of the wave numbers in the insulating material, k_2 , and the surrounding medium, k_1 , and the layer outer radius, b . For insulated wires in air, no change is necessary in maximum segment length from that for a bare wire, because the propagation wave number, k_s , (and wavelength) for current on a wire with a thin insulating layer are close to the bare wire free space values.

When the insulated wire is embedded in earth or water, the situation can be quite different, especially if $|k_1| \gg |k_2|$, because the wave number for current on the wire, k_s , can be much smaller than the wave number, k_1 , of the surrounding medium. Use of $k_s = k_1$ to establish maximum segment length, l , in these cases can still produce accurate results if the product $k_1 l$ remains small, but the solution will converge very slowly to the correct result. If the ratio

of external to internal wave numbers remains small, i.e., $|k_1/k_2| \leq 2$, then the speed of convergence will not be a problem, so k_s can be set equal to k_1 of the external medium. However, as the ratio becomes large, i.e., $|k_1/k_2| > 2$, the solution convergence rate can be markedly improved by approximating k_s by an effective propagation wave number, k_L , [9,12] derived from coaxial transmission line theory, namely,

$$k_s = k_L = k_2 \left[1 + \frac{H_0^{(2)}(k_1 b)}{(k_1 b) \ln(b/a) H_1^{(2)}(k_1 b)} \right]^{1/2} \quad (32)$$

Fortunately, the NEC solution is relatively insensitive to k_s , so the accuracy of k_s within a factor of about two is not critical.

Timing Considerations: Significant computation time can be consumed by extensive parametric analysis of model structures constructed of a large number, N , of wire segments, like the antenna, cable and shelter in this application. The developers of NEC provide useful relationships that enable users to estimate program execution times by running representative test cases. This allows better user allocation of analysis resources. The relationships show that execution time is typically given by the sum of a matrix filling term proportional to N^2 and a matrix factoring term proportional to N^3 .

SECTION 4

NUMERICAL RESULTS

4.1 MONOPOLE ANTENNA WITH RADIAL GROUND SCREEN

4.1.1 Geometry, Parameters, and NEC-GS Outputs

Figure 7 presents the spherical coordinate geometry for the general monopole antenna and its radial ground screen model. The triangular cross-section antenna tower of figure 2 is approximated by a right circular cylinder monopole element of height, h , and radius, b , passing through the vertices of the triangular cross-section. The monopole is placed above a ground screen consisting of M equally spaced radial wires of length, a , and radius, b_w , which are located at a depth, z_0 , below a flat earth surface. The earth, or ground material, is characterized by the electrical properties of conductivity, σ , in millisiemens/m and relative dielectric of constant, ϵ_r . The quantities r , θ , and ϕ are the conventional spherical coordinates, and ψ is the elevation angle measured from the horizon. Both the monopole element and the radial wire conductors are constrained to have infinite conductivity.

As stated in 3.1, the "fat" monopole of interest is best modeled by using NEC-GS. Figure 8 shows the specific geometry of the L-shaped radial wire used to form a cage of M equally spaced wires to model the monopole and its radial wire ground screen. The L-shaped radial wire consists of: a) a vertical wire section of height, h , and radius, b_w , displaced from the z -axis by a distance, b , equal to the monopole radius; b) a short vertical excitation section; and c) a horizontal wire section of radius, b_w , which begins with a short, downward sloping transition section and continues horizontally to a radial distance, a , at a depth, z_0 , beneath the surface. Each of the wire sections is suitably divided into wires and subdivided into wire segments, N_i , according to the guidelines in 3.3, where i denotes the i -th wire. The number, M , of L-shaped radials around the circumference of the monopole is also specified, as well as the earth parameters, ϵ_r , σ , and the frequencies of excitation.

The parametric analyses were conducted to characterize antenna performance relative to that of a baseline configuration and arrive at a practical final design. The baseline configuration consists of the 5.4 m FPS-118, OTH-B radar receive antenna tower structure equipped with a ground screen of 16 equally spaced radial wires 12 m long, instead of the OTH-B continuous mesh screen. The characteristic dimensions, wire coordinates, and wire segmentation of the NEG-GS model of the baseline antenna are given in table 1. Table 2 summarizes the ranges of parameter variation investigated. While many of the NEC runs were conducted for the 5.4 m tower structure, the parameter excursions in table 2 do include the dimensions of the eventually selected 6.3 m tower. It was also important to examine antenna behavior over the complete frequency range of 5 megahertz (MHz) to 30 MHz, for a wide range of ground soil conditions anticipated for the Texas site. While the five soil categories and their electrical properties provide a representative set, the average, fair, and poor categories are probably more typical for the site.

1.2780-1

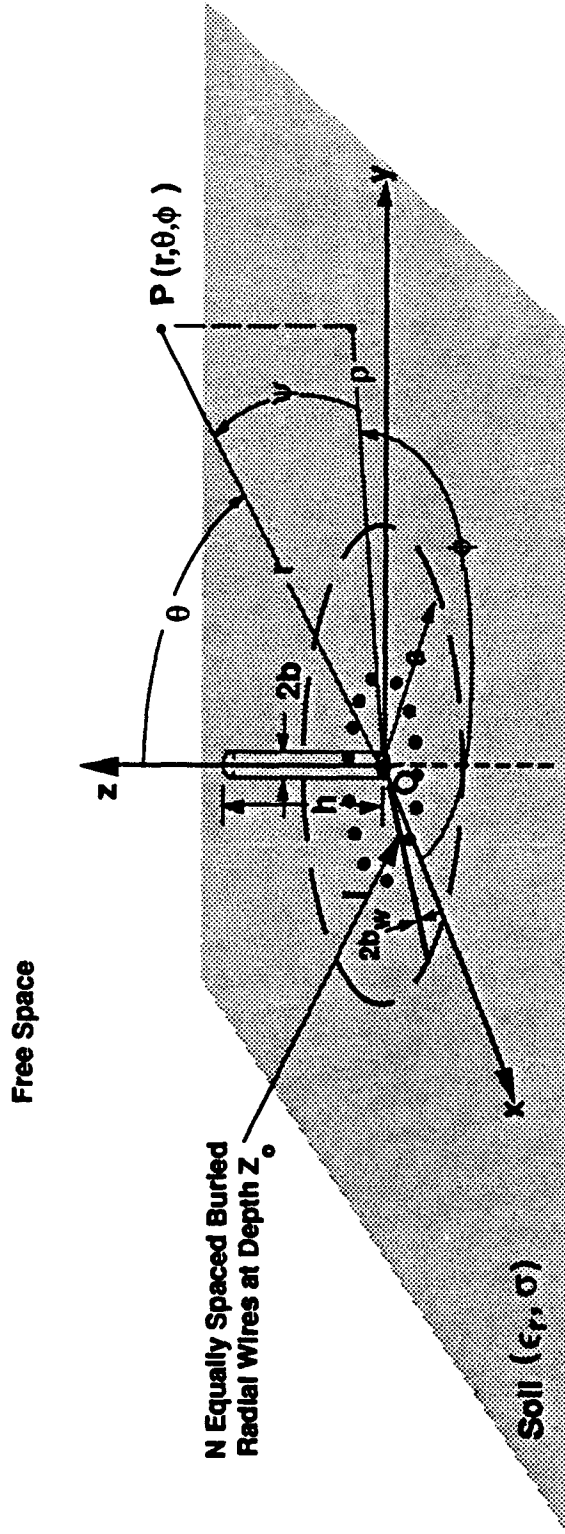


Figure 7. Spherical Coordinate Geometry for General Monopole Antenna and Ground Screen of Radial Wires

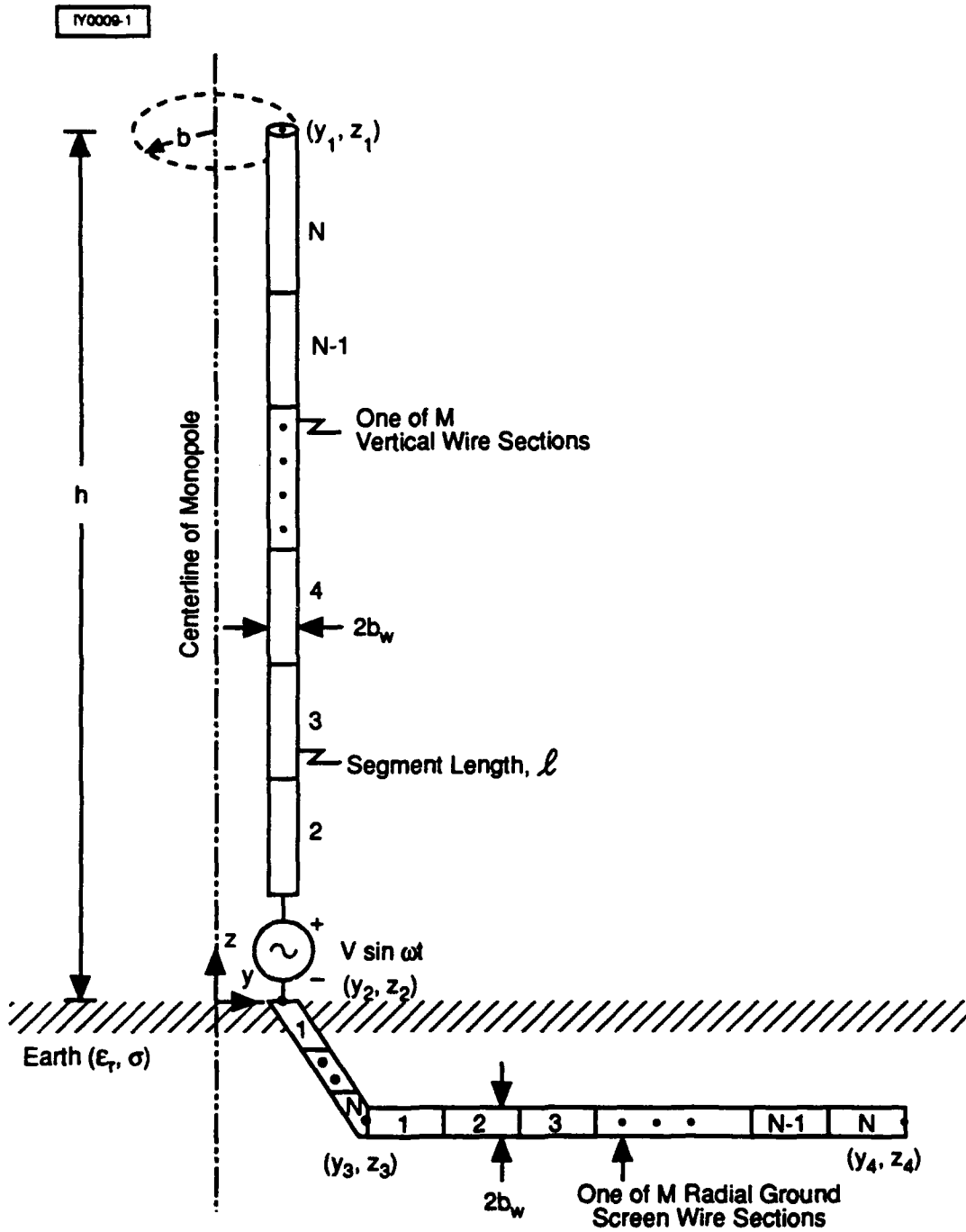


Figure 8. NEC-GS Rotational (Cage) Model Representation of Monopole Element of Radius b and Ground Screen with M L-Shaped Radial Wires

IL3081-1

Table 1. Baseline NEC-GS Rotational (Cage) Vertical Monopole Antenna Wire Model

a) Baseline Wire Model Dimensions (Figure 8)

Monopole Height (h)	5.4m	(17.7 ft)
Monopole Radius (b)	0.25m	(9.8 in)
Vertical Wire Filament Radius (b_w)	0.001m	(0.04 in)
Excitation (Feed) Section Length (l_e)	0.216m	(8.5 in)
Ground Wire Radial Extent (a)	12.0m	(39.4 ft)
Ground Wire Radius (b_w)	0.001m	(0.04 in)
Ground Wire Depth (z_o)	0.178m	(7.0 in)

b) Baseline Wire Model Coordinates (Meters) and Wire Segmentation

Monopole Vertical Wire (Includes Excitation Segment)	$y_1 = 0.25, z_1 = 5.4; y_2 = 0.25, z_2 = 0.0; N = 25, \ell = 0.216$
Ground Wire First Section	$y_2 = 0.25, z_2 = 0.0; y_3 = 0.8, z_3 = -0.178, N = 1, \ell = 0.578$
Ground Wire Horizontal Section	$y_3 = 0.8, z_3 = -0.178; y_4 = 12.0, z_4 = -0.178, N = 14, \ell = 0.8$

IL3082-1

Table 2. Parameter Variations for Performance Assessment

a) Earth (Soil) Electrical Characteristics

Category	Condition	Relative Dielectric Constant, ϵ_r	Conductivity, σ Millisiemens/m
Very Good	Wet Ground	30	15
Good	Moist Clay	10	15
Average	Medium Dry Ground	10	1.5
Fair	Sand	4	1.5
Poor	Very Dry Ground	4	0.15

b) Frequency Range

5 MHz to 30 MHz in Steps of 2.5 MHz and 5.0 MHz

c) Ground Screen Radial Wire Parameters

Number of Radials	$M = 16,32$
Radial Extent	$a = 12,24$ Meters
Burial Depth	$z_o = -0.178, -0.305$ Meters
Wire Segment Length	$\ell = 0.8, 0.4, 0.2$ Meters

d) Monopole Parameters

Monopole Height	$h = 5.4, 6.0, 6.3, 6.5, 7.0$ Meters
Base of Excitation Height	$h_e = 0.0, 0.216$ Meters

The NEC-GS computer runs explored the sensitivity of system internal noise figure and antenna directivity to: operating frequency, soil electrical properties, number, length, and burial depth of ground screen radials, and the monopole height, as well as the effects of radial wire segment size on the results.

The following key quantities were extracted from the NEC-GS output files: the real and the imaginary parts of the antenna impedance, the antenna power gain, and the average power gain. Telephone communication with NEC-GS developer, G. Burke of LLNL, alerted us to the undocumented requirement that values of several NEC-GS output file quantities must be adjusted by the number, M , of L-shaped radial wires, to obtain valid results. Namely, the input impedance and average power gain values must be divided by M , the input current must be multiplied by M , and $10 \log_{10} M$ must be subtracted from the antenna power gain, which is expressed in dB. The input impedance, Z/M , is used to compute the antenna reflection coefficient, Γ , and the associated mismatch loss factor, $1_n = 1/[1 - |\Gamma|^2]$ in the standard manner, where

$$|\Gamma|^2 = \frac{(R - Z_0)^2 + X^2}{(R + Z_0)^2 + X^2} \quad (33)$$

and

R = Resistive part of load impedance Z/M
 X = Reactive part of load impedance Z/M .

The average power gain (numeric) is used to compute the antenna efficiency

$$\eta = (\text{average power gain})/2M \quad (34)$$

and the associated antenna ohmic loss factor, $1/\eta$. The average power gain is also used, together with the power gain in dB, to compute the antenna directivity.

$$D \text{ (dBi)} = \text{power gain (dB)} - 10 \log_{10} [(\text{average power gain})/2] \quad (35)$$

4.1.2 Antenna Ohmic Loss and Cable Mismatch Loss

By accounting for the absence of a matching network, i.e. $l_m = 1$, and using the long cable worst-case, transmission line loss expression (29), the system internal noise factor and figure equations (20, 21), respectively reduce to

$$f_s = l_c l_{nm} l_{na} f_r \quad (36)$$

and

$$F_s = L_c + L_{nm} + L_{na} + F_r \text{ (dB)} \quad (37)$$

where

$$L_c = 10 \log_{10} l_c = 10 \log_{10} (1/\eta) \text{ (dB)} \quad (38)$$

$$L_{nm} = 10 \log_{10} l_{nm} = 10 \log_{10} [1/(1 - |\Gamma|^2)] \text{ (dB)} \quad (39)$$

$$L_{na} = 10 \log_{10} l_{na} = 10 \log_{10} [\exp(2\alpha d)] \text{ (dB)} \quad (40)$$

are the antenna ohmic loss, L_c , cable mismatch loss, L_{nm} , cable attenuation loss, L_{na} , and receiver noise figure, F_r , contributions to the system internal noise figure.

Each contribution was computed separately, then added together to get the total system internal noise figure. The sum $L_c + L_{nm}$ served as a secondary performance measure. This sum was used to measure the size and assess the utility of incremental gains or losses in noise figure obtainable by changing antenna geometrical parameters relative to the values for the baseline reference configuration.

Figure 9 and table 3 illustrate the dependence of antenna (ohmic loss) noise figure, L_c , on frequency and soil electrical properties, for the 16 radial baseline reference case defined by $h = 5.4$ m, $b = 0.25$ m, $l_e = 0.126$ m, $h_e = 0.0$ m, $b_w = 0.001$ m, $M = 16$, $a = 12$ m, and $z_0 = -0.178$ m in tables 1 and 2. They indicate that the resistive losses in the soil give rise to noise figure values in the range of 3.5 dB to 8 dB, thereby exhibiting only modest variability with frequency and soil condition. The loss generally increases gradually with decreasing values of conductivity and relative dielectric constant, until the trend begins to reverse itself as the conductivity becomes low enough.

Figure 10 and table 4 depict the behavior of the antenna input resistance and reactance for the baseline 16 radial configuration, as a function of frequency and soil conditions. Figure 11 presents the associated mismatch loss of equation (39) when the antenna is connected to a coaxial cable having a 75 ohm characteristic impedance. These figures demonstrate very stable impedance behavior with changes in soil electrical properties. The characteristic resonance behavior with frequency is apparent, together with the expected large increase in mismatch loss below 10 MHz, as the monopole size becomes small compared to wavelength. The following subsections, 4.1.2.1—4.1.2.3, illustrate the incremental changes in noise figure performance obtainable by changing key geometrical parameters.

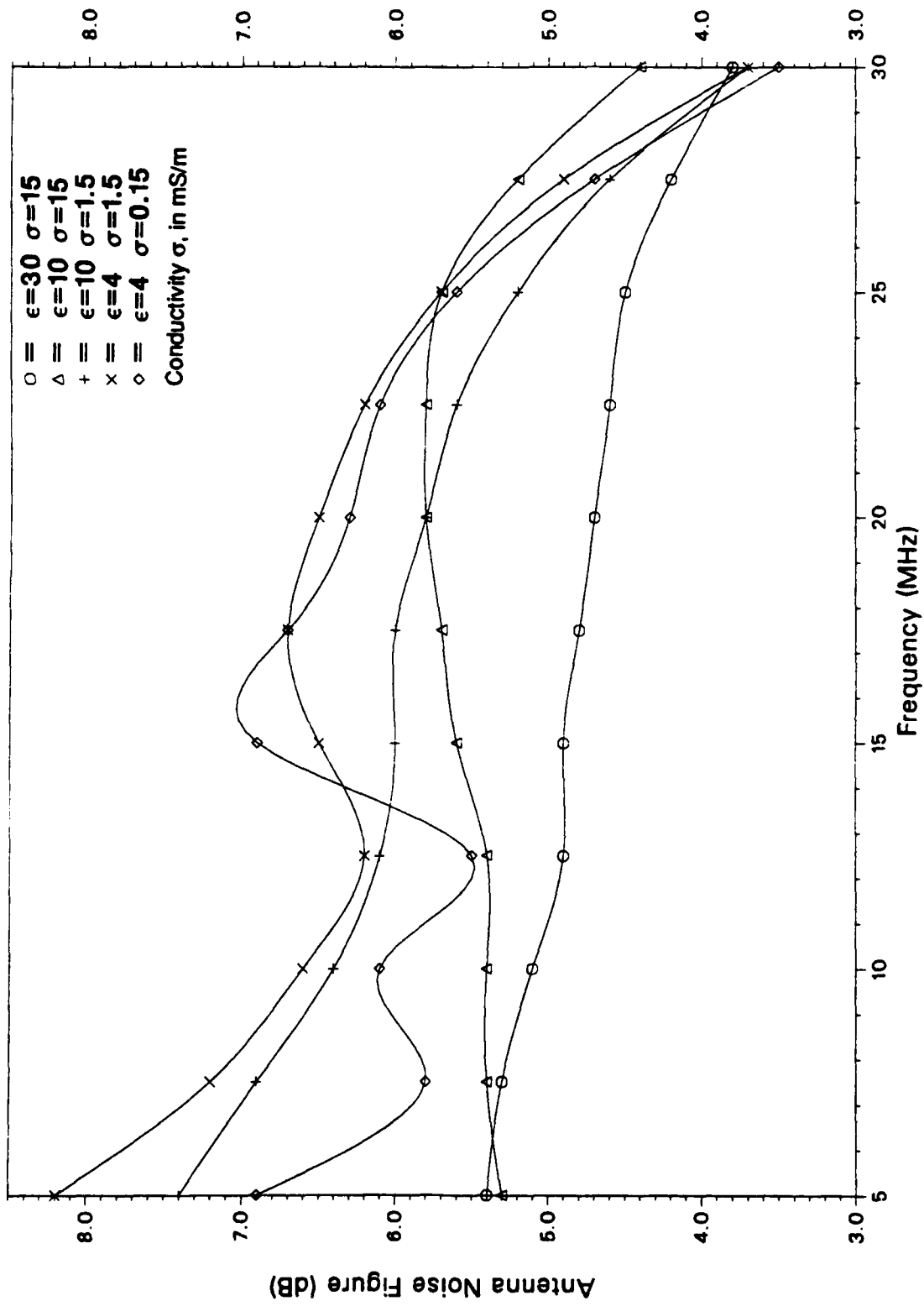


Figure 9. Antenna Noise Figure (Ohmic Loss) versus Frequency and Five Soil Conditions for 5.4 Meter High Monopole with 12 Meter Radius Ground Screen of 16 Radials

IL2766-7

Table 3. Antenna Efficiency and Noise Figure versus Frequency and Five Soil Conditions
 For 5.4 Meter High Monopole with 12 Meter Radius Ground Screen of 16 Radials, 2mm in Diameter and Buried 0.178m Deep

Frequency (MHz)	Soil Characteristics											
	Very Good (Wet Ground)		Good (Moist Clay)		Average (Medium Dry Ground)		Fair (Sand)		Poor (Very Dry Ground)			
	$\epsilon_r = 30, \sigma = 15 \text{ mS/m}$	$\epsilon_r = 10, \sigma = 1.5 \text{ mS/m}$	$\epsilon_r = 10, \sigma = 1.5 \text{ mS/m}$	$\epsilon_r = 4, \sigma = 1.5 \text{ mS/m}$	$\epsilon_r = 4, \sigma = 1.5 \text{ mS/m}$	$\epsilon_r = 4, \sigma = 0.15 \text{ mS/m}$	$\epsilon_r = 4, \sigma = 1.5 \text{ mS/m}$	$\epsilon_r = 4, \sigma = 0.15 \text{ mS/m}$				
	η (%)	NF (dB)	η (%)	NF (dB)	η (%)	NF (dB)	η (%)	NF (dB)	η (%)	NF (dB)	η (%)	NF (dB)
5.0	28.9	5.4	29.7	5.3	18.2	7.4	15.3	8.2	20.2	6.9		
7.5	29.3	5.3	28.5	5.4	20.5	6.9	19.1	7.2	26.6	5.8		
10.0	31.0	5.1	28.7	5.4	22.9	6.4	21.9	6.6	24.7	6.1		
12.5	32.1	4.9	28.6	5.4	24.4	6.1	23.8	6.2	28.1	5.5		
15.0	32.6	4.9	27.8	5.6	25.0	6.0	22.4	6.5	20.2	6.9		
17.5	33.2	4.8	27.0	5.7	25.3	6.0	21.6	6.7	21.3	6.7		
20.0	33.7	4.7	26.3	5.8	26.4	5.8	22.5	6.5	23.4	6.3		
22.5	34.5	4.6	26.3	5.8	27.8	5.6	24.2	6.2	24.4	6.1		
25.0	35.8	4.5	27.1	5.7	30.2	5.2	26.8	5.7	27.7	5.6		
27.5	38.1	4.2	29.9	5.2	34.8	4.6	32.4	4.9	33.6	4.7		
30.0	42.1	3.8	36.6	4.4	42.4	3.7	42.9	3.7	45.0	3.5		

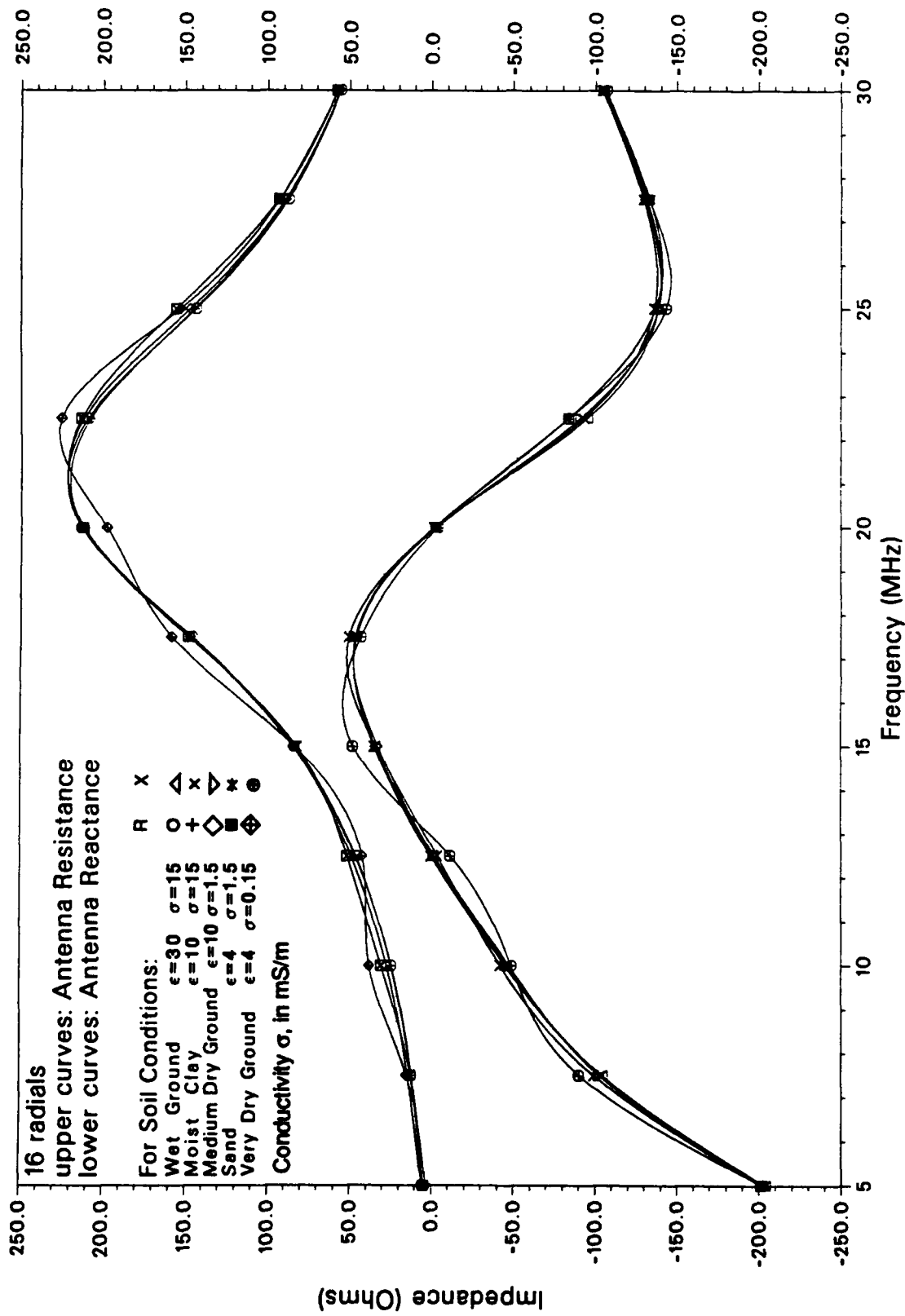


Figure 10. Antenna Input Resistance and Reactance versus Frequency and Five Soil Conditions for 5.4 Meter High Monopole with 12 Meter Radius Ground Screen of 16 Radials

IL2768-2

Table 4. Antenna Input Resistance and Reactance versus Frequency for Five Soil Conditions

For 5.4 Meter High Monopole with 12 Meter Radius Ground Screen of 16 Radials, 2 mm in Diameter and Buried 0.178m Deep

Frequency (MHz)	Soil Characteristics				
	Very Good (Wet Ground) $\epsilon_r = 30, \sigma = 15 \text{ mS/m}$	Good (Moist Clay) $\epsilon_r = 10, \sigma = 15 \text{ mS/m}$	Average (Medium Dry Ground) $\epsilon_r = 10, \sigma = 1.5 \text{ mS/m}$	Fair (Sand) $\epsilon_r = 4, \sigma = 1.5 \text{ mS/m}$	Poor (Very Dry Ground) $\epsilon_r = 4, \sigma = 0.15 \text{ mS/m}$
5.0	5.26 - j203.9	5.01 - j203.7	5.73 - j201.7	4.79 - j201.7	3.35 - j202.6
7.5	12.2 - j104.6	11.7 - j104.1	14.3 - j102.9	12.4 - j99.5	14.9 - j90.5
10.0	24.6 + j34.9	24.3 - j45.2	27.2 - j47.7	30.6 - j42.2	37.9 - j49.0
12.5	46.1 - j1.19	46.6 + j0.25	49.0 - j1.69	51.4 - j3.62	42.3 - j11.4
15.0	83.3 + j34.1	84.4 + j34.9	84.2 + j32.6	82.0 + j33.8	83.2 + j47.9
17.5	146.0 + j46.1	146.8 + j45.8	146.9 + j46.6	148.1 + j50.4	158.3 + j43.3
20.0	213.4 - j2.56	207.7 - j93.0	211.9 - j2.62	212.5 - j1.49	198.0 - j3.67
22.5	209.3 - j95.1	212.3 - j93.0	211.8 - j91.0	213.2 - j83.6	225.3 - j83.9
25.0	143.7 - j138.4	144.5 - j135.9	147.3 - j138.4	155.6 - j136.6	153.3 - j143.0
27.5	87.5 - j130.3	88.7 - j129.4	89.2 - j131.2	93.1 - j133.1	92.8 - j132.7
30.0	55.7 - j104.9	55.8 - j104.3	56.1 - j105.1	57.8 - j105.8	57.5 - j106.8

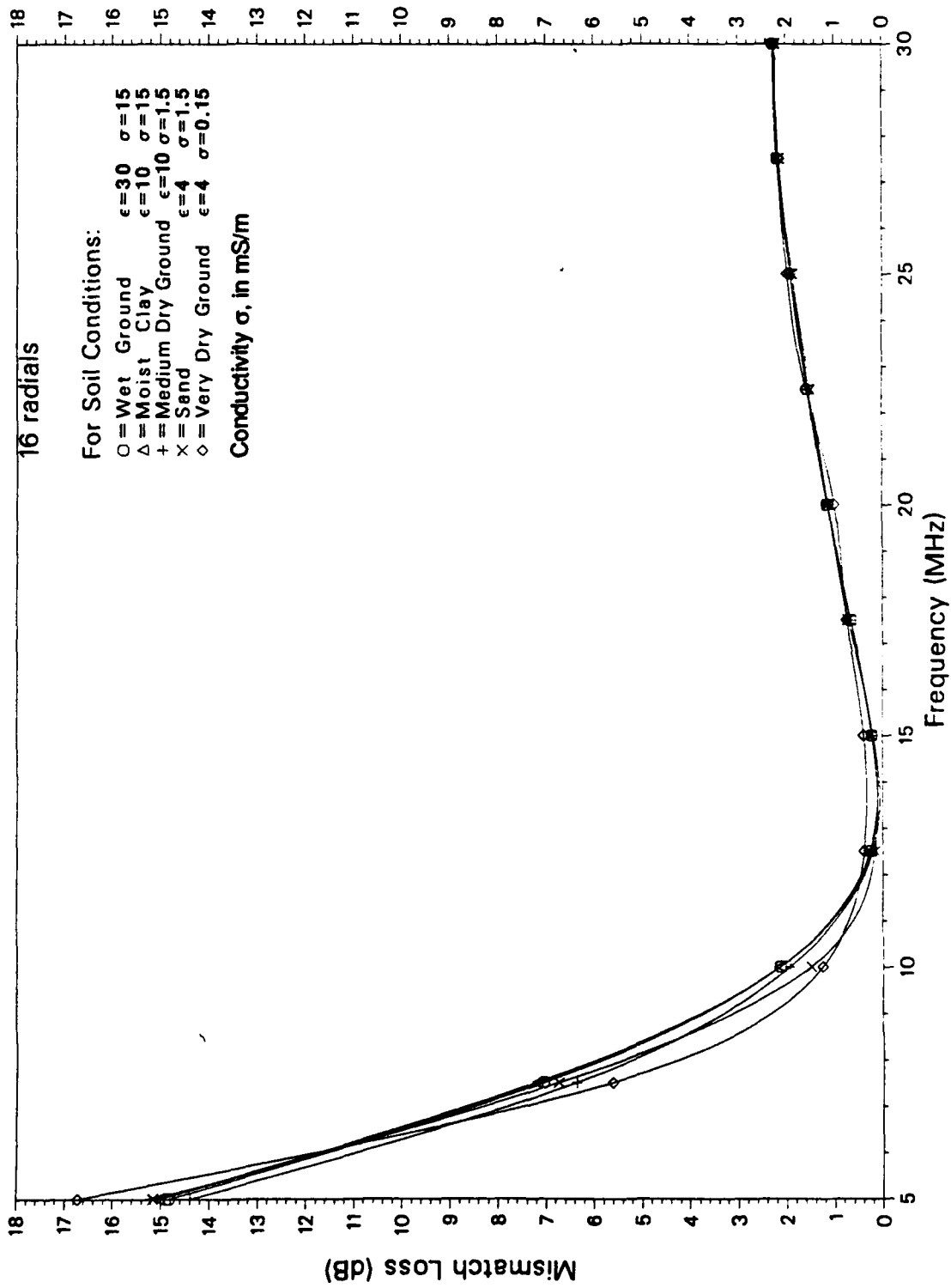


Figure 11. Cable Mismatch Loss versus Frequency and Five Soil Conditions for 75 ohm Coaxial Cable Feeding 5.4 Meter High Monopole with 12 Meter Radius Ground Screen of 16 Radials

4.1.2.1 Effect of Increasing the Number of Radials

Figures 12 and 13 show that doubling the number of radials to 32 lowers the maximum antenna noise figure somewhat and compresses the range of values to between 4 dB and 6 dB. Figures 14 and 15 directly compare the 32 radial input impedance and mismatch loss behavior (dashed curves) with that for the 16 radial case (solid curves). The 32 radial case exhibits performance similar to that for the 16 radial case, namely, it is relatively independent of soil condition and displays the characteristic resonance behavior. The main differences involve the first anti-resonant frequency for the 32 radials, which is shifted downward slightly, and the mismatch loss values below 10 MHz, which have increased by about 0.5 dB to 3 dB, relative to those for the 16 radial case. Table 5 tabulates the net changes in the noise figure sum ($L_c + L_{nm}$) that occur when the number of radials is doubled from 16 to 32, for a 12 m radius ground screen. Negative changes indicate improvements in noise figure performance. The achievable improvements are only minor and generally greatest in the frequency mid-range where the performance is already better.

4.1.2.2 Effect of Increasing the Length of the Radials

Tables 6 and 7 show the impact of increasing the ground screen radius. Tabulated are the net changes that occur in noise figure when the radius is doubled from 12 m to 24 m for ground screens having 16 and 32 radials, respectively. Table 8 shows the resultant impact on noise figure if both the number and length of the radials are increased, from a ground screen having 16 radials 12 m in length, to one having 32 radials 24 m in length. The tables and plots indicate that notwithstanding the approximately 5 dB improvement in noise figure attainable at the lowest frequency, for the worst case ground condition, the amount of improvement realized is generally mixed and marginal.

Consideration of the marginal, performance gains achievable, and the significant cost increases incurred by installing additional or longer buried radial wires, led to selection of the baseline ground screen configuration of 16 radials, each 12 m (40 ft) in length. If the unlikely worst-case soil condition does, in fact, become the predominant one at the Texas site and improved performance is desired at the low end of the frequency band, then the improvement can be economically achieved by adding a simple matching network at the base of the monopole antenna.

4.1.2.3 Effects of Radial Wire Burial Depth and Feed Section Height

Table 9 shows the effect of increasing the burial depth of a 16 radial 12 m radius ground screen from 7 in to 12 in (0.178 m to 0.305 m). Namely, performance is generally reduced slightly, making it undesirable to bury the radials any deeper than the approximately 7 in required to achieve adequate physical protection. Table 10 shows that raising the feed

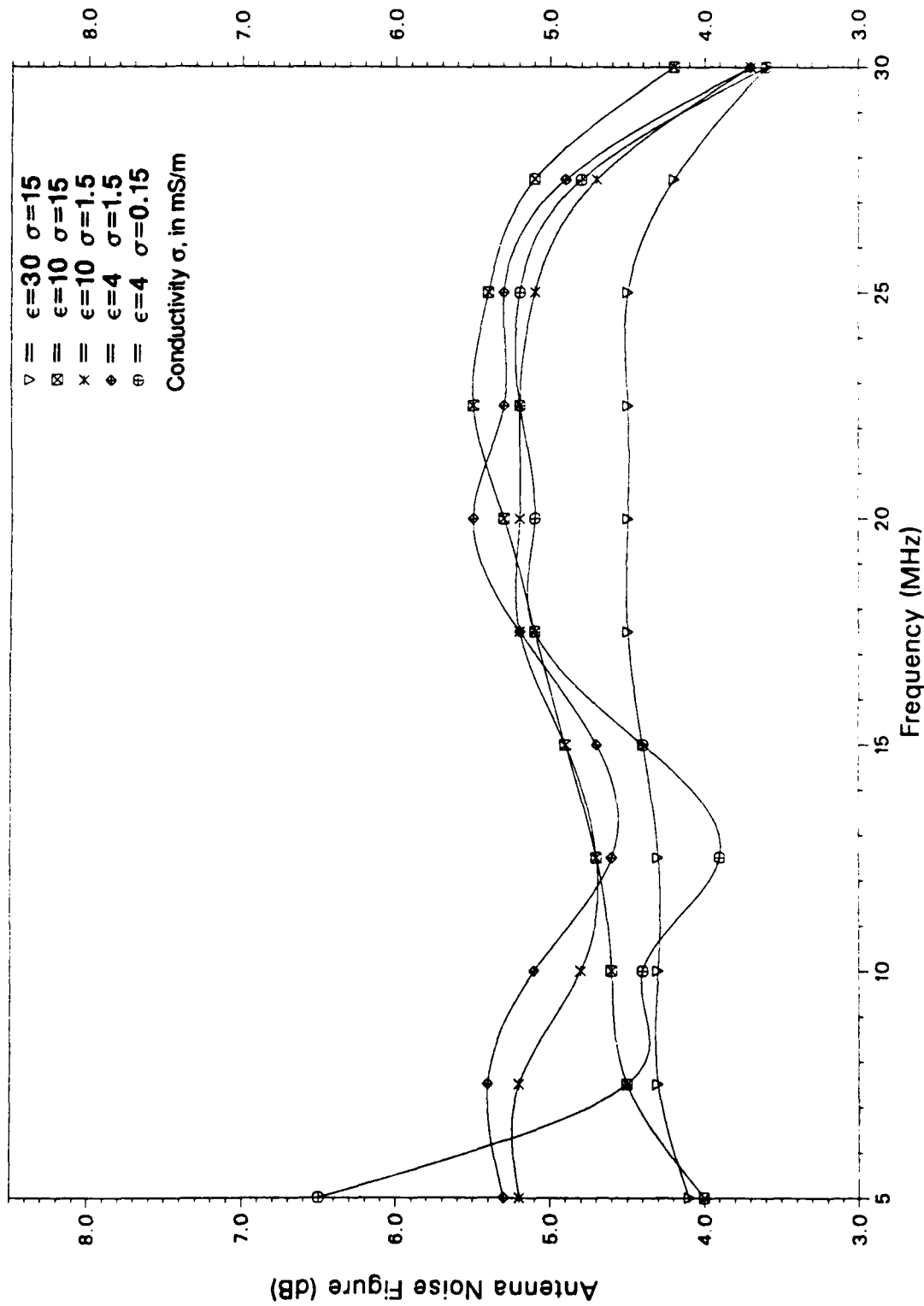


Figure 12. Antenna Noise Figure (Ohmic Loss) versus Frequency and Five Soil Conditions for 5.4 Meter High Monopole with 12 Meter Radius Ground Screen of 32 Radials

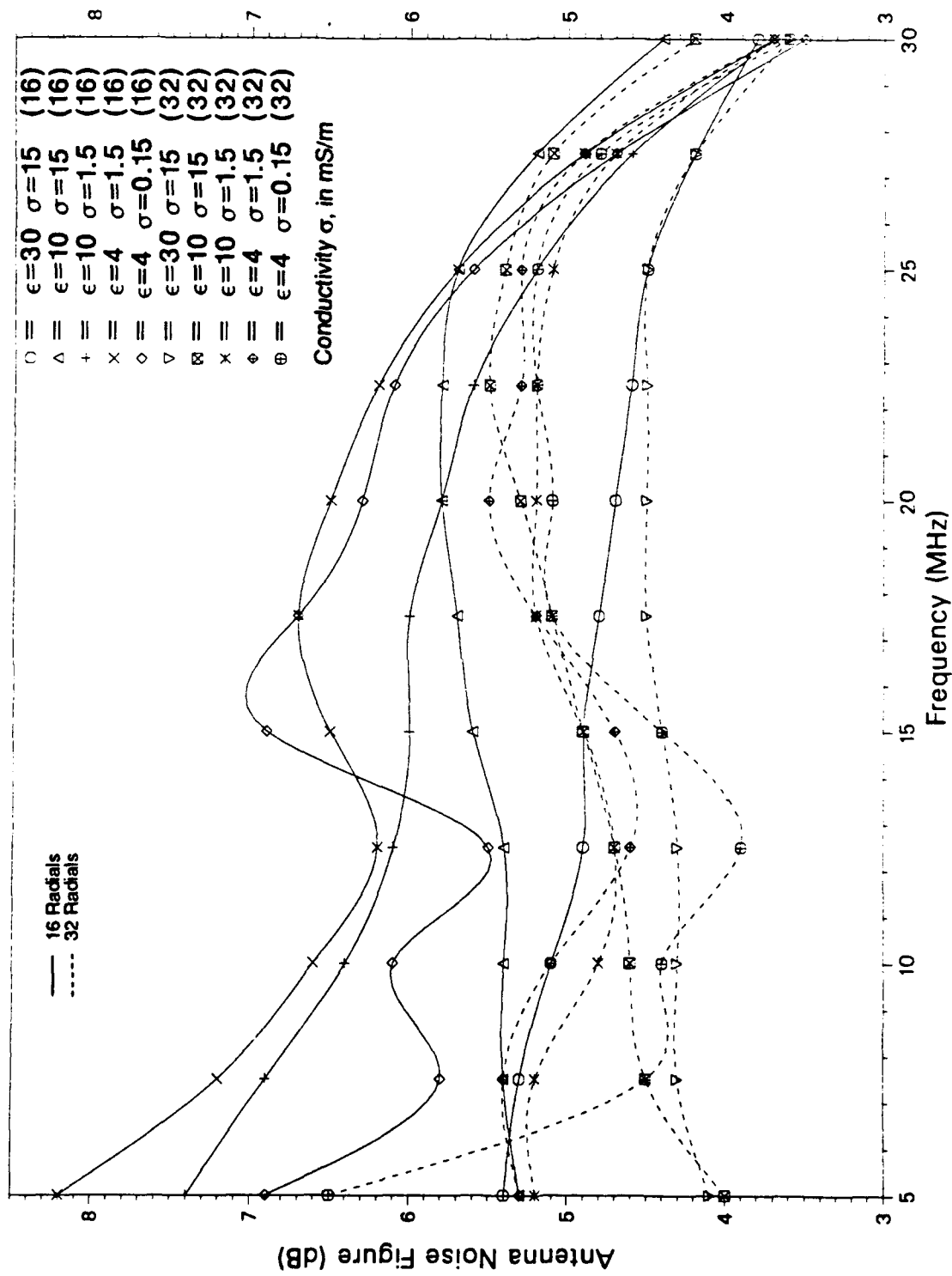


Figure 13. Antenna Noise Figure (Ohmic Loss) versus Frequency and Five Soil Conditions for 5.4 Meter High Monopole with 12 Meter Radius Ground Screen Having Either 16 or 32 Radials

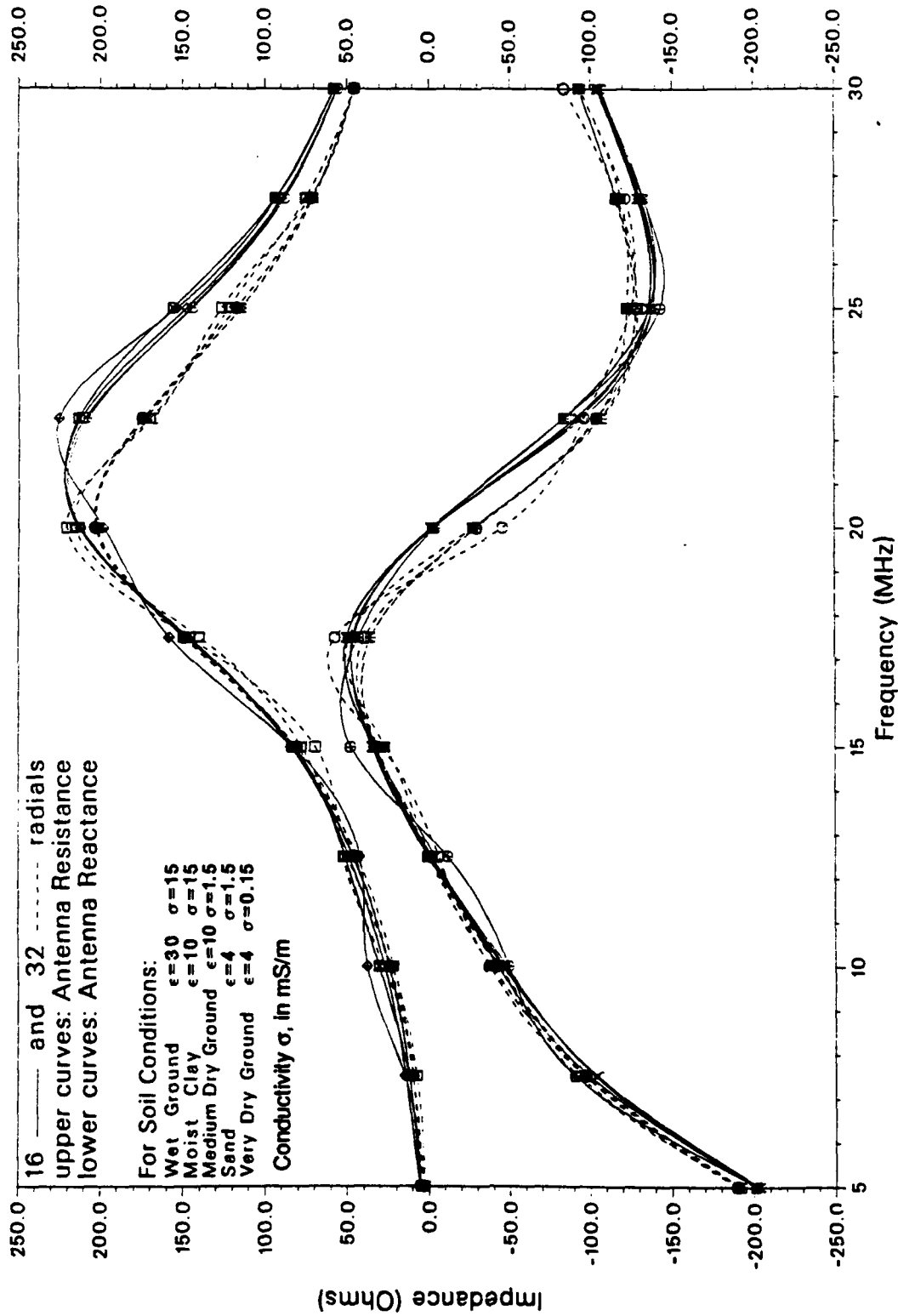


Figure 14. Antenna Input Resistance and Reactance versus Frequency and Five Ground Conditions for 5.4 Meter High Monopole with 12 Meter Radius Ground Screen Having Either 16 or 32 Radials

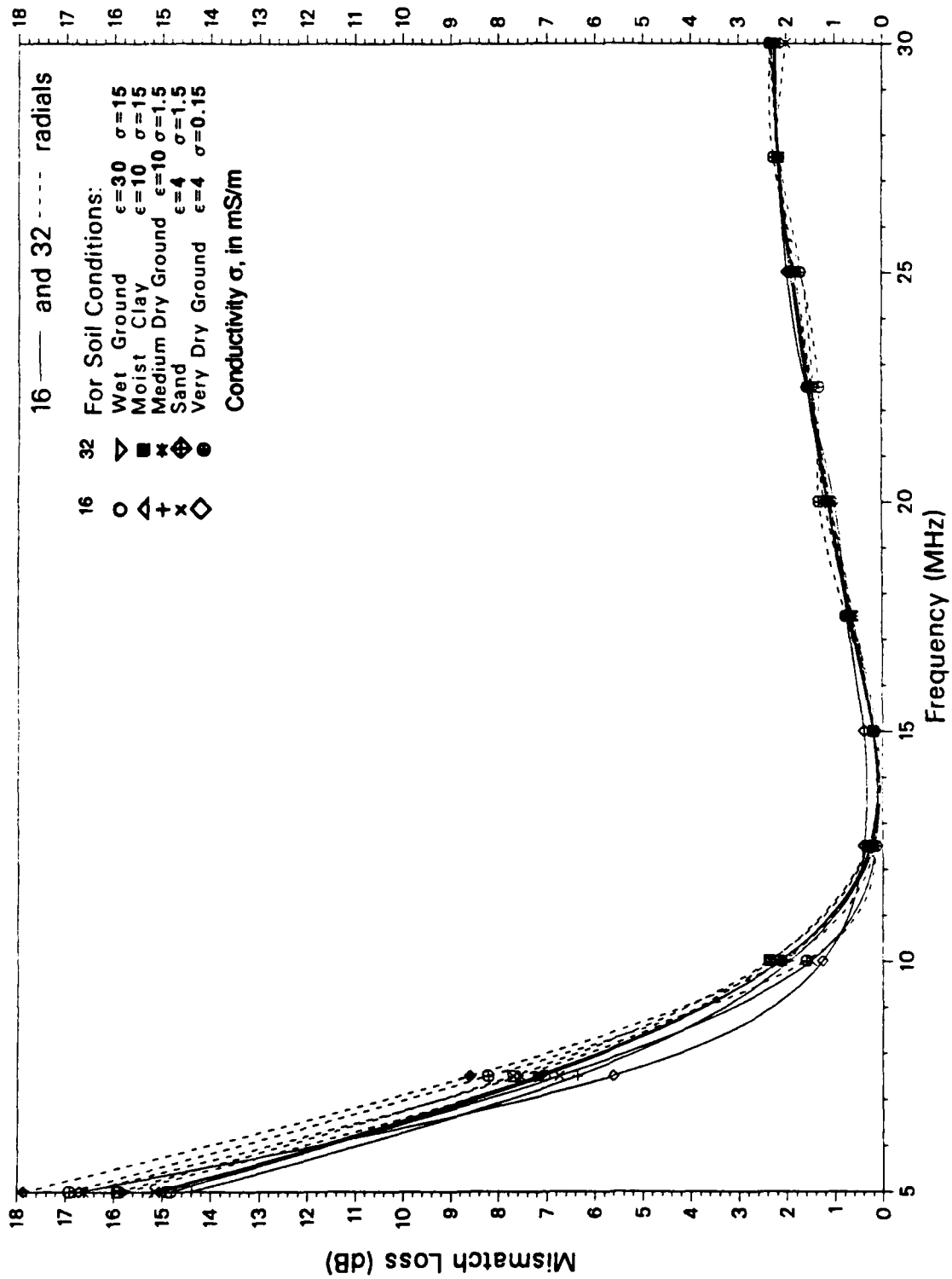


Figure 15. Cable Mismatch Loss versus Frequency and Five Soil Conditions for 75 ohm Coaxial Cable Feeding 5.4 Meter High Monopole with 12 Meter Radius Ground Screen Having Either 16 or 32 Radials

L3075

Table 5. Change in Noise Figure Sum ($L_c + L_{nm}$) in dB as Number of Radials of 12 Meter Radius Ground Screen is Increased from 16 to 32

For 5.4 Meter High Monopole

Frequency (MHz)	Soil Characteristics				
	Very Good	Good	Medium	Fair	Poor
	$\epsilon_r = 30, \sigma = 15 \text{ mS/m}$	$\epsilon_r = 10, \sigma = 15 \text{ mS/m}$	$\epsilon_r = 10, \sigma = 1.5 \text{ mS/m}$	$\epsilon_r = 4, \sigma = 1.5 \text{ mS/m}$	$\epsilon_r = 4, \sigma = 0.15 \text{ mS/m}$
5.0	-0.4	-0.4	0.0	-0.2	-0.2
7.5	-0.9	-0.4	-0.5	+0.1	+1.3
10.0	-0.6	-0.6	-1.4	-1.0	-1.4
12.5	-0.5	-0.6	-1.3	-1.6	-1.4
15.0	-0.5	-0.7	-1.1	-1.7	-2.7
12.5	-0.3	-0.7	-0.8	-1.6	-1.6
20.0	-0.3	-0.6	-0.6	-1.0	-0.9
22.5	-0.2	-0.4	-0.5	-1.0	-1.2
25.0	-0.1	-0.4	-0.2	-0.6	-0.7
27.5	0.0	-0.1	+0.1	0.0	+0.2
20.0	-0.1	-0.1	-0.3	+0.1	+0.2

IL3076-1

Table 6. Change in Noise Figure Sum ($L_c + L_{nm}$) in dB as Radius of 16 Radial Ground Screen Is Increased from 12 to 24 Meters For 5.4 Meter High Monopole

Frequency (MHz)	Soil Characteristics			
	Good	Medium	Fair	Poor
	$\epsilon_r = 10, \sigma = 15 \text{ mS/m}$	$\epsilon_r = 10, \sigma = 1.5 \text{ mS/m}$	$\epsilon_r = 4, \sigma = 1.5 \text{ mS/m}$	$\epsilon_r = 4, \sigma = 0.15 \text{ mS/m}$
5.0	-0.2	-0.6	-2.0	-4.7
10.0	0.0	+0.1	-0.4	+1.7
15.0	0.0	+0.2	+0.4	-0.2
20.0	0.0	+0.1	+0.2	+0.5
25.0	0.0	+0.1	+0.1	-0.1
30.0	0.0	0.0	-0.1	+0.1

Table 7. Change in Noise Figure Sum ($L_c + L_{nm}$) in dB as Radius of 32 Radial Ground Screen is Increased from 12 to 24 Meters For 5.4 Meter High Monopole

Frequency (MHz)	Soil Characteristics			
	Good	Medium	Fair	Poor
	$\epsilon_r = 10, \sigma = 15 \text{ mS/m}$	$\epsilon_r = 10, \sigma = 1.5 \text{ mS/m}$	$\epsilon_r = 4, \sigma = 1.5 \text{ mS/m}$	$\epsilon_r = 4, \sigma = 0.15 \text{ mS/m}$
5.0	-0.2	-1.6	-2.3	-4.8
10.0	-0.1	+0.6	+0.4	+1.3
15.0	+0.1	+0.4	+1.0	+1.2
20.0	+0.1	+0.3	+0.3	+0.6
25.0	+0.2	+0.2	+0.6	+0.6
30.0	0.0	+0.3	0.0	0.0

Table 8. Change in Noise Figure Sum ($L_c + L_{nm}$) in dB as Ground Screen is Changed from 16 Radials, 12 Meters Long to 32 Radials, 24 Meters Long For 5.4 Meter High Monopole

Frequency (MHz)	Soil Characteristics			
	Good	Medium	Fair	Poor
	$\epsilon_r = 10, \sigma = 15 \text{ mS/m}$	$\epsilon_r = 10, \sigma = 1.5 \text{ mS/m}$	$\epsilon_r = 4, \sigma = 1.5 \text{ mS/m}$	$\epsilon_r = 4, \sigma = 0.15 \text{ mS/m}$
5.0	-0.6	-1.6	-2.4	-5.0
10.0	-0.6	-0.9	-0.5	0.0
15.0	-0.6	-0.7	-0.9	-1.5
20.0	-0.5	-0.4	-0.7	-0.3
25.0	-0.2	0.0	0.0	-0.0
30.0	-0.1	+0.1	+0.1	+0.2

L3077

Table 9. Change in Noise Figure Sum ($L_c + L_{\text{min}}$) in dB as Burial Depth of 12 Meter Radius Ground Screen of 16 Radials is Increased from 0.178m (7 inches) to 0.305m (12 inches)

For 5.4 Meter High Monopole

Frequency (MHz)	Soil Characteristics				
	Very Good	Good	Medium	Fair	Poor
	$\epsilon_r = 30, \sigma = 15 \text{ mS/m}$	$\epsilon_r = 10, \sigma = 15 \text{ mS/m}$	$\epsilon_r = 10, \sigma = 1.5 \text{ mS/m}$	$\epsilon_r = 4, \sigma = 1.5 \text{ mS/m}$	$\epsilon_r = 4, \sigma = 0.15 \text{ mS/m}$
5.0	0.0	-0.1	-0.1	-0.2	-0.2
10.0	-0.1	+0.3	0.0	-0.1	0.0
15.0	+0.3	+0.3	+0.4	+0.4	+0.6
20.0	+0.3	+0.3	+0.4	+0.3	+0.4
25.0	+0.1	+0.2	+0.2	+0.2	+0.2
30.0	0.0	-0.1	-0.1	-0.2	-0.3

Table 10. Change in Noise Figure Sum ($L_c + L_{\text{min}}$) in dB as Base of Monopole Feed Section is Raised from 0.0 to 0.2 Meter Above Ground Surface

For 5.4 Meter High Reference Monopole with 12 Meter Radius Reference Ground Screen of 16 Radials

Frequency (MHz)	Soil Characteristics				
	Very Good	Good	Medium	Fair	Poor
	$\epsilon_r = 30, \sigma = 15 \text{ mS/m}$	$\epsilon_r = 10, \sigma = 15 \text{ mS/m}$	$\epsilon_r = 10, \sigma = 1.5 \text{ mS/m}$	$\epsilon_r = 4, \sigma = 1.5 \text{ mS/m}$	$\epsilon_r = 4, \sigma = 0.15 \text{ mS/m}$
5.0	0.0	-0.1	0.0	0.0	+0.2
10.0	-0.1	-0.4	-0.2	0.0	0.0
15.0	+0.1	+0.1	+0.2	+0.2	+0.3
20.0	-0.1	+0.1	+0.2	+0.2	+0.2
25.0	0.0	0.0	+0.1	+0.1	+0.2
0.0	-0.3	-0.2	-0.1	0.0	0.0

section a distance of 0.2 m above the surface of the ground (approximately equal to the height of the section), produces a negligibly small decrease in performance. Additional tables of antenna efficiency, noise figure, impedance, and cable mismatch loss are given in Volume 2—Appendices.

4.1.3 Cable Attenuation Loss and Receiver Noise Figure

The cable attenuation loss is defined in the conventional exponential form by equation (40), and represents the resistive power loss suffered by a simple traveling wave on a matched transmission line. The objective was to minimize the loss contributed by the long cable runs, while satisfactorily addressing the important considerations of physical handling, burial, and reasonable cost-per-unit length. Consequently, the decision was made to use proven economical high-volume 75 ohm aluminum coaxial cable widely used by the cable television industry.

Specifically, the selected cable is a Times Fiber Communications, Inc. TX840JBA, 0.84 inch diameter, 75 ohm jacketed aluminum direct burial coaxial cable, with steel armoring and polyisobutylene flooding compound. The specified attenuation rates of 0.09 dB/100 ft maximum at 5 MHz and 0.24 dB/100 ft maximum at 30 MHz translates into the cable attenuation losses tabulated in table 11 and plotted in figure 16. Cable loss values are presented for four cable lengths: maximum, 4,454.2 ft (1,357.6 m); reference, 4,000 ft (1,219.2 m); average 2,536.4 ft (773.1 m); and minimum, 660.4 ft (201.3 m). As indicated, cable losses become moderately large for the longest cables at the high end of the frequency band.

The receiver noise figure is specified as constant and equal to 8 dB across the 5 MHz to 30 MHz frequency band of interest for a 50 ohm source impedance. This is based on the performance of the MITRE-developed experimental wideband HF receiver. A 75-to-50 ohm impedance step-down transformer at the receiver end of the coaxial cable produces the desired 50 ohm source impedance to the receiver for a matched 75 ohm feed cable (long cable condition). A production version of this receiver has been manufactured, to MITRE specification, by a division of Harris Corporation for the Texas application. Any noise figure improvements achieved in the production version of this receiver will correspondingly reduce the system internal noise figure values predicted in this analysis.¹

Predictions of receiver noise figure performance as a function of source impedance values presented by mismatched feed cables can be obtained after the receiver empirical constants, r_n and Y_{no} , have also been measured. However, as discussed in section 2.1.1.2, inclusion of receiver noise factor variation as a function of source impedance, as defined by equation (30), should be accompanied by use of the more exact transmission line loss factor equation (28) that includes the $[1 - |\Gamma|^2 \exp(-4\alpha d)]$ term in the numerator.

¹ Test data from the 110 production receivers shows a relatively consistent value of 6 dB for these receivers.

IL3079-1

**Table 11. Cable Attenuation Loss (dB) versus Frequency for Four Cable Lengths
(for Times Fiber TX840JBA 75 ohm Coaxial Cable)**

Frequency (MHz)	Cable Lengths			
	Maximum	Reference	Average	Minimum
	4,454.2 ft, 1,357.6m	4,000 Ft, 1,219.2m	2,536.4 ft, 773.1m	660.4 ft, 201.3m
5.0	4.3	3.9	2.5	0.64
7.5	5.3	4.8	3.0	0.74
10.0	6.1	5.5	3.5	0.91
12.5	6.9	6.2	3.9	1.02
15.0	7.6	6.8	4.3	1.12
17.5	8.1	7.3	4.6	1.21
20.0	8.7	7.8	4.9	1.29
22.5	9.2	8.3	5.3	1.37
25.0	9.8	8.8	5.6	1.45
27.5	10.2	9.2	5.8	1.52
30.0	10.7	9.6	6.1	1.63

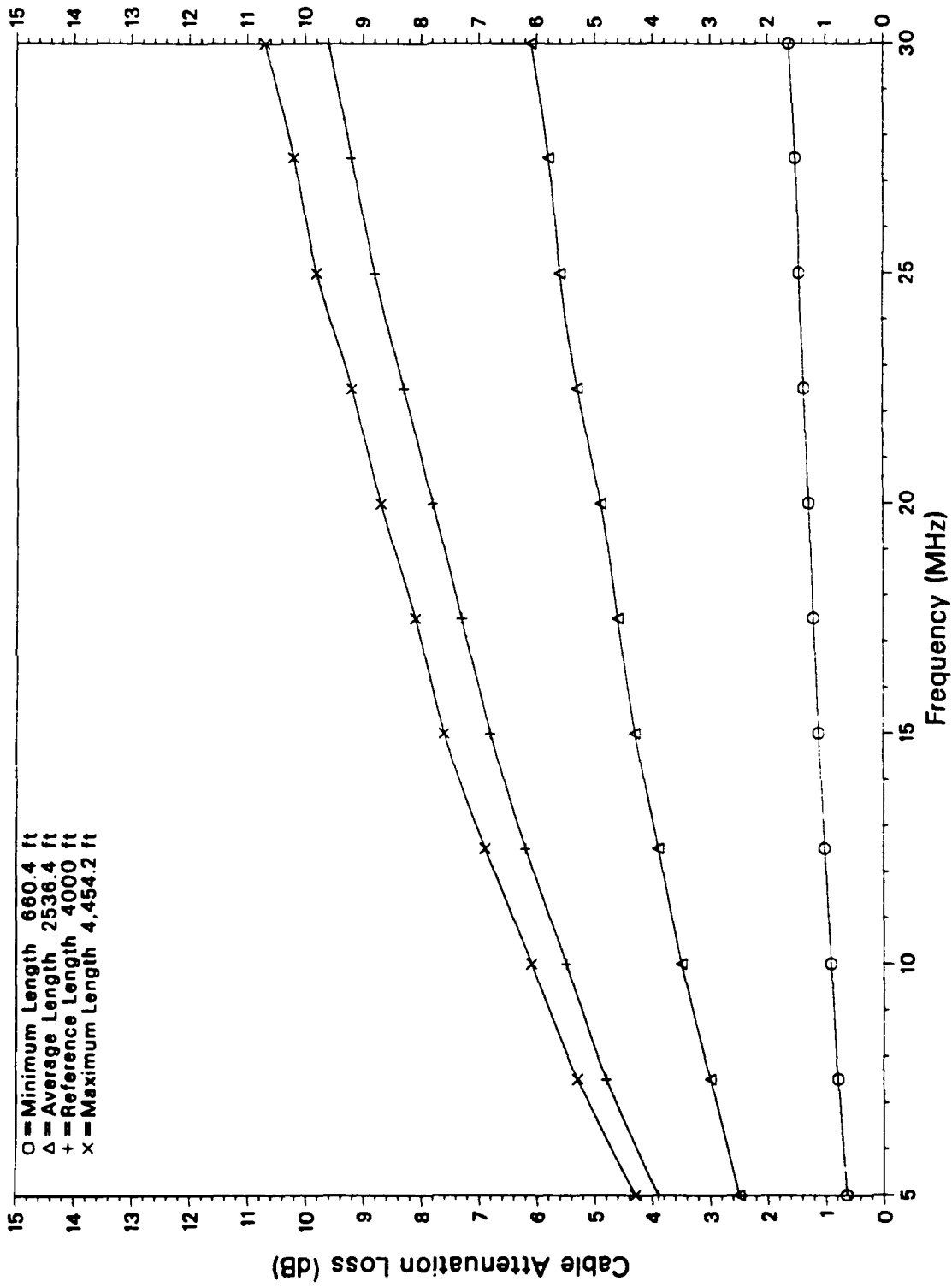


Figure 16. Cable Attenuation Loss versus Frequency for Four Cable Lengths

4.1.4 System Internal Noise Figure

Figure 17 presents the system internal noise figure, F_S , in a way that dramatically illustrates the cumulative contributions of the four noise figure components in equation (37). The curves are for a reference configuration, 5.4 m monopole antenna with a 16 radial, 12 m radius ground screen, located on sandy soil ($\epsilon_r = 4$, $\sigma = 1.5$ millisiemens/m), representative of the Texas array site, and connected to a 4454 ft (1,358 m) maximum length coaxial feed cable terminated with a receiver having a constant noise figure of 8 dB. The dominating effect below about 10 MHz is mismatch loss, which causes a significant rise in noise figure as the monopole height becomes small compared to wavelength. If necessary, a substantial portion of this mismatch loss can be alleviated by inserting a matching network at the base of the monopole. However, the matching network's ohmic loss contribution to the system internal noise figure must then be included, as indicated in equations (22) and (24). Corresponding plots for the other four ground conditions and the 32 radial ground screen configuration are given in Volume 2—Appendices.

Figures 18 and 19 reveal the favorable insensitivity of system internal noise figure to variations in soil condition for the case of a 5.4 m monopole using a 12 m radius ground screen with either 16 or 32 radials, respectively. The figures also support the results of table 5, by showing that little is gained by doubling the number of radials to 32. In addition, by including both maximum and minimum cable lengths, the plots provide realistic upper bounds on the expected variations in system internal noise figure between the 96 different antenna-cable-receiver combinations of the array. More accurate estimates of system internal noise figure can be obtained if desired, particularly at the lower frequencies for antenna/receiver pairs connected by relatively short cables, by following the suggestions given in section 2.1.1.2.

4.1.5 Antenna Directivity

A series of polar plots were generated, using equation (35), to examine antenna directivity behavior as a function of frequency, soil condition, and number of ground screen radials. Figures 20 through 23 were selected to illustrate representative behavior; a complete set of plots is presented in Volume 2—Appendices. The figures plot directivity in dBi (relative to an isotropic antenna) along the radial coordinate versus either the elevation angle measured from the horizontal axis (horizon) or the polar angle measured from the vertical axis (zenith).

Figures 20 and 21 are polar plots for the 5.4 m reference monopole having a 12 m radius ground screen, with either 16 or 32 radials, respectively, at the representative frequency of 10 MHz. They illustrate the favorable weak dependence of directivity on soil conditions and the nearly identical results for 16 and 32 radials. Elevation angles below about 30° to 40° are the important ones for OTH HF applications. In this angular range, variations in soil condition cause variations in directivity ranging from about 0 dB to 3 dB. In the direction of peak directivity, between about 20° to 30° elevation, the variation is reduced to nearly 0 dB. For the balance of the angular span between 0° and 30° to 40°, the directivity at a given elevation angle can vary gradually, over approximately a 3 dB range, as the soil becomes less conductive.

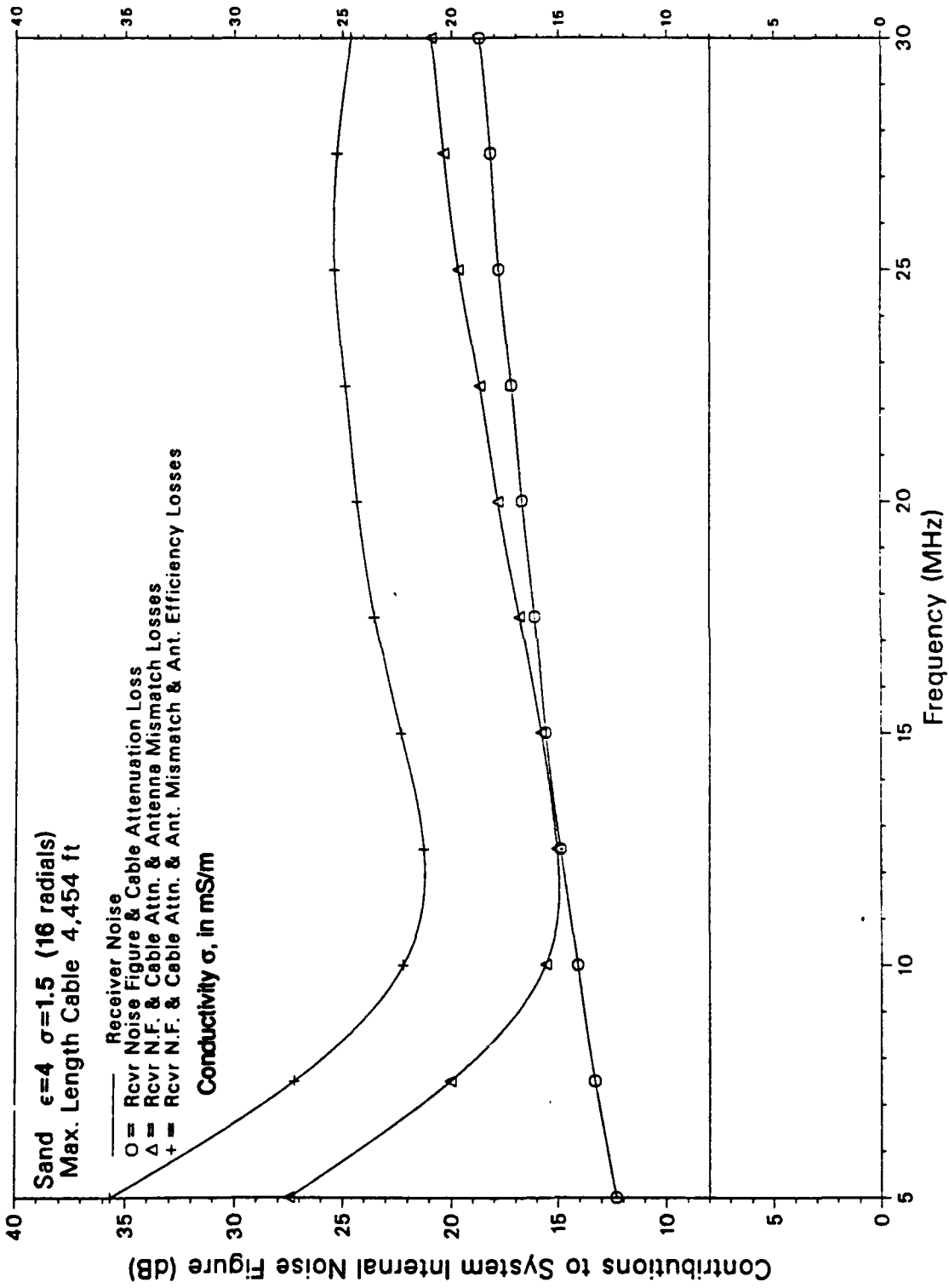


Figure 17. System Internal Noise Figure Cumulative Contributions for Case of Sandy Soil and Maximum Length Cable for 5.4 Meter High Monopole with 12 Meter Radius Ground Screen of 16 Radials

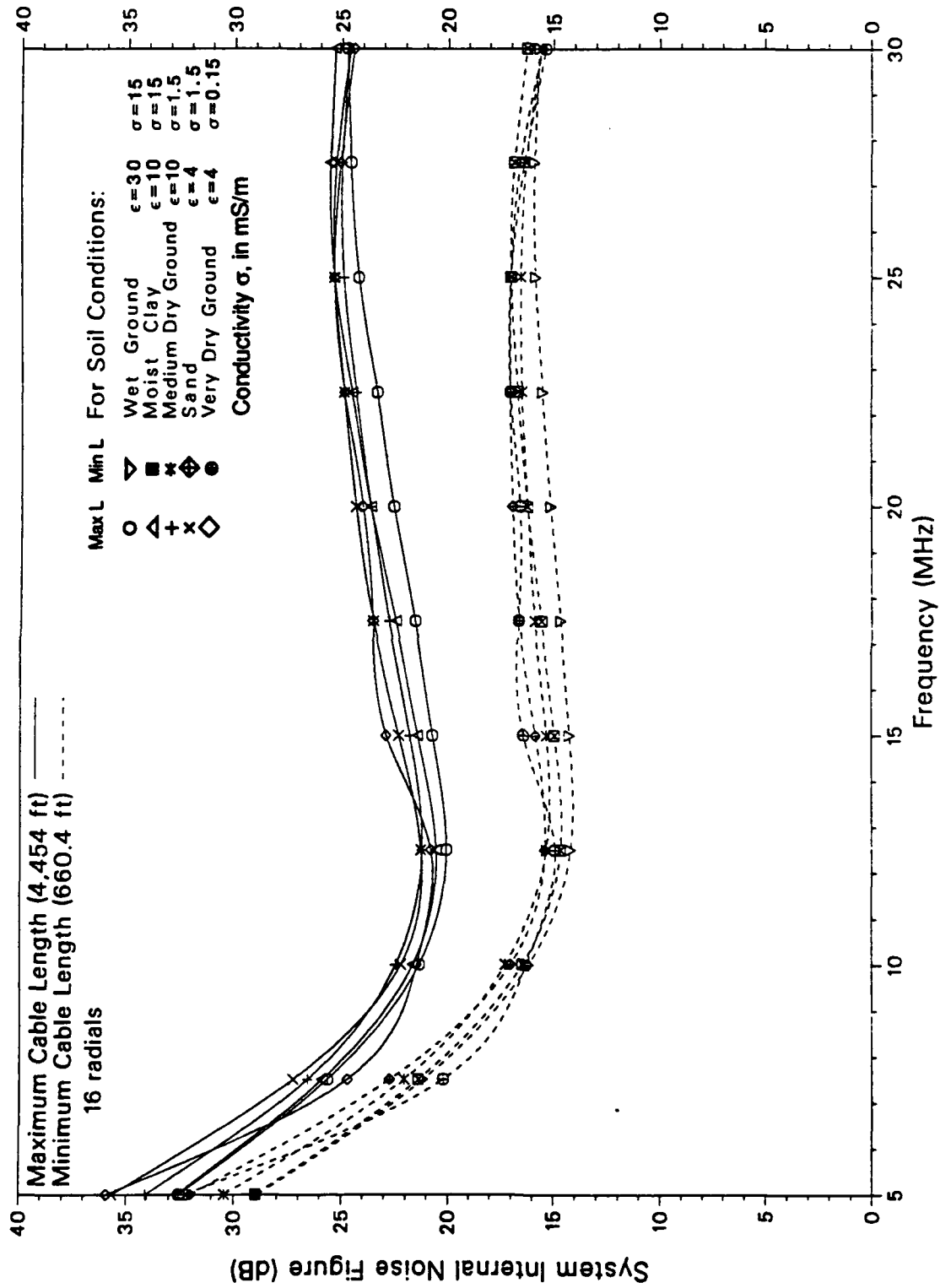


Figure 18. System Internal Noise Figures versus Frequency, Soil Condition, and Maximum and Minimum Cable Lengths for 5.4 Meter High Monopole Antenna with 12 Meter Radius Ground Screen of 16 Radials

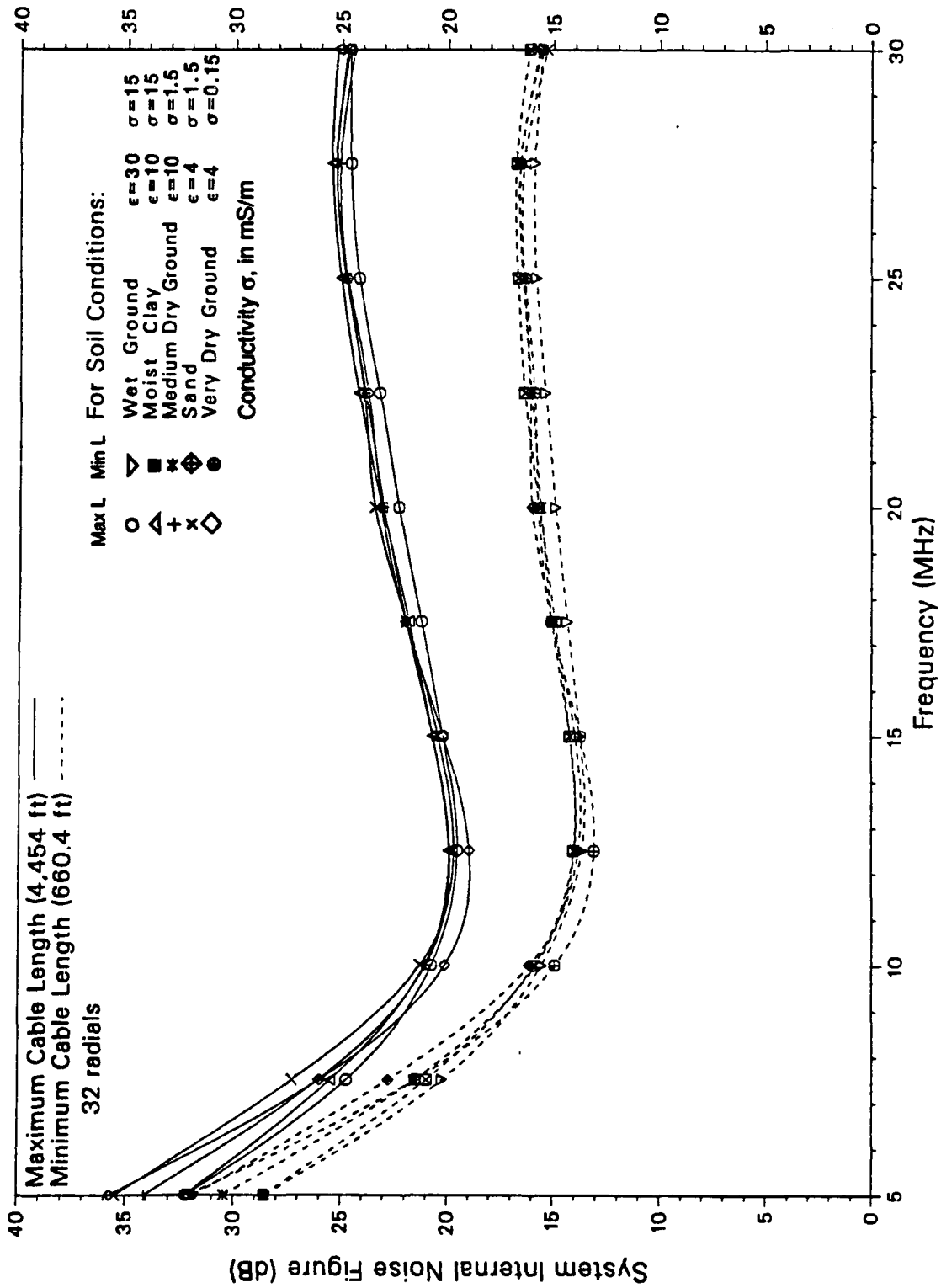


Figure 19. System Internal Noise Figure versus Frequency, Soil Condition, and Maximum and Minimum Cable Lengths for 5.4 Meter High Monopole with 12 Meter Radius Ground Screen of 32 Radials

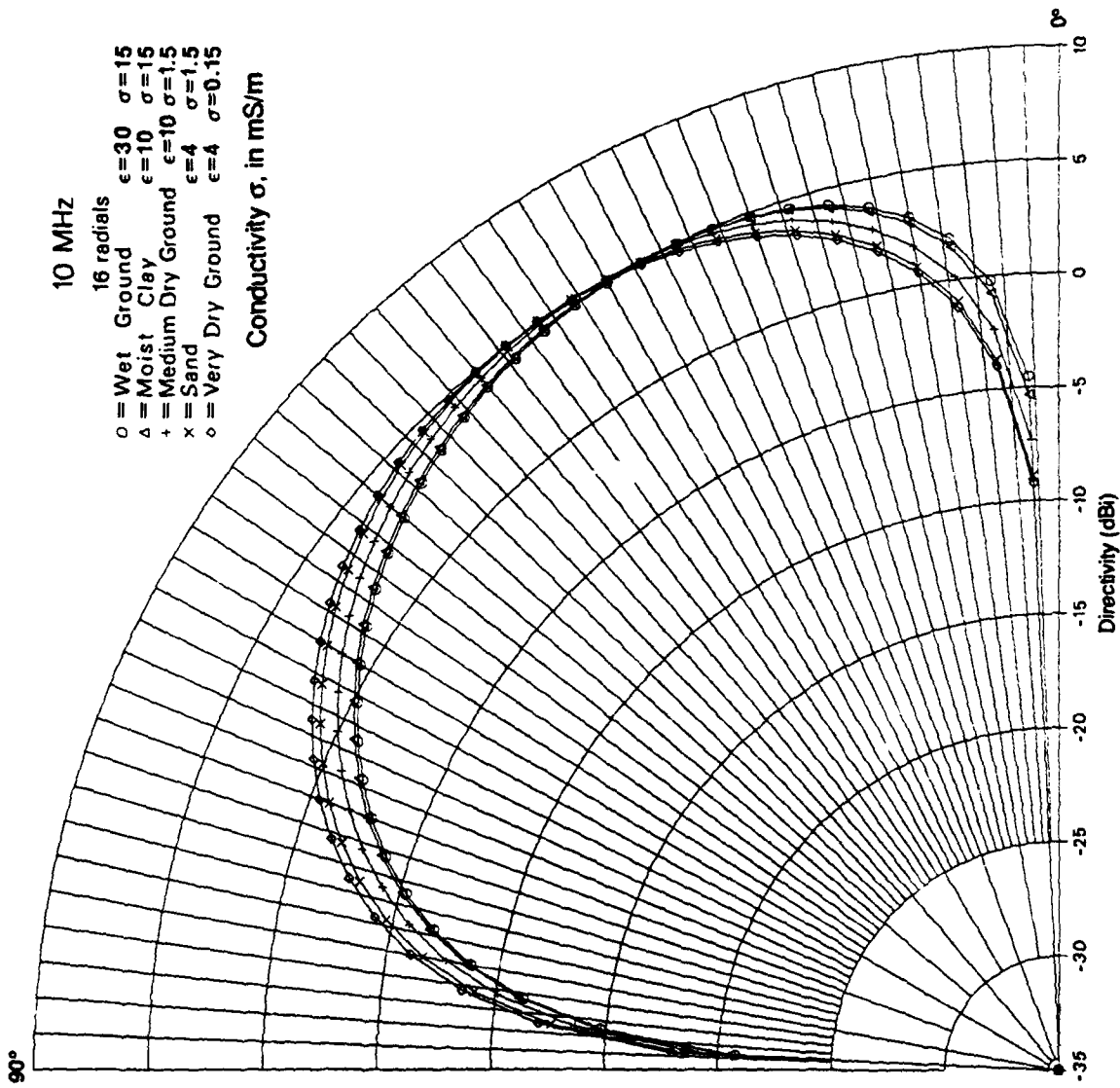


Figure 20. Antenna Directivity versus Elevation Angle and Five Soil Conditions at Frequency of 10 MHz, for 5.4 Meter High Monopole with 12 Meters Radius Ground Screen of 16 Radials

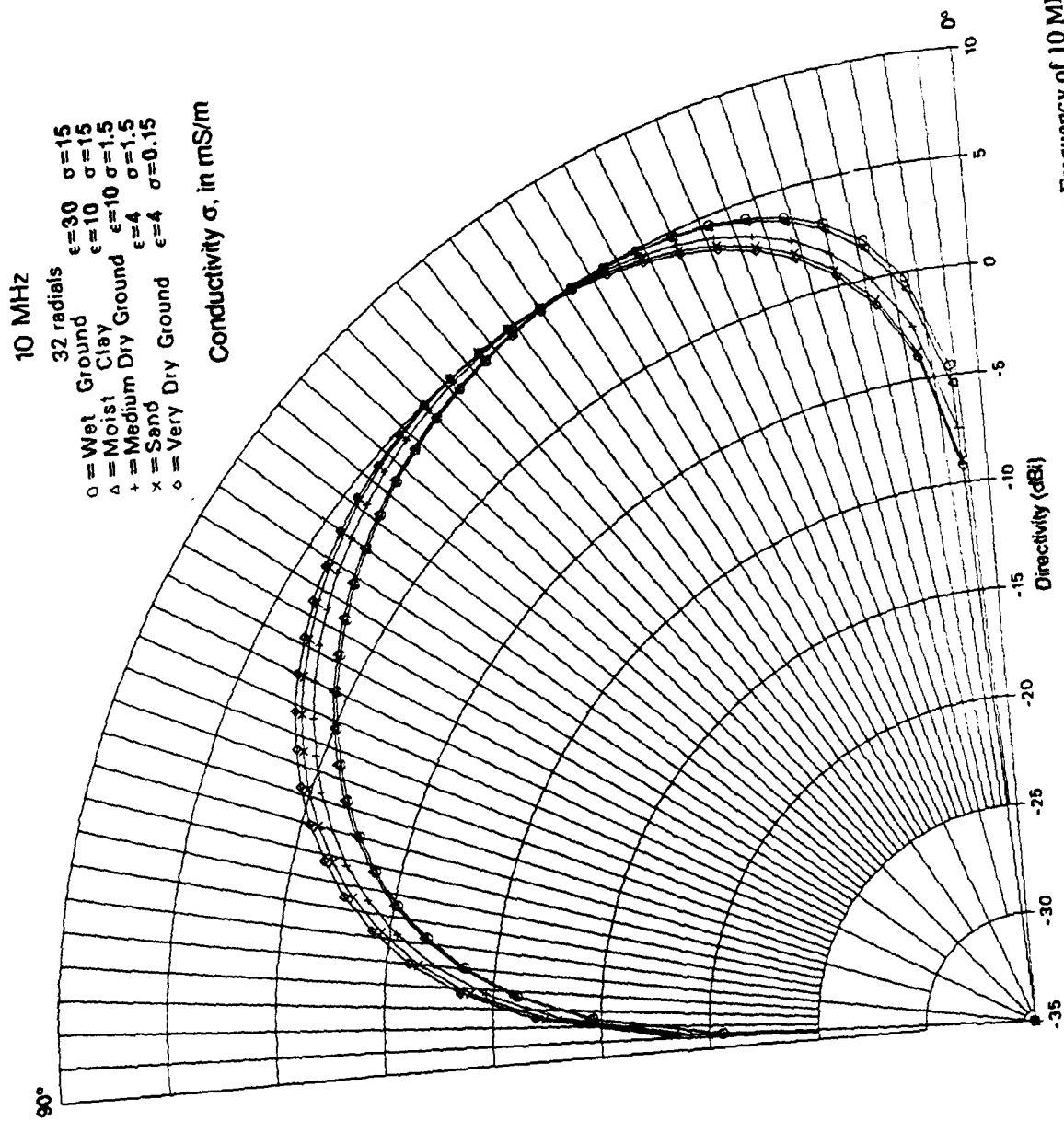


Figure 21. Antenna Directivity versus Elevation Angle and Five Soil Conditions at Frequency of 10 MHz, for 5.4 Meter High Monopole with 12 Meters Radius Ground Screen of 32 Radials

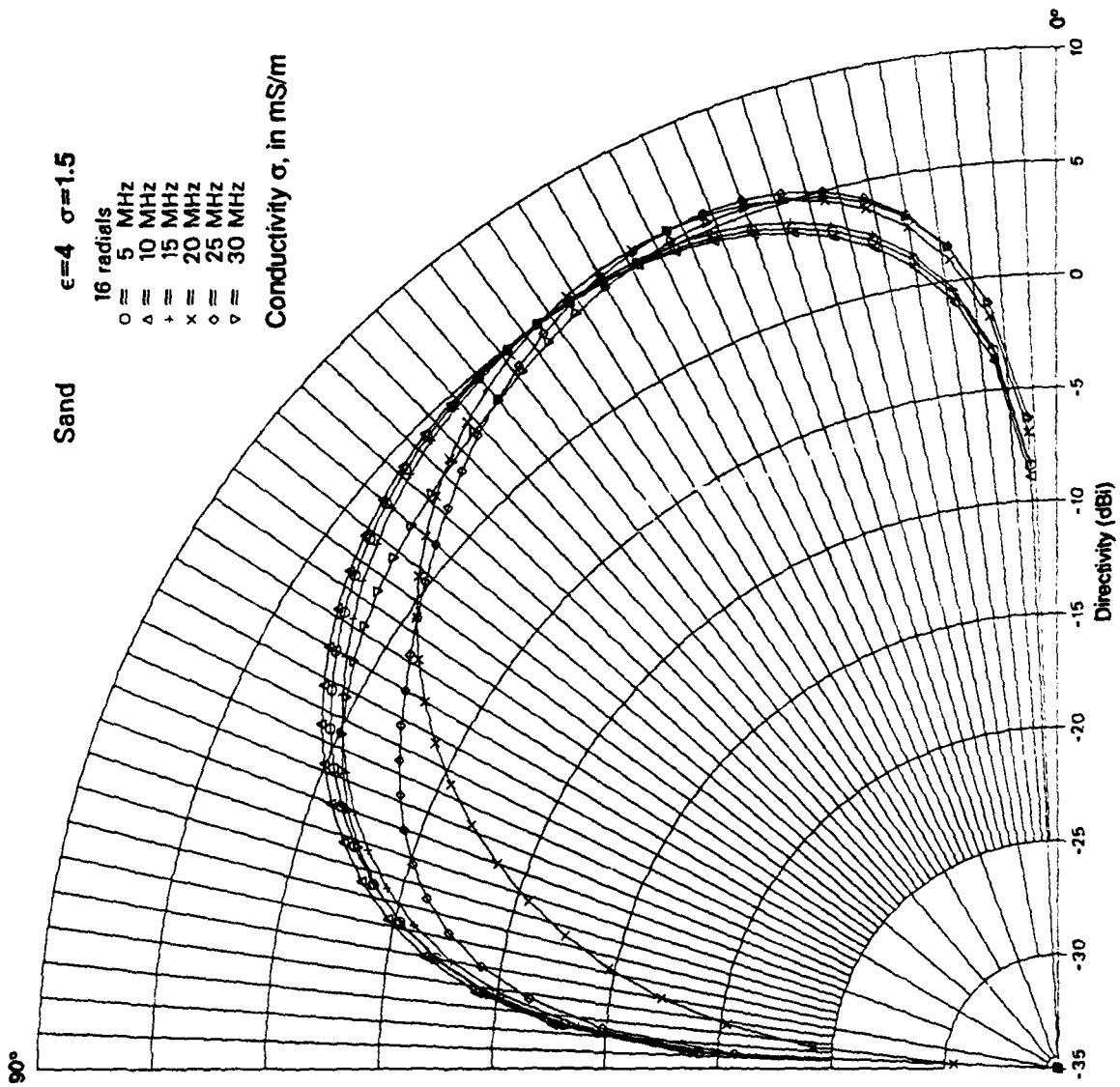


Figure 22. Antenna Directivity versus Elevation Angle and Frequency for 5.4 Meter High Monopole with 12 Meter Radius Ground Screen of 16 Radials for a Sandy Soil Condition

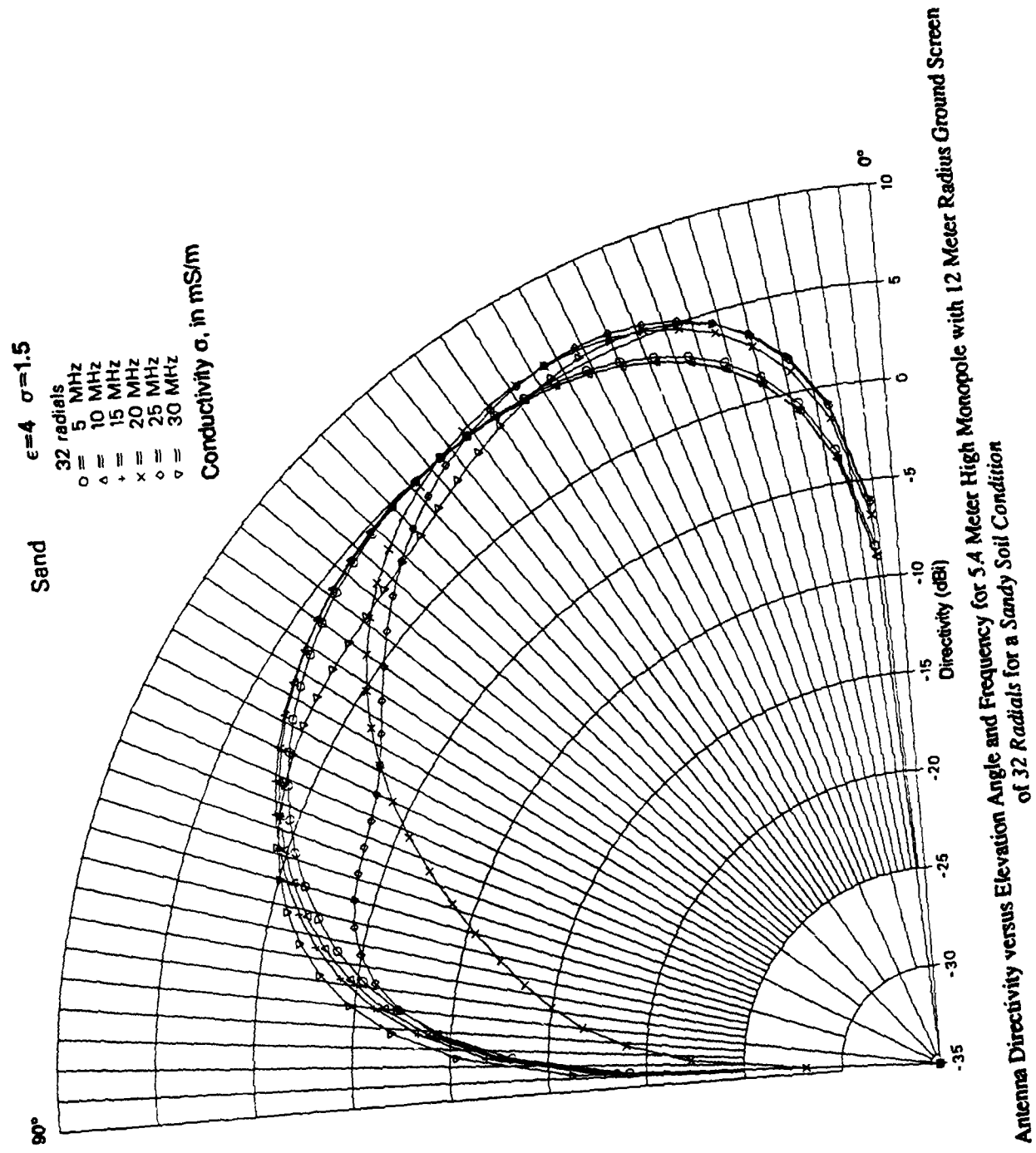


Figure 23. Antenna Directivity versus Elevation Angle and Frequency for 5.4 Meter High Monopole with 12 Meter Radius Ground Screen of 32 Radials for a Sandy Soil Condition

Similar behavior is observed in figures 22 and 23, which show the dependence of directivity on frequency for the same monopole, with a 16 or 32 radial ground screen, respectively, for a representative sandy soil condition. The figures illustrate the relatively weak dependence of directivity on frequency for elevation angles below 30° to 40°. Above this angular range, the dependence of directivity on both frequency and the number of radials is stronger, but of little consequence to the applications of interest. Below 30° to 40° elevation, the directivity can change by 1 dB to 3 dB over the 5 MHz to 30 MHz band. In the vicinity of peak directivity, between about 20° to 30° elevation, the variation is constrained to approximately 1 dB. For the balance of the angular span between 0° and 30° to 40°, the directivity at a given elevation angle can generally increase and decrease over approximately a 3 dB range, depending on the specific soil condition, as the frequency increases from 5 MHz to 30 MHz.

4.2 FINAL 6.3 METER MONOPOLE ANTENNA AND GROUND SCREEN CONFIGURATION

The effect of monopole height on system internal noise figure and antenna directivity was also examined to guide if necessary the selection of a monopole antenna tower other than the baseline 5.4 m monopole structure. Cost and some logistics considerations eventually led to the selection of a somewhat taller, less expensive monopole tower.

Table 12 tabulates the changes relative to the 5.4 m monopole case, in the noise figure sum ($L_c + L_{nm}$) at three frequencies, 5 MHz, 17.5 MHz, and 30 MHz, spanning the 5 MHz to 30 MHz band, for four different monopole antenna heights. The table indicates that the primary, and similar, benefits of reduced noise figure occur at the upper and lower ends of the band, and they remain relatively independent of soil condition. All results are for the chosen ground screen consisting of 16 radials, each 12 m in length. The attainable noise figure improvements at 5 MHz and 30 MHz, relative to the 5.4 m high case, range from slightly under 2 dB for a 6.0 m monopole to slightly greater than 4 dB for a 7.0 m monopole.

In addition, the antenna directivity was examined at the upper end of the frequency band, to determine whether increasing the monopole height relative to wavelength produced undesirable pattern lobing. Figures 24 to 28 present plots of the antenna directivity versus soil condition at the highest expected frequency of 30 MHz. Examination of the figures reveals that the directivity patterns at 30 MHz remain well behaved, but suffer small to moderate decreases in directivity in the primary elevation angle region below 30° to 40°. However, review of table 12 indicates that these decreases in directivity are fortunately offset by compensating decreases (improvements) in system internal noise figure. In some cases, noise figure improvements can exceed decreases in directivity, especially at the low end of the band, leading to improved overall performance.

A 6.3 m high monopole tower was finally selected over the competing 5.4 m high tower, based on cost, logistics, and performance factors. The 6.3 m monopole is a ROHN self-supporting tower consisting of two 10-ft triangular tower sections mounted to a 20 cm base feed section. Summary performance results for the final configuration of a 6.3 m monopole

L3080

Table 12. Change in Noise Figure Sum ($L_c + L_{nm}$) in dB as Monopole Height is Increased from Reference Monopole Height of 5.4 Meters to Heights of 6.0, 6.3, 6.5, and 7.0 Meters
For 12 Meter Radius Reference Ground Screen of 16 Radials

Frequency (MHz)	Soil Characteristics				
	Very Good	Good	Medium	Fair	Poor
	$\epsilon_r = 30, \sigma = 15 \text{ mS/m}$	$\epsilon_r = 10, \sigma = 15 \text{ mS/m}$	$\epsilon_r = 10, \sigma = 1.5 \text{ mS/m}$	$\epsilon_r = 4, \sigma = 1.5 \text{ mS/m}$	$\epsilon_r = 4, \sigma = 0.15 \text{ mS/m}$
Height = 6.0m					
5.0	-1.7	-1.8	-1.8	-1.9	-1.8
17.5	+0.4	+0.5	+0.3	+0.3	+0.3
30.0	-1.1	-1.8	-1.5	-1.9	-1.9
Height = 6.3m					
5.0	-2.6	-2.6	-2.6	-2.6	-2.6
17.5	+0.6	+0.7	+0.4	+0.4	+0.4
30.0	-2.0	-2.8	-2.3	-2.7	-2.5
Height = 6.5m					
5.0	-3.1	-3.2	-3.0	-3.1	-3.0
17.5	+0.7	+0.8	+0.5	+0.6	+0.4
30.0	-2.5	-2.5	-2.9	-3.3	-3.1
Height = 7.0m					
5.0	-4.4	-4.3	-4.3	-4.4	-4.4
17.5	-1.0	+1.2	+0.7	+0.8	+0.6
30.0	-3.6	-4.5	-3.6	-4.0	-3.7

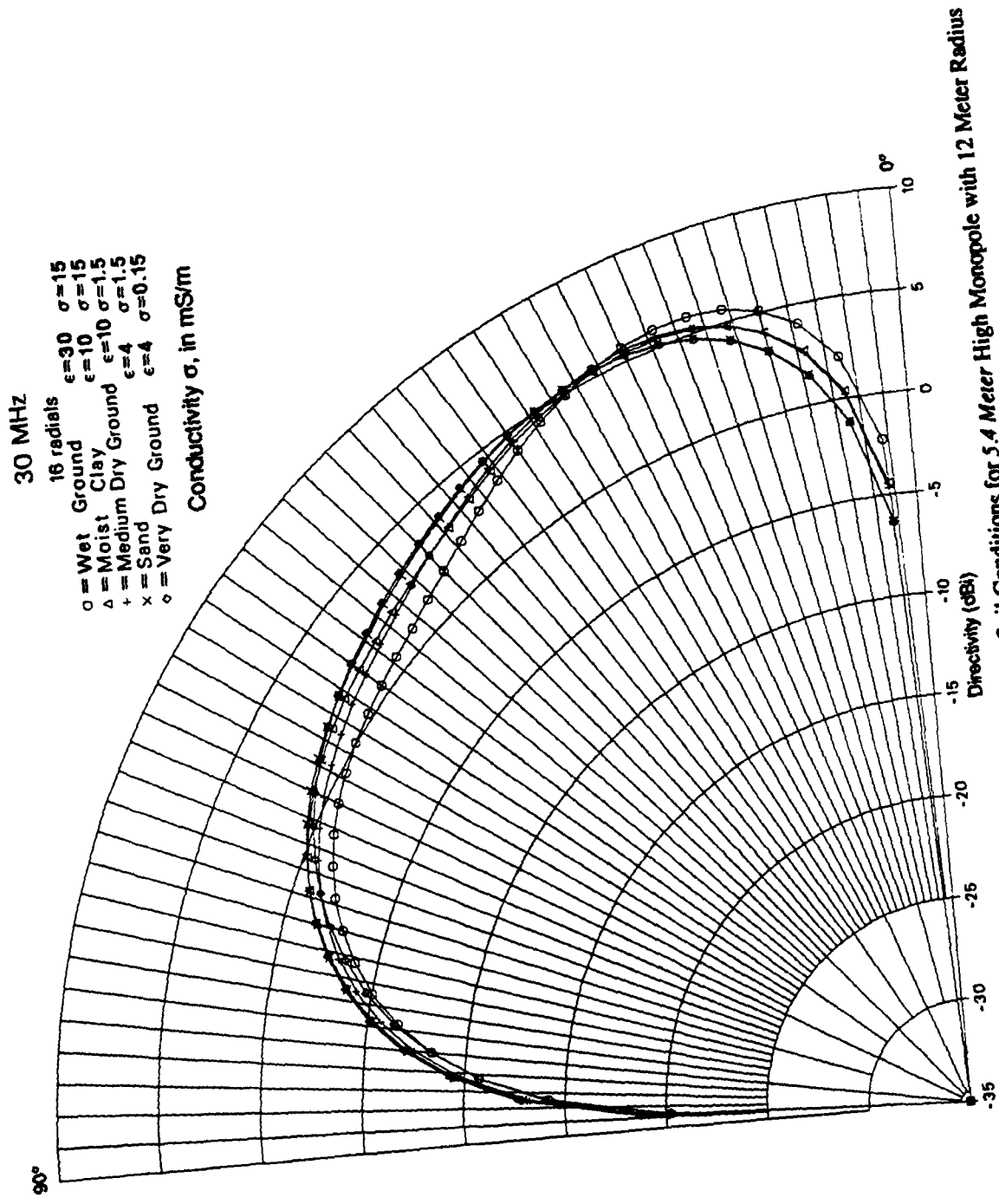


Figure 24. Antenna Directivity versus Elevation Angle and Five Soil Conditions for 5.4 Meter High Monopole with 12 Meter Radius Ground Screen of 16 Radials at Frequency of 30MHz

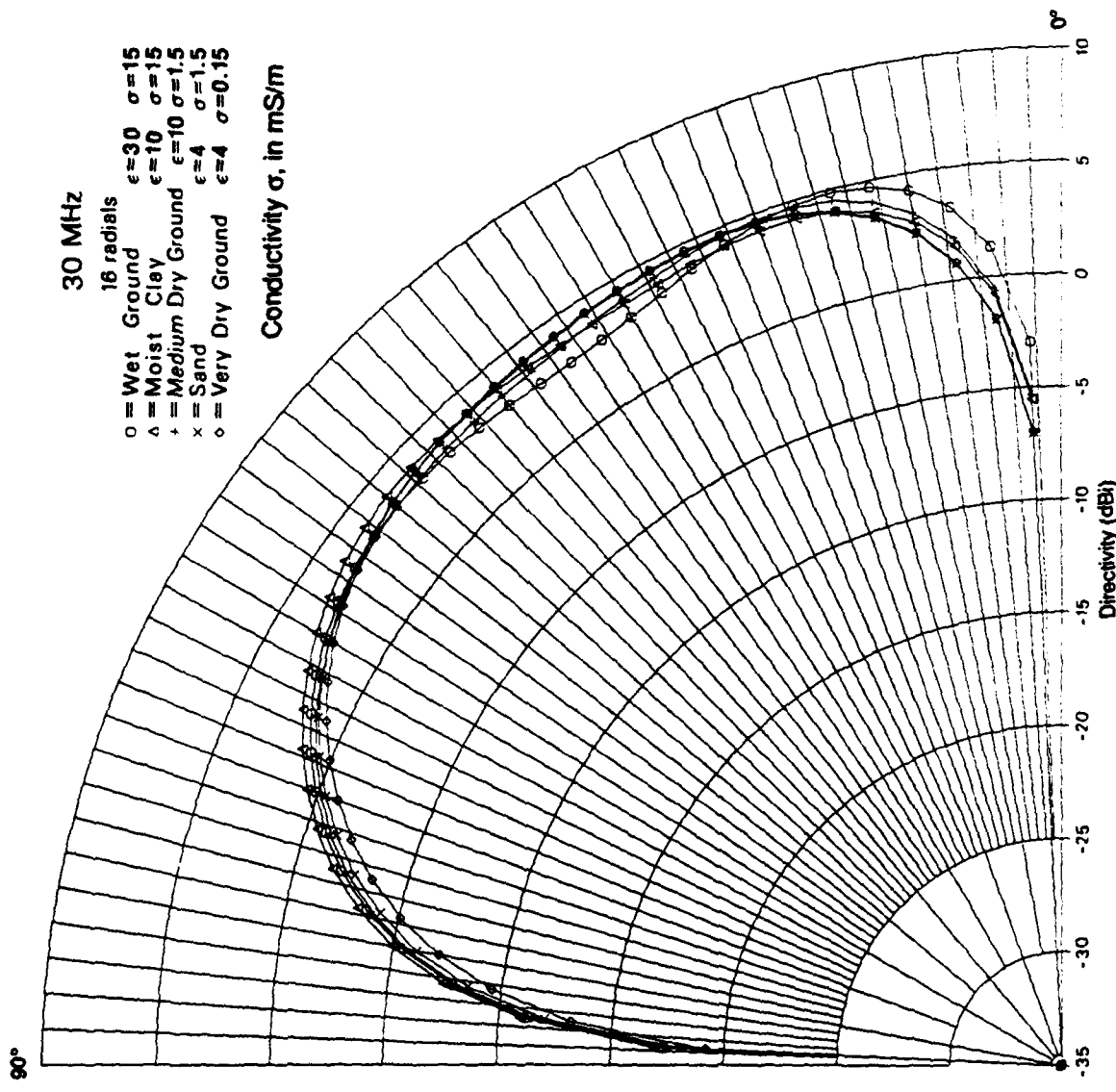
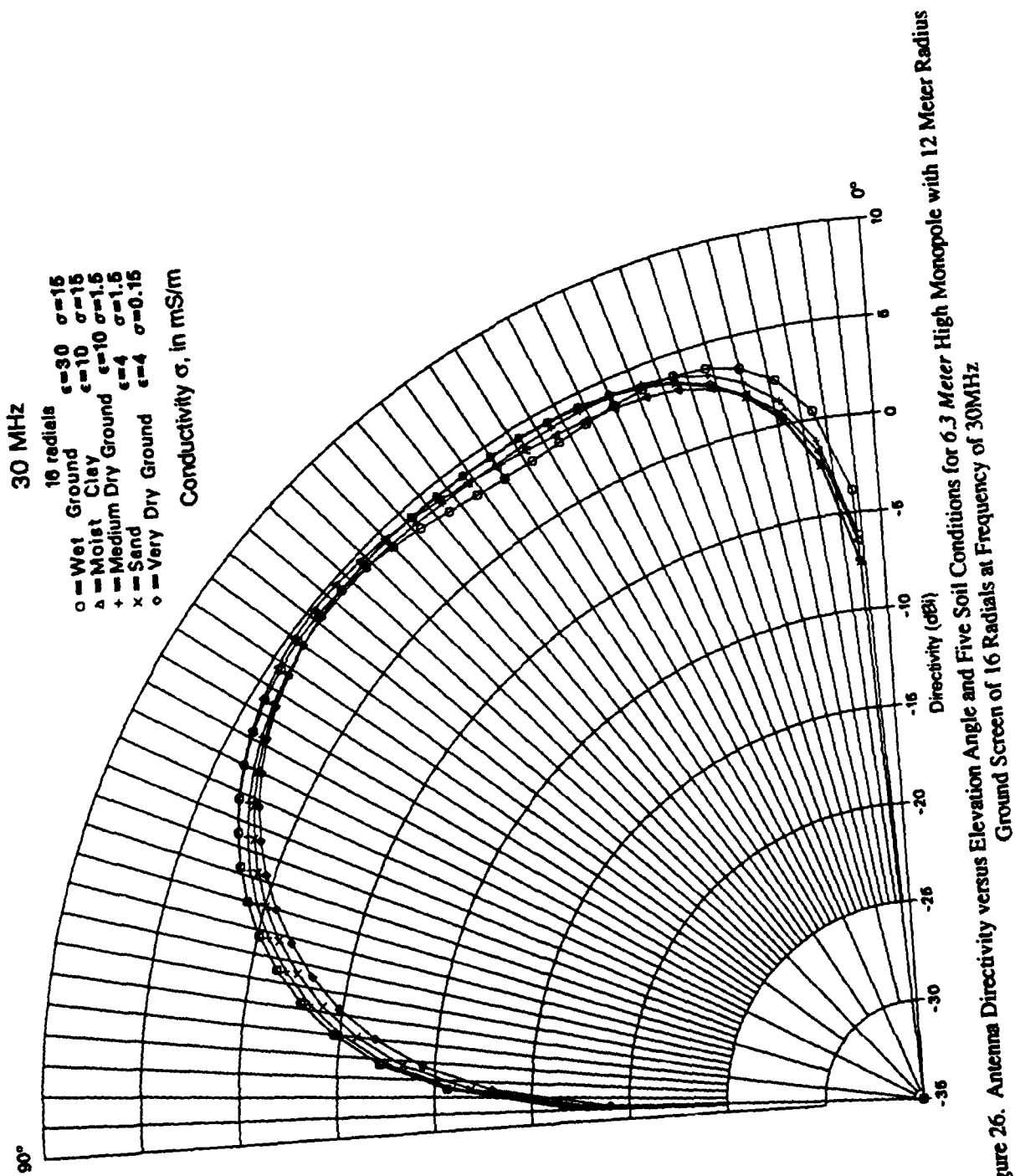


Figure 25. Antenna Directivity versus Elevation Angle and Five Soil Conditions for 6.0 Meter High Monopole with 12 Meter Radius Ground Screen of 16 Radials at Frequency of 30MHz



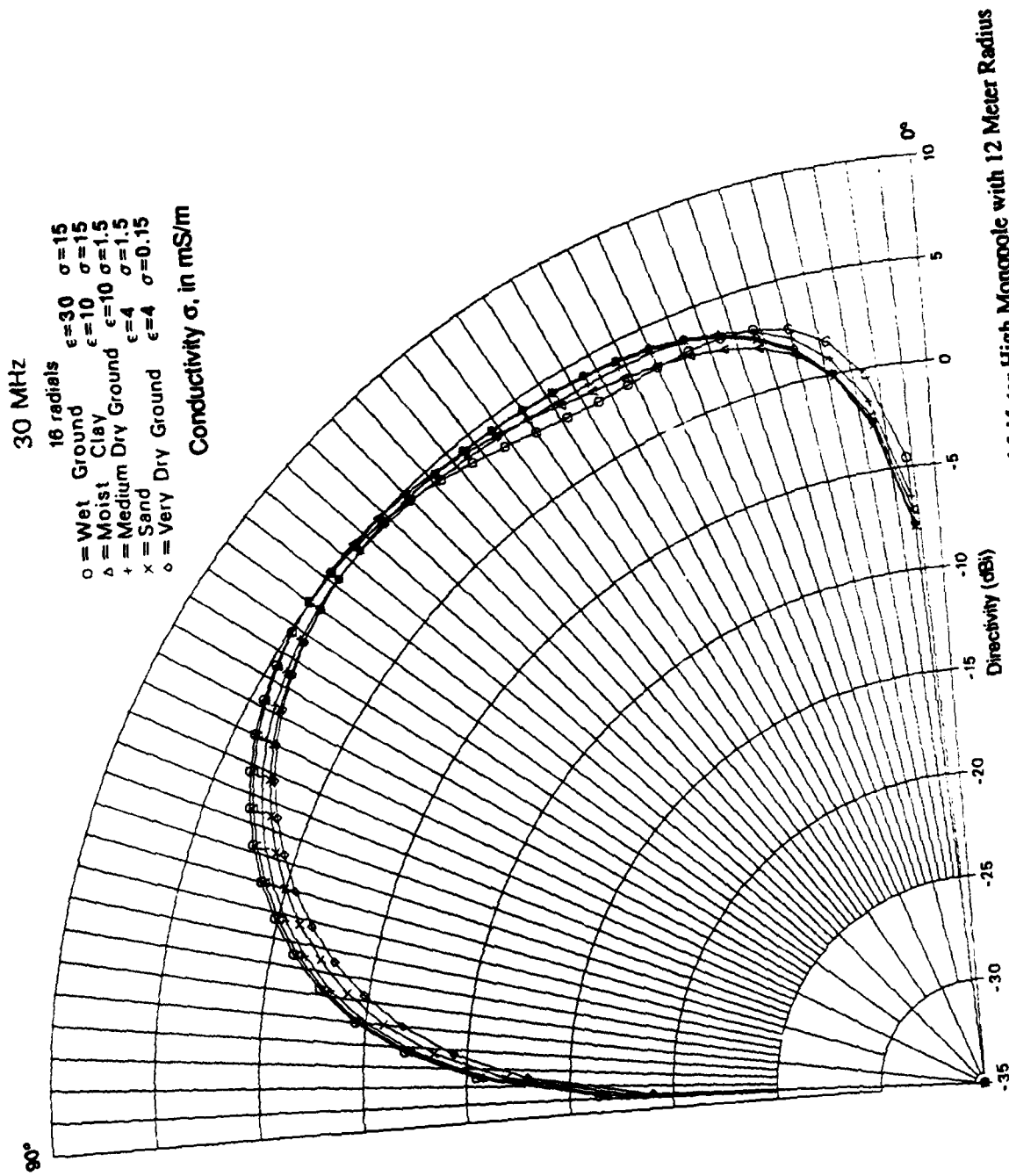


Figure 27. Antenna Directivity versus Elevation Angle and Five Soil Conditions for 6.5 Meter High Monopole with 12 Meter Radius Ground Screen of 16 Radials at Frequency of 30MHz

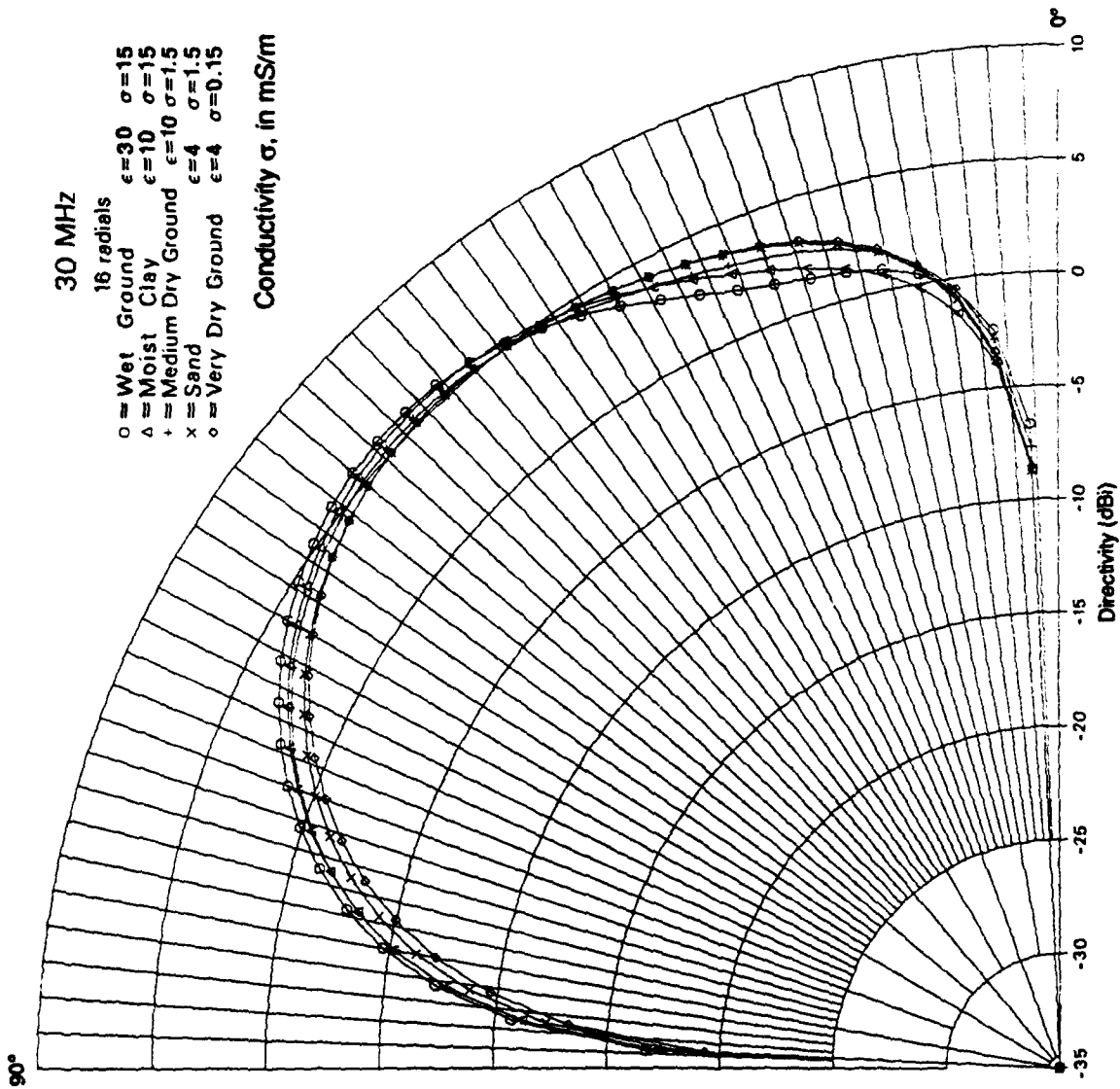


Figure 28. Antenna Directivity versus Elevation Angle and Five Soil Conditions for 7.0 Meter High Monopole with 12 Meter Radius Ground Screen of 16 Radials at Frequency of 30MHz

antenna with a 12 m radius ground screen of 16 radial wires are presented in figures 29 to 35. A complete set of performance results is given in Volume 2—Appendices.

Figure 29 and table 13 present the antenna (ohmic loss) noise figure, figure 30 and table 14 present the antenna input impedance, and figure 31 shows the corresponding plots of cable mismatch loss. Figure 32 presents the system internal noise figure by illustrating the cumulative behavior of each noise figure contribution, for the representative sandy soil condition. Figure 33 depicts the associated upper bounds for system internal noise figure for all five soil conditions and the maximum and minimum cable length. Figure 34 illustrates the antenna directivity dependence on soil condition at the representative frequency of 10 MHz, while figure 35 shows the directivity dependence on frequency for the representative sand soil condition. The performance results in these figures can be compared with those in the corresponding figures for the 5.4 m high monopole in section 4.1.1, and can be further refined if desired as discussed in section 2.1.1.2.

4.3 ALTERNATIVE DIPOLE ANTENNA CONFIGURATIONS

A dipole antenna design was also briefly examined as a potential alternative to the primary monopole antenna configuration in the unlikely case that the monopole and its ground radials became physically impractical and/or produced unsatisfactory electrical performance. By using dipole configurations having the same triangular cross-section tower structure as the monopole, similarities in cost, installation, and mechanical strength were retained. Two basic configurations were considered: (a) a center-fed dipole equal in length to the comparison monopole for three feed heights above the surface of the earth; and (b) a center-fed dipole twice the length of the monopole for one feed height above the surface. In each case, the dipole base was insulated from the surface by a height not less than 0.2 m.

4.3.1 Geometry and Parameters for NEC-GS Model

Like the monopole, the dipole, triangular cross-section antenna tower was approximated by a right circular cylinder element of length, h , and radius, b , passing through the vertices of the triangular cross-section. The center-fed, vertical dipole is located above the earth as indicated in figure 36a. As stated in 3.1, the "fat" dipoles and monopoles of interest are best modeled by using NEC-GS. Figure 36b shows the specific geometry used to form a cage of M equally spaced vertical wires to model the dipole. The vertical wire is of length, h , and radius, b_w , displaced from the z -axis by a distance, b , equal to the dipole radius, and is center-fed at a height $|z_0|$. Each of the wires is subdivided into wire segments, N_i , according to the guidelines in 3.3, where i denotes the i -th wire. The number, M , of vertical wires around the circumference of the dipole is specified, as well as the earth electrical parameters, ϵ_r , σ , and the frequencies of excitation. The characteristic dimensions, wire coordinates, wire segmentation and the ranges of parameter variation for the NEC-GS model of the dipole antenna are given in table 15.

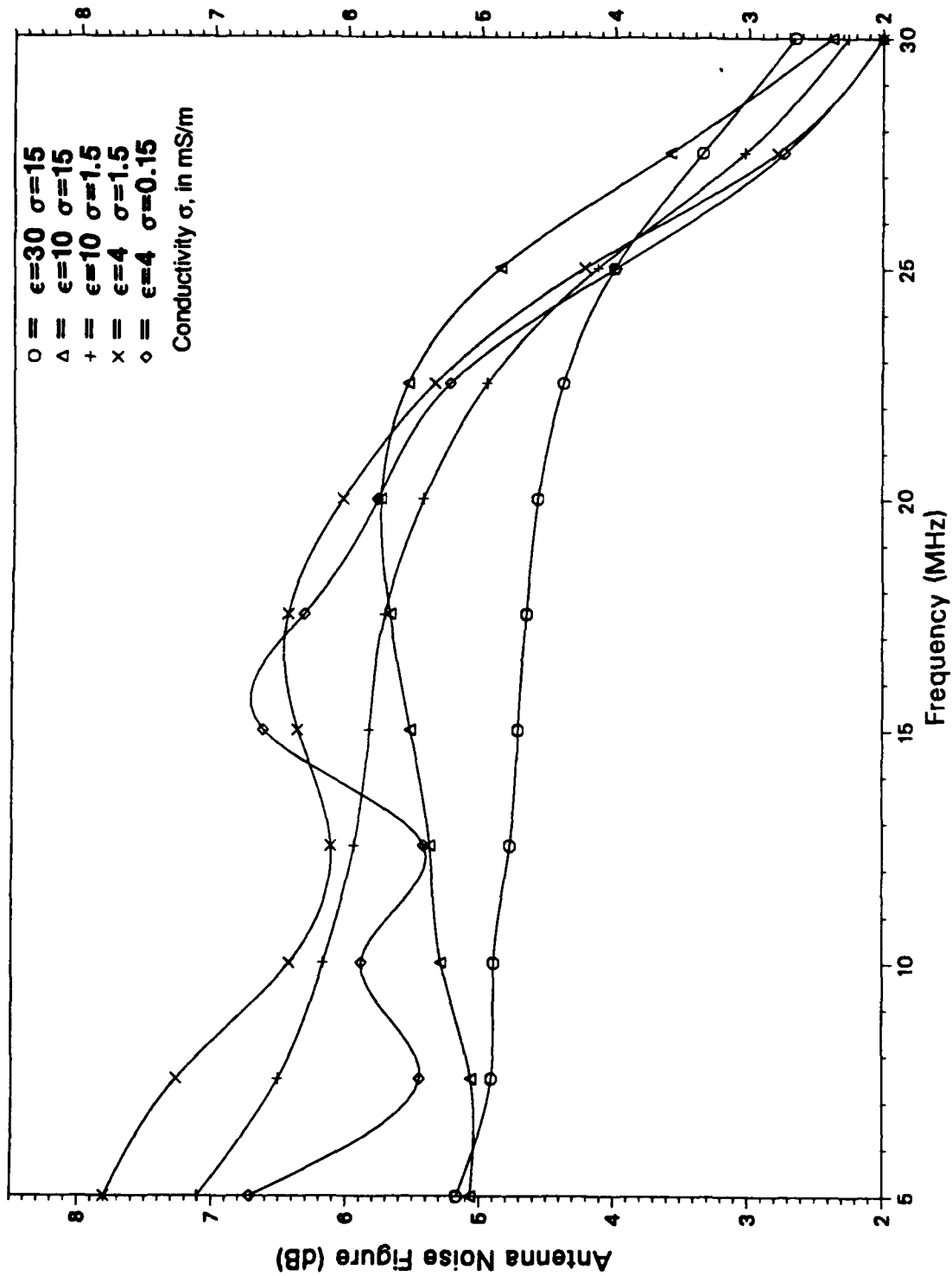


Figure 29. Antenna Noise Figure (Ohmic Loss) versus Frequency and Five Soil Conditions, for 6.3 Meter High Monopole with 12 Meter Radius Ground Screen of 16 Radials

IA9844-3

Table 13. 6.3 Meter High Monopole Antenna: Efficiency and Noise Figure versus Frequency for Five Soil Conditions

For 12 Meter Radius Ground Screen of 16 Radials, 2mm in Diameter and Buried 0.178m Deep

Frequency (MHz)	Soil Characteristics									
	Very Good (Wet Ground)		Good (Moist Clay)		Average (Medium Dry Ground)		Fair (Sand)		Poor (Very Dry Ground)	
	$\epsilon_r = 30, \sigma = 15 \text{ mS/m}$		$\epsilon_r = 10, \sigma = 15 \text{ mS/m}$		$\epsilon_r = 10, \sigma = 1.5 \text{ mS/m}$		$\epsilon_r = 4, \sigma = 1.5 \text{ mS/m}$		$\epsilon_r = 4, \sigma = 0.15 \text{ mS/m}$	
	η (%)	NF (dB)	η (%)	NF (dB)	η (%)	NF (dB)	η (%)	NF (dB)	η (%)	NF (dB)
5.0	9.7	5.2	10.0	5.1	6.2	7.1	5.3	7.8	6.8	6.7
7.5	10.3	4.9	10.0	5.1	7.1	6.5	6.0	7.3	9.1	5.4
10.0	10.4	4.9	9.5	5.3	7.7	6.2	7.3	6.4	8.3	5.9
12.5	10.7	4.8	9.3	5.4	8.1	5.9	7.8	6.1	9.2	5.4
15.0	10.8	4.7	9.0	5.5	8.4	5.8	7.4	6.4	7.0	6.6
17.5	10.9	4.7	8.6	5.7	8.6	5.7	7.3	6.4	7.5	6.3
20.0	11.2	4.6	8.5	5.8	9.2	5.4	8.0	6.0	8.5	5.8
22.5	11.7	4.4	8.9	5.5	10.2	5.0	9.3	5.3	9.6	5.2
25.0	12.7	4.0	10.5	4.9	12.4	4.1	12.1	4.2	12.8	4.0
27.5	14.8	3.3	14.0	3.6	15.9	3.0	16.8	2.8	17.0	2.7
30.0	17.4	2.7	18.5	2.4	19.0	2.3	20.8	2.0	21.0	2.0

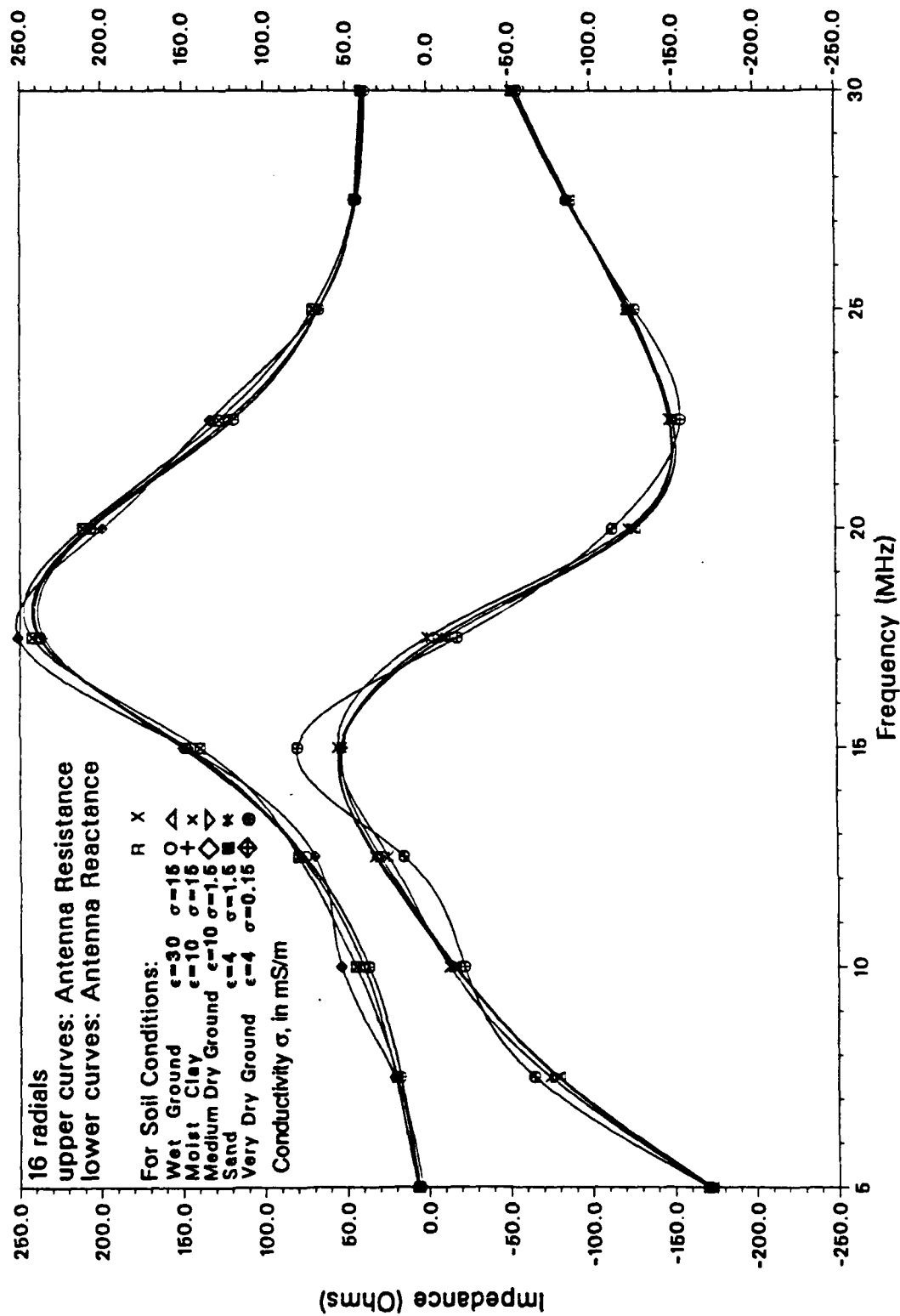


Figure 30. Antenna Input Resistance and Reactance versus Frequency for Five Soil Conditions, for 6.3 Meter High Monopole with 12 Meter Radius Ground Screen of 16 Radials

IA9843-3

Table 14. 6.3 Meter High Monopole Antenna: Input Resistance and Reactance versus Frequency for Five Soil Conditions

For 12 Meter Radius Ground Screen of 16 Radials, 2mm in Diameter and Buried 0.178m Deep

Frequency (MHz)	Soil Characteristics				
	Very Good (Wet Ground) $\epsilon_r = 30, \sigma = 15 \text{ mS/m}$	Good (Moist Clay) $\epsilon_r = 10, \sigma = 15 \text{ mS/m}$	Average (Medium Dry Ground) $\epsilon_r = 10, \sigma = 1.5 \text{ mS/m}$	Fair (Sand) $\epsilon_r = 4, \sigma = 1.5 \text{ mS/m}$	Poor (Very Dry Ground) $\epsilon_r = 4, \sigma = 0.15 \text{ mS/m}$
5.0	6.9 - j172.9	6.6 - j172.7	7.3 - j170.2	6.1 - j170.5	4.4 - j171.0
7.5	17.5 - j79.7	17.1 - j79.4	20.5 - j78.3	19.4 - j74.2	20.8 - j64.7
10.0	36.7 - j16.8	36.6 - j15.4	39.8 - j16.6	44.6 - j12.8	53.5 - j21.9
12.5	75.3 + j31.6	76.6 + j32.7	77.7 + j29.4	79.6 + j24.6	69.5 + j15.1
15.0	149.2 + j54.3	150.3 + j53.3	146.9 + j52.6	140.0 + j55.7	147.8 + j80.6
17.5	237.1 - j10.5	234.9 - j10.8	238.0 - j6.6	242.4 + j0.6	251.0 - j18.1
20.0	206.7 - j127.2	206.0 - j124.9	208.5 - j125.4	211.2 - j122.8	199.3 - j112.9
22.5	118.7 - j150.0	119.5 - j148.5	122.1 - j150.4	127.5 - j148.3	132.9 - j155.0
25.0	66.0 - j122.8	66.4 - j122.2	66.7 - j123.4	69.9 - j124.8	67.0 - j127.3
27.5	42.9 - j87.9	42.5 - j87.0	43.2 - j87.1	44.1 - j87.1	44.7 - j85.9
30.0	38.1 - j55.1	37.6 - j53.3	39.1 - j53.5	40.2 - j52.1	40.7 - j53.2

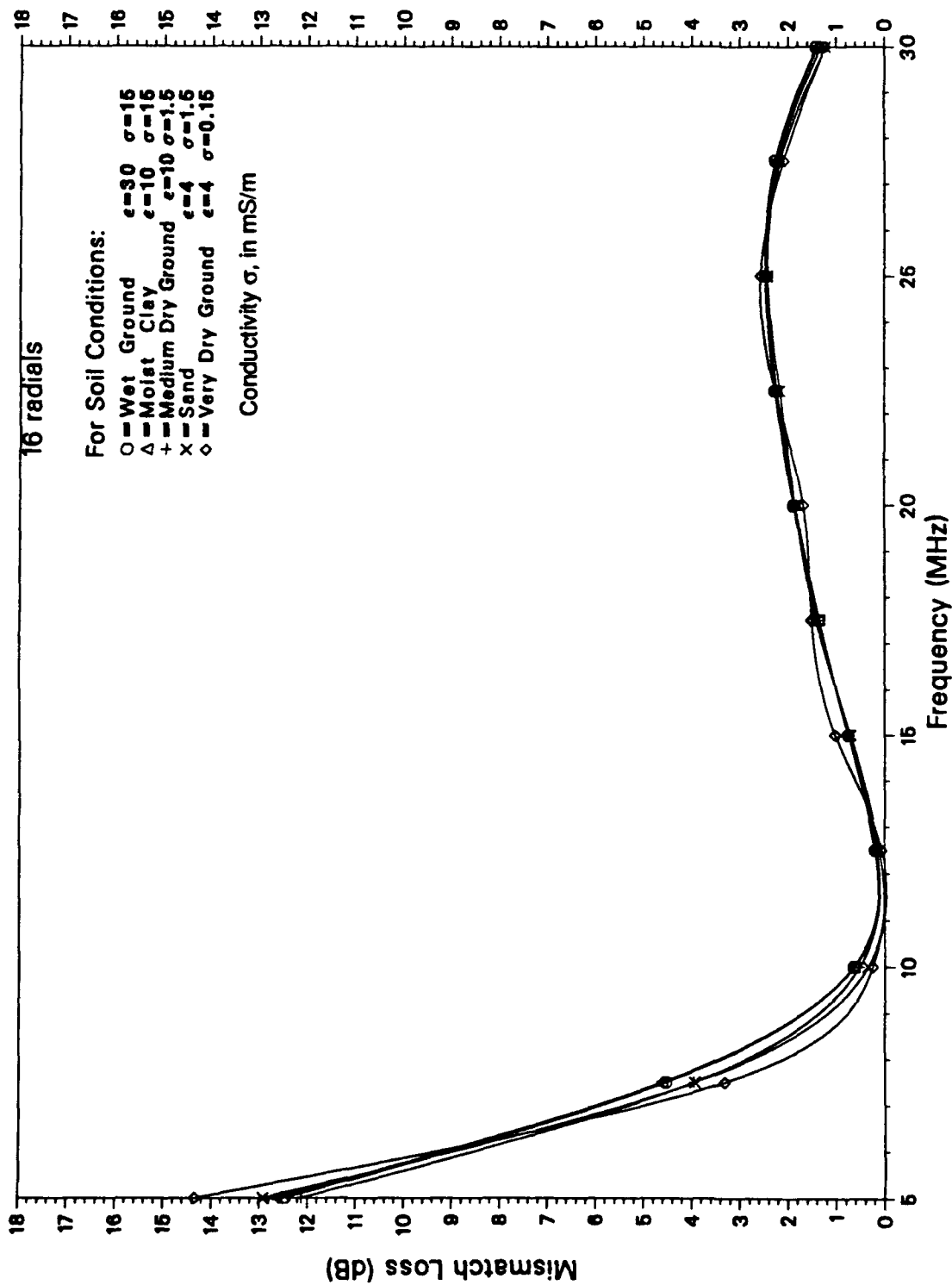


Figure 31. Cable Mismatch Loss versus Frequency and Five Soil Conditions for 75 ohm Coaxial Cable Feeding 6.3 Meter High Monopole with 12 Meter Radius Ground Screen of 16 Radials

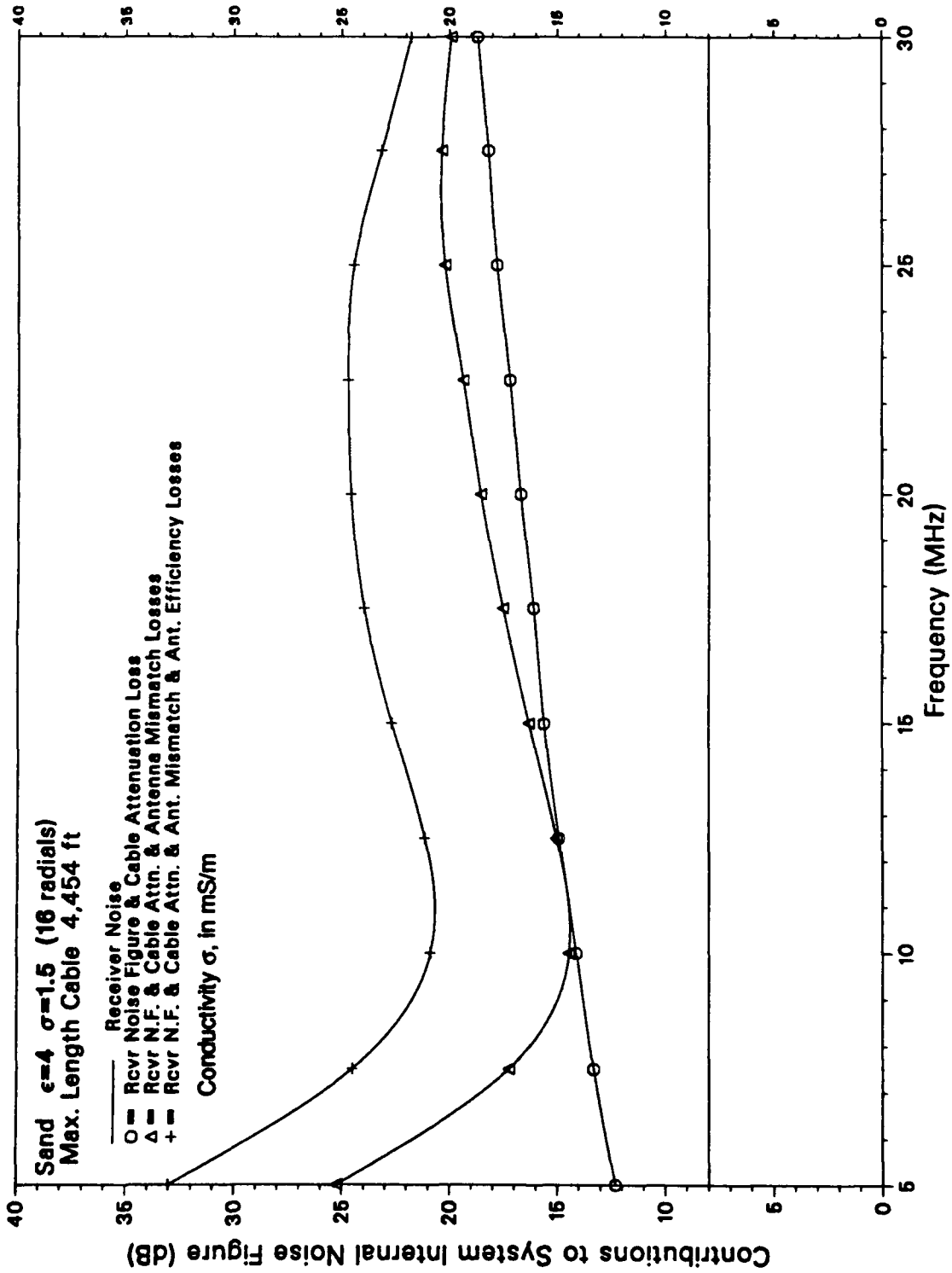


Figure 32. System Internal Noise Figure Cumulative Contributions for Case of Sandy Soil and Maximum Length Cable for 6.3 Meter High Monopole with 12 Meter Radius Ground Screen of 16 Radials

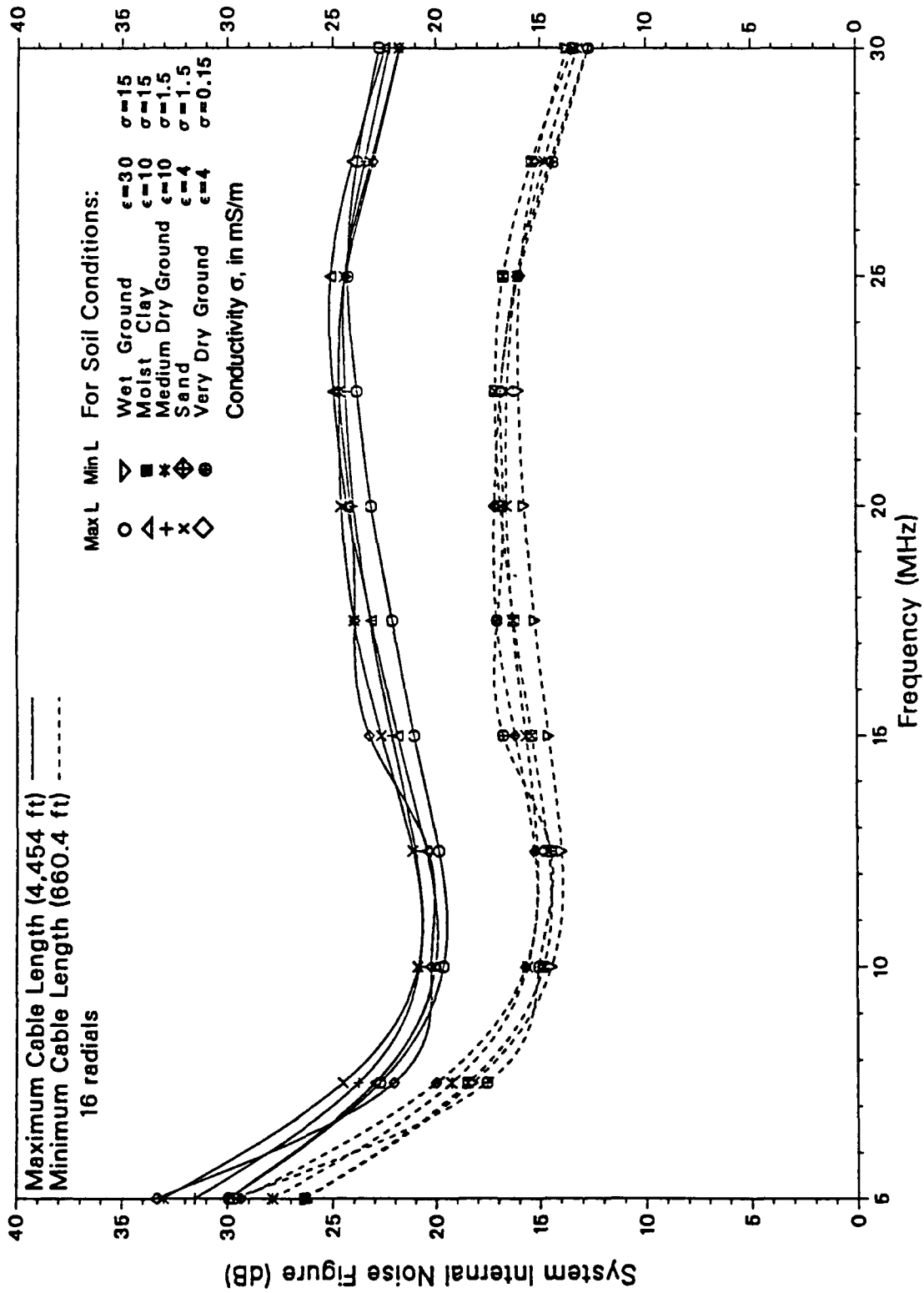


Figure 33. System Internal Noise Figures versus Frequency, Soil Condition, and Maximum and Minimum Cable Lengths for 6.3 Meter High Monopole Antenna with 12 Meter Radius Ground Screen of 16 Radial Wires

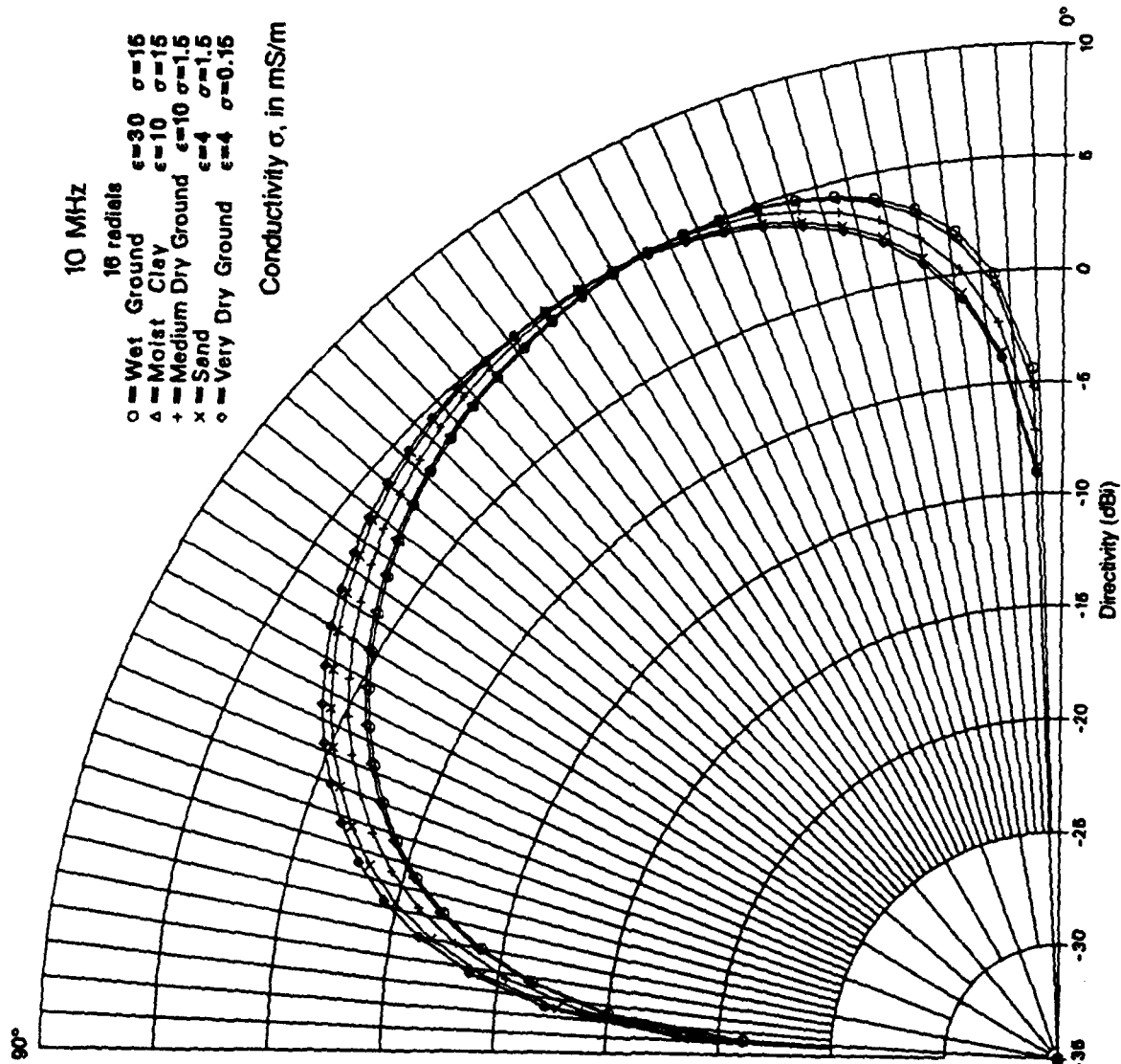


Figure 34. Antenna Directivity versus Elevation Angle and Five Soil Conditions at Frequency of 10 MHz, for 6.3 Meter High Monopole with 12 Meters Radius Ground Screen of 16 Radials

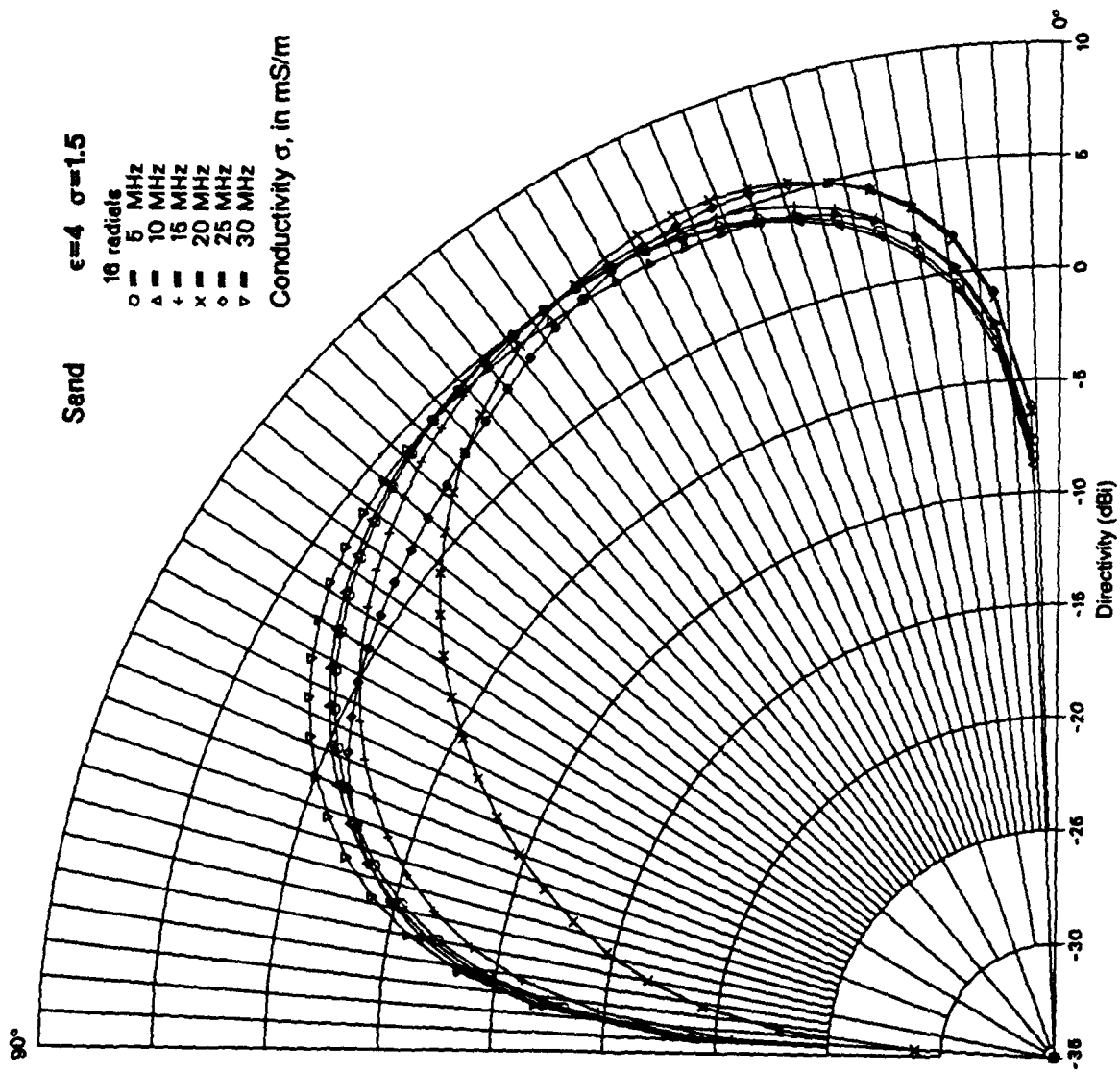


Figure 35. Antenna Directivity versus Elevation Angle and Frequency, for 6.3 Meter High Monopole with 12 Meter Radius Ground Screen of 16 Radials, for a Sandy Soil Condition

1Y0007-1

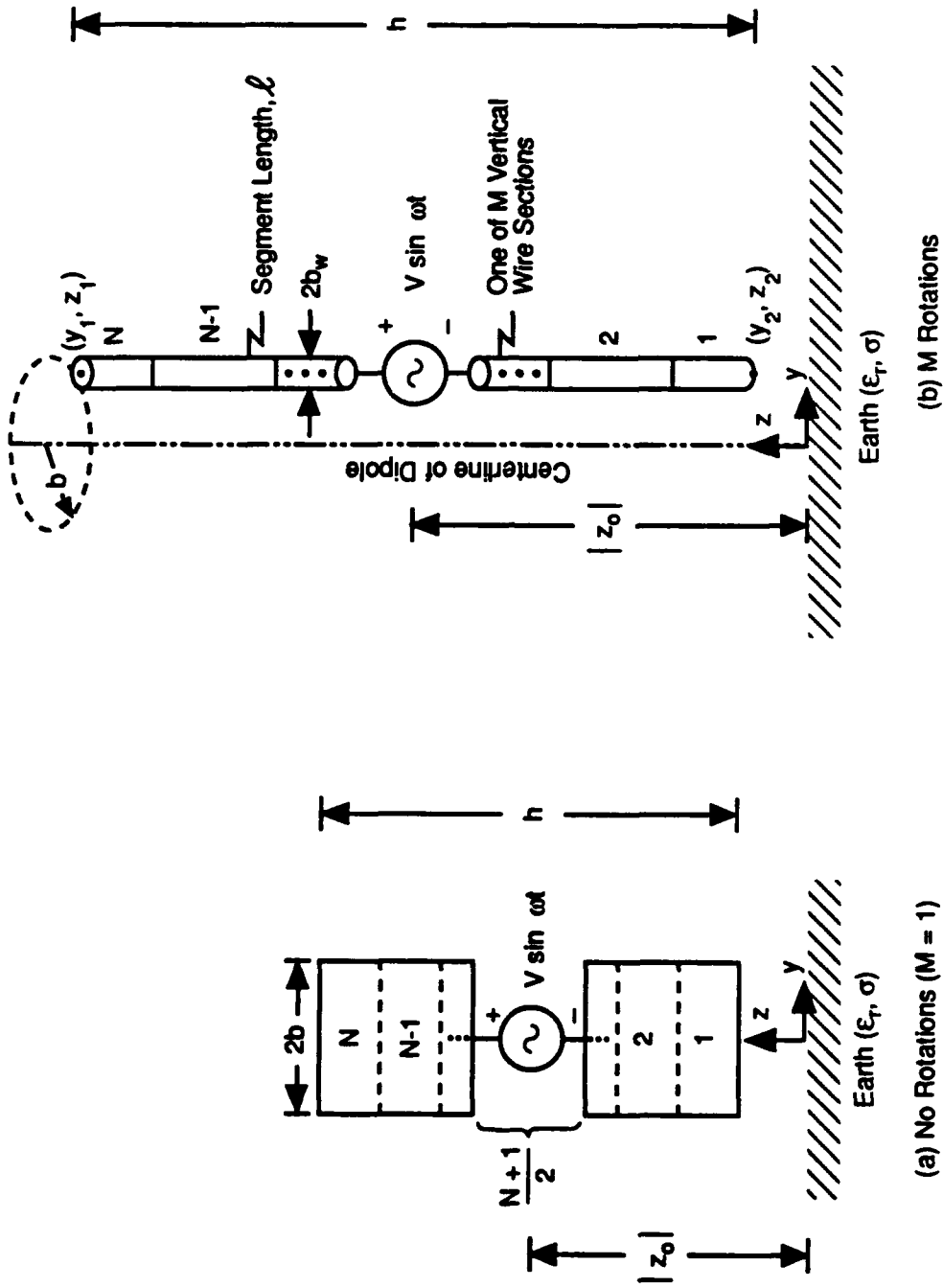


Figure 36. Rotational (Cage) NEC-GS Model Representation of a Fat Vertical Dipole Element of Radius b in Proximity to Earth

IL3083-1

Table 15. NEC-GS Rotational (Cage) Vertical Dipole Antenna Wire Model

a) Wire Model Dimensions (Figure 36)

Dipole Length (h)	5.0m, 10.0m	(16.4 or 32.8 ft)
Dipole Radius (b)	0.25m	(9.8 in)
Dipole Feed height (z_0)	2.7, 3.2, 5.2m*	(8.9, 10.5, 17.1 ft)
Vertical Wire Filament Radius (b_w)	0.001m	(0.04 in)
Excitation (Feed) Section Length (ℓ_e)	0.4m	(0.38)
Number of Rotations (Filaments) (M)	16	16

* 10m Dipole Examined for 5.2m Feed Height Only; 5m Dipole for all Three Heights

b) Vertical Wire Model Coordinates (Meters) and Wire Segmentation

Feed Height	5 Meter Dipole	
2.7m	$y_1 = 0.25, z_1 = 5.2; y_2 = 0.25, z_2 = 0.2; N = 13, \ell = 0.38$	
3.2m	$y_1 = 0.25, z_1 = 5.7; y_2 = 0.25, z_2 = 0.7; N = 13, \ell = 0.38$	
5.2m	$y_1 = 0.25, z_1 = 7.7; y_2 = 0.25, z_2 = 2.7; N = 13, \ell = 0.38$	
Feed Height	10 Meter Dipole	
5.2m	$y_1 = 0.25, z_1 = 10.2; y_2 = 0.25, z_2 = 0.2; N = 25, \ell = 0.40$	

4.3.2 Antenna Ohmic Loss and Cable Mismatch Loss

System internal noise figure performance was characterized for the dipole relative to that for a 5 m high monopole with 12 m radius ground screen having 16 radial wires. Noise figure behavior was examined as a function of dipole length and feed height above ground, at the three frequencies of 5 MHz, 15 MHz, and 25 MHz in the 5 to 30 MHz band for the representative sandy soil condition ($\epsilon_r = 3.5$, $\sigma = 2.3$ millisiemens/m). As in 4.1.2, the sum ($L_c + L_{nm}$) served as the key measure for assessing changes in noise figure performance as a function of antenna geometrical parameters and frequency. The average power gain and the real and imaginary parts of the antenna input impedance were extracted from NEC-GS output files as before to compute the antenna efficiency loss, L_c , and the antenna reflection coefficient and its associated cable mismatch loss, L_{nm} . Like the monopole case, the mismatch loss was calculated for a 75 ohm coaxial cable, which, for connection to the balanced dipole antenna, was assumed to be equipped with a suitable, lossless balun.

Table 16 illustrates the dependence on frequency and dipole geometry of the dipole antenna efficiency, η , antenna noise figure (ohmic loss), L_c , reflection coefficient squared, $|\Gamma|^2$, cable mismatch loss, L_{nm} , and the noise figure sum ($L_c + L_{nm}$), together with the corresponding values for a 5 m reference monopole with a 12 m radius ground screen of 16 radials, all for the representative sandy soil condition. The tabulated results indicate that the noise figure sums ($L_c + L_{nm}$) for the 5 m, center-fed dipole configuration are significantly larger than those for the monopole case, independent of feed height, except at the less important, upper end of the frequency band. Even doubling the dipole length to 10 m produces only marginally improved noise figure performance relative to that of the monopole. However, even this marginal improvement for the 10 m dipole is at the expense of a less desirable mechanical structure, twice the height of the monopole, and an undesirable decrease in antenna elevation pattern beamwidth at the upper end of the frequency band. Consequently, the simple triangular tower dipole antenna structures were judged unfavorable alternatives to the selected monopole configuration.

4.4 FEED CABLE EFFECTS ON RADIATION PATTERN

As stated in 2.2.1, undesired electrical currents will be induced along the external surface of the coaxial feed cable when the monopole antenna feed cable is not completely shielded beneath a large continuous conducting ground screen, from EM fields radiated from, or incident upon, the antenna. These undesired cable currents can disturb the azimuthal symmetry of the antenna and modify the directivity pattern and phase center of the antenna. The potential seriousness of these cable effects were evaluated by using NEC-3I computer software to model a monopole antenna and radial wire ground screen, fed by a long jacketed feed cable. The three conditions of no cable, unburied cable, and buried cable were examined and the associated directivities and phases of the radiation fields were compared.

4.4.1 Geometry, Parameters, and NEC-3I Model

Figure 37 presents the coordinate geometry for the monopole antenna, its radial ground screen, and feed cable. The asymmetric geometry of the antenna with its jacketed (insulated)

IL3084-1

Table 16. Comparison of 5 and 10 Meter Dipole Performance versus Frequency with Performance of a 5 Meter Monopole with 16 Radial, 12 Meter Radius Ground Screen for a Sandy Soil Condition ($\epsilon_r = 3.5, \sigma = 2.3 \text{ mS/m}$)

For Performance Measures of Antenna Noise Figure (Ohmic Loss, L_o), Cable Mismatch Loss (L_{cm}), Noise Figure Sum ($L_c + \frac{1}{2} L_{cm}$), Efficiency (%), Magnitude Squared of Reflection Coefficient $|\Gamma|^2$ and Antenna Input Impedance, Z_{in}

Frequency (Mhz)	5.0 Meter Monopole with 16 Radial, 12 Meter Radius Ground Screen										5.0 Meter Dipole										10.0 Meter Dipole																													
	Feed Height = 2.7m					Feed Height = 3.2m					Feed Height = 5.2m					Feed Height = 5.2m					Feed Height = 5.2m																													
	η (%)	$ \Gamma ^2$	L_o (dB)	L_{cm} (dB)	$L_c + L_{cm}$ (dB)	η (%)	$ \Gamma ^2$	L_o (dB)	L_{cm} (dB)	$L_c + L_{cm}$ (dB)	η (%)	$ \Gamma ^2$	L_o (dB)	L_{cm} (dB)	$L_c + L_{cm}$ (dB)	η (%)	$ \Gamma ^2$	L_o (dB)	L_{cm} (dB)	$L_c + L_{cm}$ (dB)	η (%)	$ \Gamma ^2$	L_o (dB)	L_{cm} (dB)	$L_c + L_{cm}$ (dB)	η (%)	$ \Gamma ^2$	L_o (dB)	L_{cm} (dB)	$L_c + L_{cm}$ (dB)																				
5	18.9	.979	7.2	16.9	24.1	4.5	.991	13.5	20.4	33.9	7.5	.995	11.3	23.3	34.6	14.0	.998	8.5	26.8	35.3	10.6	.963	9.7	14.3	24.0	21.8	.963	9.7	14.3	24.0																				
15	22.1	.020	6.6	0.1	6.7	14.4	.785	8.4	6.7	15.1	17.0	.842	7.7	8.0	15.7	22.2	.896	6.5	9.8	16.3	17.8	.081	7.5	0.4	7.9	17.8	.081	7.5	0.4	7.9																				
25	23.9	.287	6.2	1.5	7.7	20.3	.046	6.9	0.2	7.1	23.7	.072	6.3	0.3	6.6	36.7	.077	4.3	0.3	4.6	28.2	.527	5.5	3.2	8.7	308.6	.527	5.5	3.2	8.7																				
Frequency	Z_{in} (ohm)										Z_{in} (ohm)										Z_{in} (ohm)																													
5	3.6 - j215.6										14.5 - j687.5										8.1 - j711.9										21.8 - j407.3																			
15	65.9 - j17.9										28.8 - j171.3										22.0 - j179.6										14.5 - j184.0										129.5 + j21.3									
25	188.0 - j99.9										73.0 - j32.5										60.8 - j34.8										52.9 - j28.9										308.6 - j220.2									

L3063

16 Radials, 12 Meters Long, Buried at 0.178m (7in)

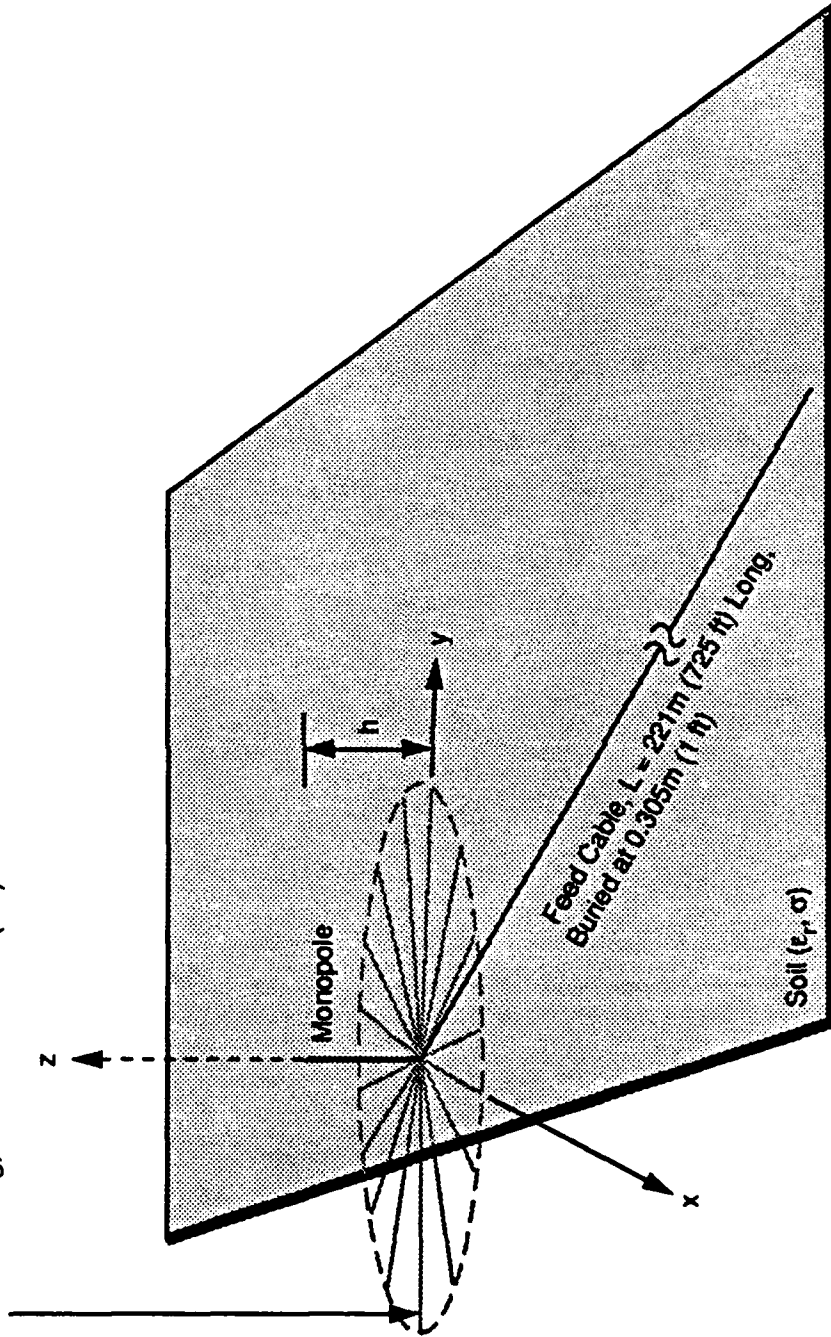


Figure 37. Coordinate Geometry for Investigation of Antenna Pattern Effects Due to Presence of Long Coaxial Feed Cable

cable requires the use of NEC-3I, not the more convenient NEC-GS software. In addition, the constraint concerning the wire segment length-to-diameter ratio, discussed in 3.3, requires that the triangular cross-section antenna tower of figure 2 be approximated by a thinner solid monopole element of height, h , with reduced radius, b . Use of this reduced monopole radius does not detract from the assessment of cable effects on the monopole radiation pattern.

As indicated in figure 37, the thin monopole is placed above a ground screen consisting of M equally spaced radial wires of length, a , and radius, b_w , which are located at a depth, z_0 , below a flat earth surface. To account for the current induced on the external surface of the cable's outer conductor and estimate its corresponding effects on the antenna radiation pattern, the feed cable is modeled as a longer and larger diameter additional radial wire, because the outer conductor of the coaxial feed cable is connected (grounded) to the ground screen. This longer radial wire is placed either above or below the surface to represent the case of an unburied or buried cable, respectively. The earth, or soil material, is characterized, as before, by the conductivity, σ , in milliseimens/m and relative dielectric permittivity, ϵ_r .

The quantities x , y , z , and r , θ , ϕ are the conventional cartesian and spherical coordinates, respectively, and ψ is the elevation angle measured from the horizon. The monopole element, the radial wire conductors, and the long radial wire representing the feed cable are all constrained to have infinite conductivity.

The specific NEC-3I wire geometry used to model the thin monopole, its radial wire ground screen, and the feed cable is described below. The monopole consists of a vertical wire section of height, h , and radius, b , with a short vertical excitation segment at its base. However, unlike the NEC-GS model for a fat monopole in figure 8, the vertical wire section for the thin monopole is centered on the z -axis, not displaced from it. Each of the M (16) radials consists of a mostly horizontal wire section of radius, b_w , which begins at the base of the monopole wire section with a short downward sloping transition section, and continues horizontally to a radial distance, a , at a depth, z_0 , beneath the surface. Similarly, the jacketed feed cable is modelled by a mostly horizontal, but *insulated*, wire section having wire conductor radius, b_c , insulating jacket radius, b_j , and material dielectric constant, $\epsilon_c = 2.25$. This insulated cable wire also begins at the base of the monopole wire section, with a short downward sloping transition section when buried (upward sloping, when unburied), and continues horizontally to a radial distance, c , at a depth, d , beneath the surface (or height h_c above the surface, when unburied). This radial cable wire is located at the azimuth angle of 32.5° , nearly halfway between two ground screen radial wires.

Each of the wire sections is, as before, suitably divided into wires and subdivided into wire segments, N_i , according to the guidelines in 3.3, where i denotes the i -th wire. In addition, the radial cable wire has been modeled to include, after the sloping transition section, a short tapered-segment section containing six wire segments of gradually increasing length according to the taper ratio of 1.5. This allows the wire junction constraints of 3.3 to be conveniently satisfied for the case of an unburied cable located close to the surface. Unlike NEC-GS, NEC-3 and NEC-3I require that each of the ($M = 16$) individual ground radial wires, with their associated coordinates and numbers of wire segments, must be individually

specified. The earth parameters, ϵ_r , σ , and the frequencies of excitation are specified as in NEC-GS.

4.4.2 Radiation Patterns-Effects of Buried versus Unburied Cables and Antenna Height

A variety of computer runs were completed to characterize the primary effects of the feed cable on the antenna directivity pattern and phase front in the radiation field. The following quantities: antenna power gain, average power gain, phase of the E_θ component, and magnitude of the currents along the feed cable, ground radials, and monopole, were extracted from the NEC-3I output files to assess the cable-based effects. Attention was directed at the influence of cable burial, operating frequency, monopole height, cable burial depth, cable length, presence of insulating cable jacket, number of radials, and soil electrical properties.

Comprehensive results were obtained on the effects of cable burial for two configurations of primary interest, namely, a monopole of reference height 5.4 m, and another 2.4 m high. Each monopole is mounted on a 12 m radius ground screen having 16 radials buried to a depth of 0.178 m (7 in), and fed by a jacketed, coaxial cable 221 m (725 ft) long. The cable length is slightly longer than the minimum cable length of 201 m used in the Texas array.

The pattern behavior was examined for a representative sandy soil condition ($\epsilon_r = 3.5$, $\sigma = 2.3$ millisiemens/m), at three frequencies: 5 MHz, 15 MHz, and 25 MHz across the HF band, and three cable conditions: no cable, an unburied cable 0.075 m (3 in) above the surface, and a cable buried at a depth of 0.305 m (12 in). The characteristic dimensions and ranges of parameters examined are given in table 17. The 2.4 m monopole configuration was included because of the following: (a) it has been used as a reference antenna during airborne pattern measurements of HF ground-based antennas, and (b) the asymmetric pattern distortions were first observed during such tests, when using a 2.4 m monopole, fed by a 221 m coaxial cable [20].

For completeness, results were also obtained for the least favorable soil condition of table 2 ($\epsilon_r = 4$, $\sigma = 0.15$ millisiemens/m), in the unlikely event that it should be encountered. The analysis included directivity and phase behavior for the monopole heights, 5.4 m and 6.3 m, and two burial depths of 0.305m (12in) and 0.457m (18in).

4.4.2.1 Directivity Effects at 5 MHz

Figures 38 through 43 are polar plots of antenna directivity versus elevation angle and azimuth angle. Figures 38 through 40 illustrate the distortions produced in the directivity pattern of the 2.4 m monopole antenna by the presence of the 221 m long feed cable, while figures 41 through 43 illustrate similar but smaller distortions for the 5.4 m reference monopole in the presence of the same 221 m feed cable, all for the *worst-case frequency* of 5 MHz. Cable effects on antenna radiation patterns become less pronounced at the high end of the HF frequency band, as shown in subsection 4.4.2.3. Comparison of the 2.4 m and 5.4 m cases reveals that the "bulge" distortion in the directivity patterns in the general direction of the cable is more pronounced for the shorter antenna. This occurs because the undesired

IL3118 1

Table 17. NEC-3I Wire Model and Parameters for Cable Effects Analysis

a) Wire Model Dimensions (Figure 37)

Monopole Height (h)	5.4, 2.4m	(17.7, 7.9ft)
Monopole Wire Filament Radius (b)	0.01, 0.0013m	(0.39, 0.05in)
Excitation (Feed) Section Length (l_c)	0.1m	(3.9in)
Ground Wire Radial Extent (a)	12.0m	(39.4ft)
Ground Wire Radius (b_w)	0.0013m	(0.05in)
Ground Wire Depth (z_c)	0.178m	(7.0in)
Number of Radials (M)	16	16
Cable Length (D)	221m	(725ft)
Cable Radius (b_c)	0.007m	(0.28in)
Cable Insulation Thickness (t)	0.001m	(0.04in)
Cable Unburied Height (h_c)	0.075m	(3.0in)
Cable Burial Depth (d_c)	-0.178, -0.305, -0.457m	(-7, -12, -18in)
Cable Orientation (ϕ_c)	32.5°	32.5°

b) Soil Characteristics

Sandy Soil	$\epsilon_r = 3.5$, $\sigma = 2.3$ millisiemens/m
Very Dry Ground	$\epsilon_r = 4$, $\sigma = 0.15$ millisiemens/m

c) Frequencies 5, 15, 25 MHz

E3118-1

**Table 17. NEC-3I Wire Model and Parameters for Cable Effects Analysis
(Concluded)**

d) Wire Model Coordinates (meters) and Wire Segmentation

Monopole – 5.4m high, 0.01m radius

Vertical Wire – Section 1 $x_1 = 0.0, y_1 = 0.0, z_1 = 0.0; x_2 = 0.0, y_2 = 0.0, z_2 = 1.0, N = 10, \ell = 0.1$
(Includes Excitation Segment at Base)

– Section 2 $x_2 = 0.0, y_2 = 0.0, z_2 = 1.0; x_3 = 0.0, y_3 = 0.0, z_3 = 5.4, N = 14, \ell = 0.314$

Monopole – 2.4m high, 0.0013m radius

Vertical Wire – Section 1 $x_1 = 0.0, y_1 = 0.0, z_1 = 0.0; x_2 = 0.0, y_2 = 0.0, z_2 = 2.4; N = 24, \ell = 0.1$
(Includes Excitation Segment at Base)

Ground Screen – 16 Radials, 12m in length, 0.0013m radius, -0.178m depth

Radial Wire 1 – Section 1 $x_1 = 0.0, y_1 = 0.0, z_1 = 0.0; x_2 = 0.8, y_2 = 0.0, z_2 = -0.178, N = 1, \ell = 0.82$

– Section 2 $x_2 = 0.8, y_2 = 0.0, z_2 = -0.178; x_3 = 12.0, y_3 = 0.0, z_3 = -0.178, N = 14, \ell = 0.8$

Radial Wires 2 through 16 – Repeat radial wire 1 geometry around monopole, one every 22.5° with corresponding coordinates

Radial Feed Cable – 221m long, 0.007m radius, 0.001m insulation thickness

Unburied Case – height = 0.075m, orientation – $\phi = 32.5^\circ$

Wire 1 $x_1 = 0.0, y_1 = 0.0, z_1 = 0.0; x_2 = 0.67, y_2 = 0.43, z_2 = 0.075, N = 10, \ell = 0.08$

Wire 2 $x_1 = 0.67, y_1 = 0.43, z_1 = 0.075; x_2 = 2.08, y_2 = 1.32, z_2 = 0.075, N = 6,$
(tapered segments) $\ell = 0.08$ to 0.61, with adjacent segments increasing by ratio of 1.5

Wire 3 $x_1 = 2.08, y_1 = 1.32, z_1 = 0.075; x_2 = 186.39, y_2 = 118.74, z_2 = 0.075, N = 269, \ell = 0.82$

Buried Case – depth = -0.178, -0.305 or -0.457m, orientation – $\phi = 32.5^\circ$

Wire 1 $x_1 = 0.0, y_1 = 0.0, z_1 = 0.0; x_2 = 0.67, y_2 = 0.43, z_2 = -0.305; N = 10, \ell = 0.085$

Wire 2 $x_1 = 0.67, y_1 = 0.43, z_1 = -0.305; x_2 = 2.08, y_2 = 1.32, z_2 = -0.305; N = 6,$
(tapered segments) $\ell = 0.08$ to 0.61, with adjacent segments increasing by ratio of 1.5

Wire 3 $x_1 = 2.08, y_1 = 1.32, z_1 = -0.305; x_2 = 186.39, y_2 = 118.74, z_2 = -0.305; N = 269, \ell = 0.82$

2.4 m Monopole. 12 m radials (16), buried 7"
 Elevation Principal Plane Cuts
 Vertical plane through the 221 m feed cable
 at Azimuth of 32.5 degrees
 Frequency 5 MHz

○ = Without feed cable
 △ = Cable above ground (3")
 + = Cable below ground (12")
 Sandy Ground $\epsilon=3.5$ $\sigma=2.3$
 Conductivity σ in mS/m

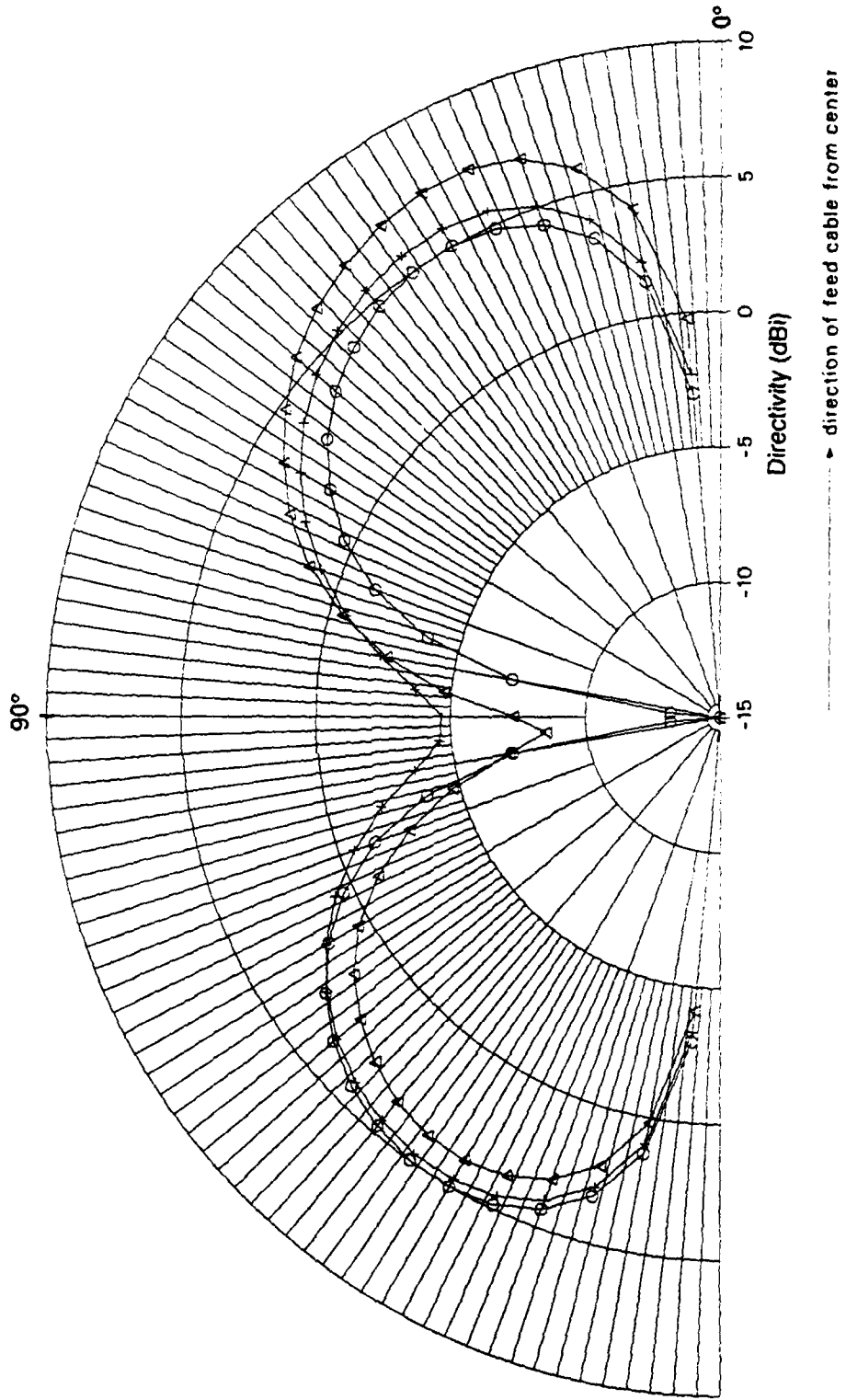


Figure 38. Principal Plane Elevation Plots of Cable Directivity Effects, for 2.4 Meter Monopole on Sandy Soil

2.4 m Monopole, 12 m radials (16), buried 7"
 Elevation Principal Plane Cuts
 Vertical plane across 221 m feed cable
 at Azimuth of 122.5 degrees
 Frequency 5 MHz

○ = Without feed cable
 △ = Cable above ground (3")
 + = Cable below ground (12")
 Sandy Ground $\epsilon=3.5$ $\sigma=2.3$
 Conductivity σ in mS/m

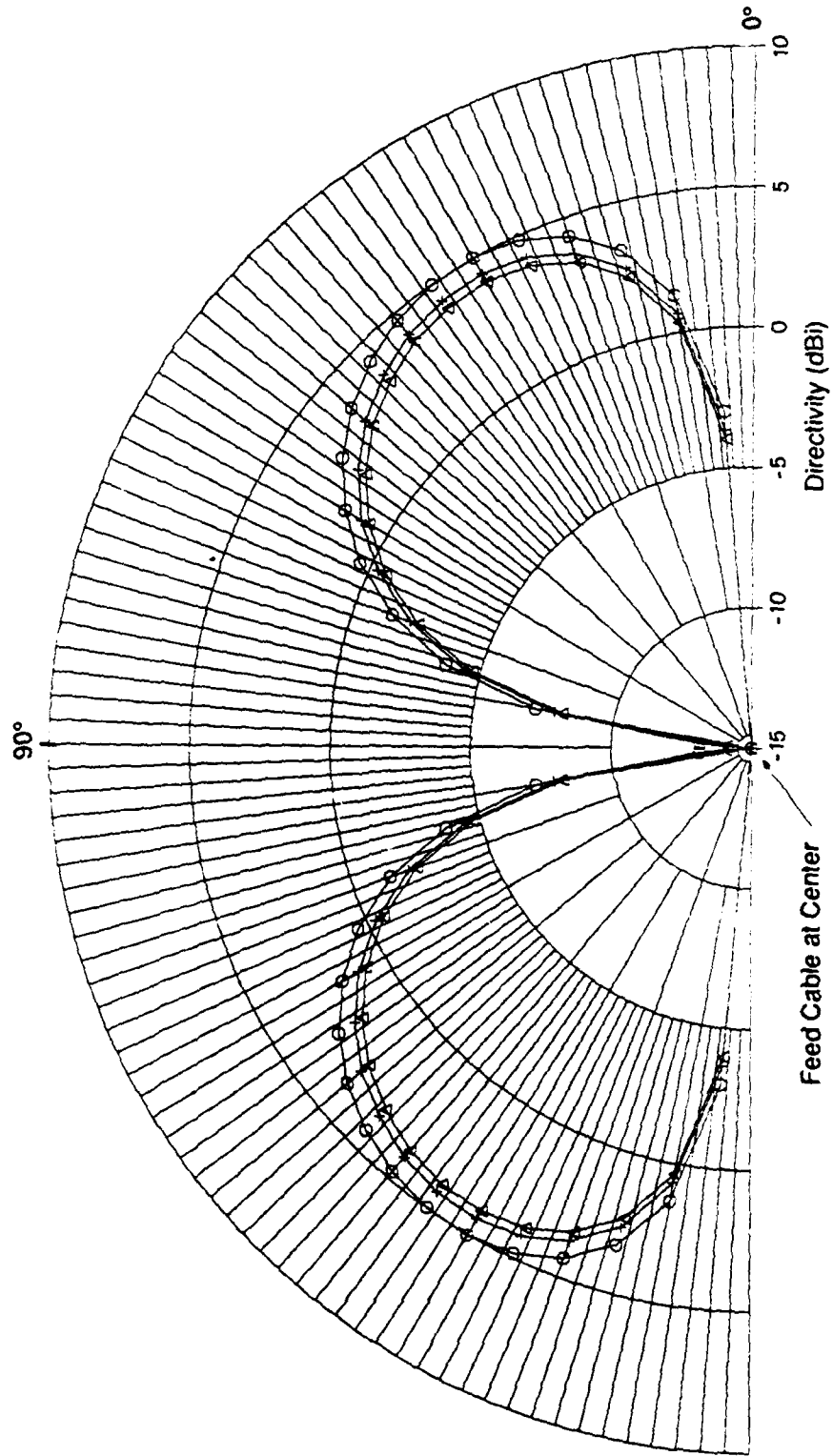


Figure 39. Perpendicular Plane Elevation Plots of Cable Directivity Effects, for 2.4 Meter Monopole on Sandy Soil

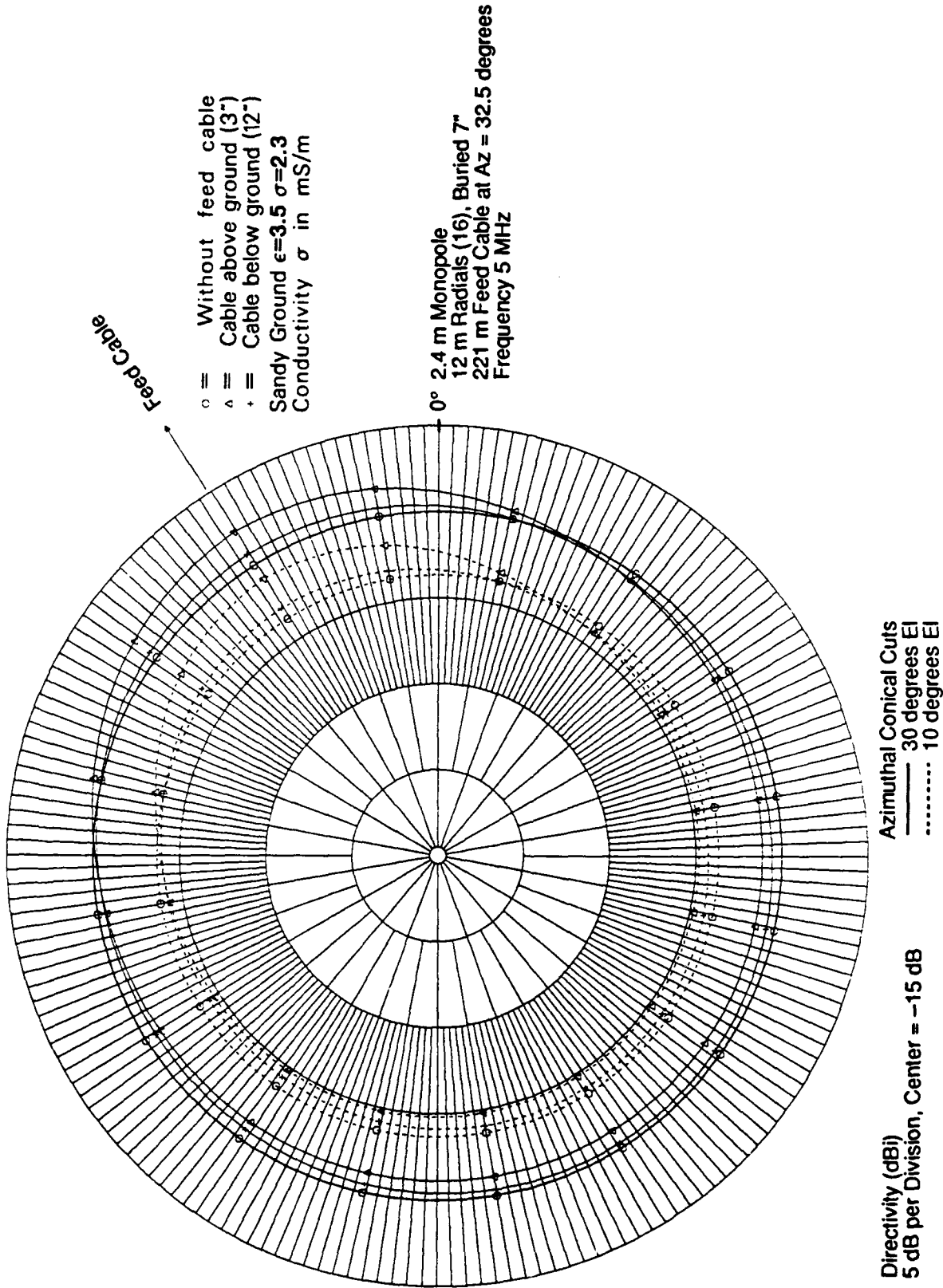


Figure 40. Azimuthal Conical Cut Plots of Cable Directivity Effects at Two Elevation Angles, for 2.4 Meter Monopole on Sandy Soil

5.4 m Monopole, 12 m radials (16), buried 7"
 Elevation Principal Plane Cuts
 Vertical plane through the 221 m feed cable
 at Azimuth of 32.5 degrees
 Frequency 5 MHz

○ = Without feed cable
 △ = Cable above ground (3")
 + = Cable below ground (12")
 Sandy Ground $\epsilon=3.5$ $\sigma=2.3$
 Conductivity σ in mS/m

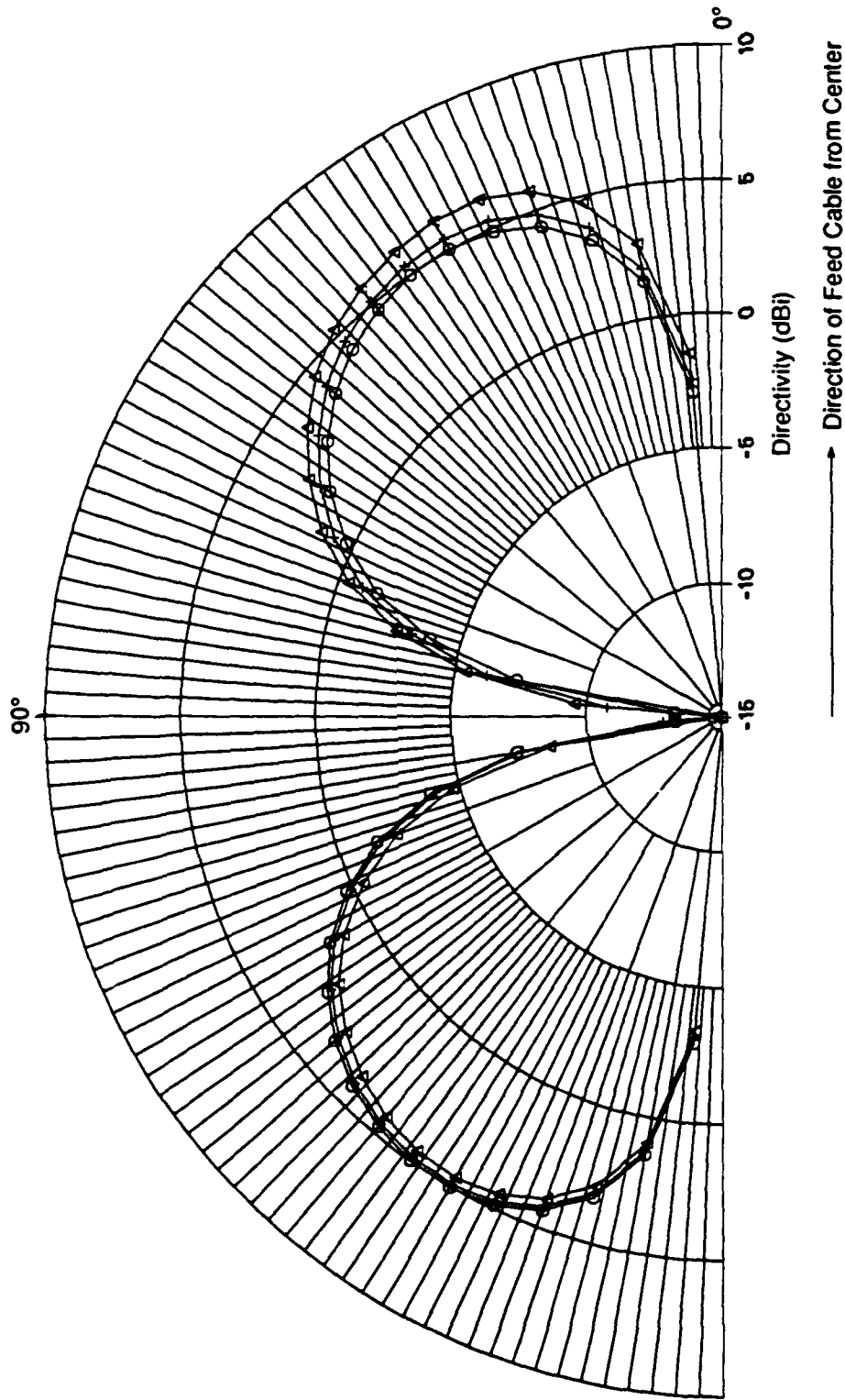


Figure 41. Principal Plane Elevation Plots of Cable Directivity Effects, for 5.4 Meter Monopole on Sandy Soil

5.4 m Monopole, 12 m radials (16), buried 7"
 Elevation Principal Plane Cuts
 Vertical plane across 221 m feed cable
 at Azimuth of 122.5 degrees
 Frequency 5 MHz

○ = Without feed cable
 △ = Cable above ground (3")
 + = Cable below ground (12")
 Sandy Ground $\epsilon=3.5$ $\sigma=2.3$
 Conductivity σ in mS/m

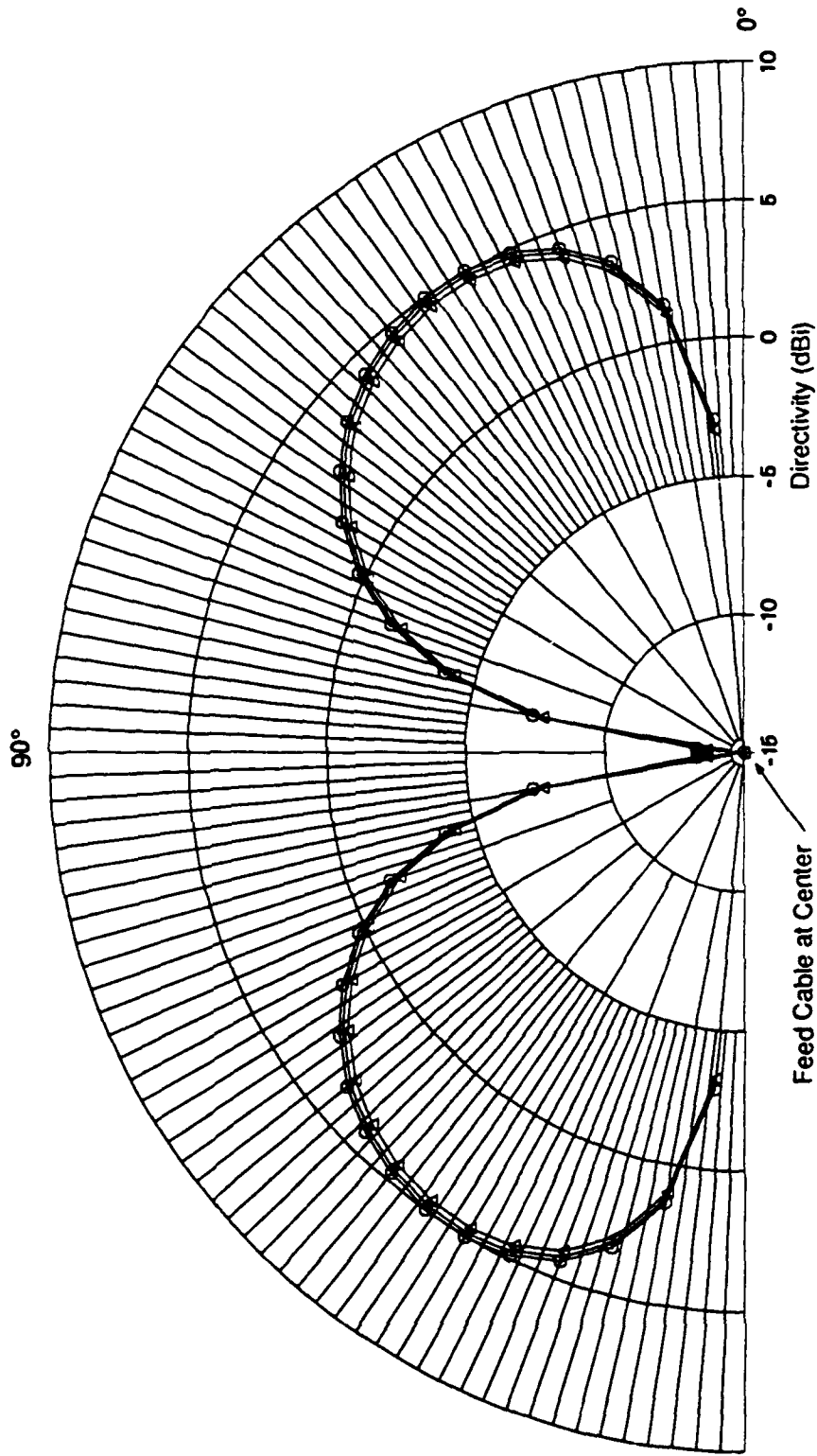


Figure 42. Perpendicular Plane Elevation Plots of Cable Directivity Effects, for 5.4 Meter Monopole on Sandy Soil

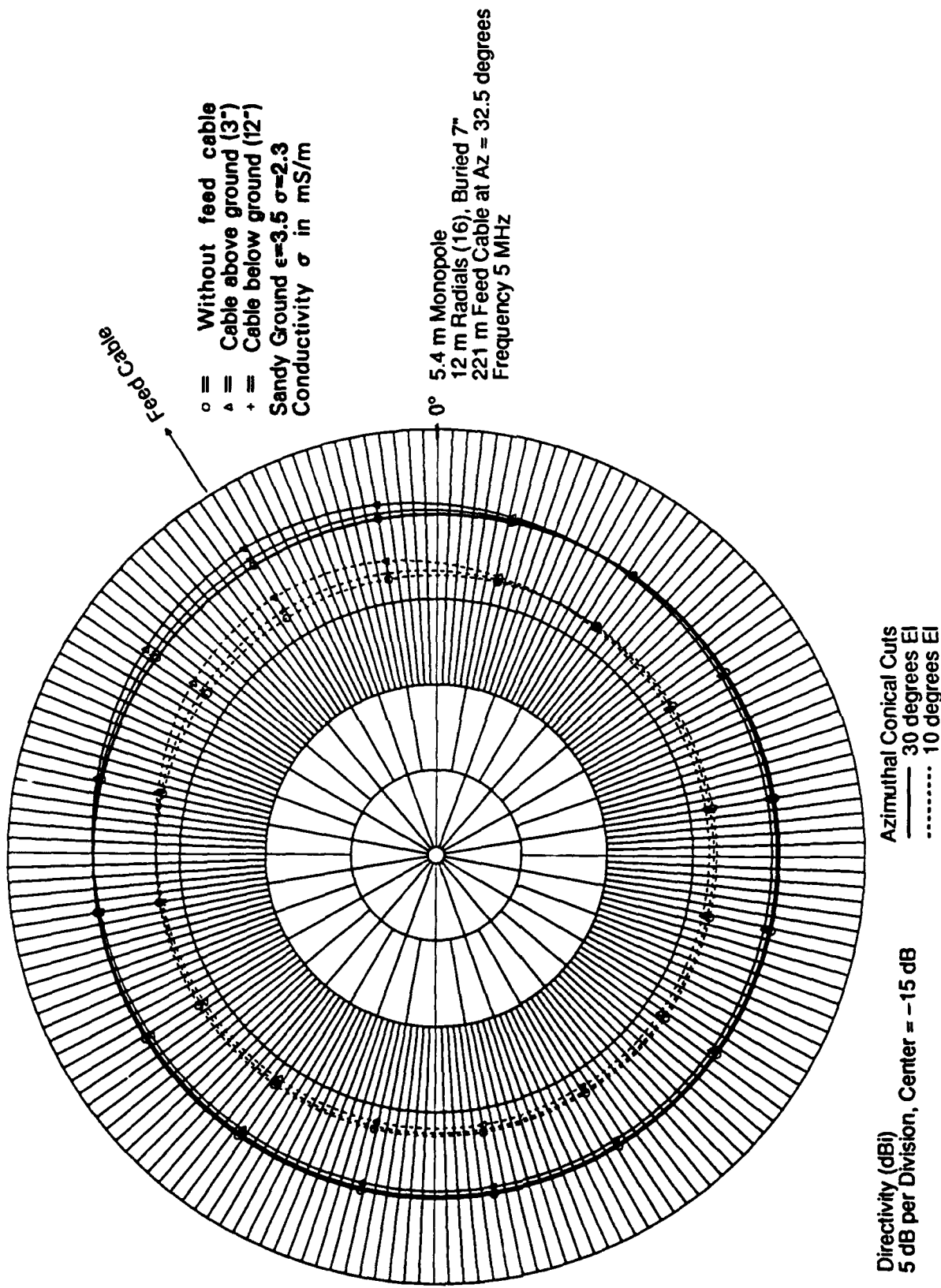


Figure 43. Azimuthal Conical Cut Plots of Cable Directivity Effects at Two Elevation Angles, for 5.4 Meter Monopole on Sandy Soil

component of receive signal contributed by the cable current represents a greater fraction of the total received power in the case of the shorter 2.4 m monopole than in the case of the taller more effective 5.4 m monopole receive antenna. Each figure depicts the three cable conditions of no cable, unburied cable, and buried cable. Figures 38 and 39 for the 2.4 m monopole, and 41 and 42 for the 5.4 m monopole, present elevation cuts in two principal planes, the one that contains the cable, and a second that is perpendicular to the cable, respectively. Figure 40 and 43 each present azimuthal conical cuts at two elevation angles; 30° in the vicinity of peak directivity, and a low elevation angle of 10° , for the 2.4 m and 5.4 m antennas, respectively.

Examination of the polar plots with circular symbols in these figures reveals the characteristic, symmetrical, "doughnut-like" cross-section, elevation pattern, and corresponding omnidirectional azimuth pattern, of an isolated monopole antenna with no feed cable. The azimuthal conical cut polar plots with triangle symbols in figures 40 and 43 apply to the *unburied* cable condition, and show the bulge in directivity within an approximately $\pm 60^\circ$ angular sector centered on the cable, accompanied by corresponding decreases in directivity outside of this sector. The triangle symbol plots for the unburied cable in figures 38 and 39 (for 2.4 m) and 41 and 42 (for 5.4 m) illustrate the associated elevation pattern behavior in the plane of the cable and perpendicular to the cable, respectively.

The elevation plane polar plots of figures 38 and 40 for the 2.4 m monopole show that marked increases in directivity, greater than 3 dB relative to the no cable case, can occur in the direction of an *unburied* feed cable. Figures 41 and 43 for the 5.4 m monopole show maximum directivity increases between about 1.5 dB to 2 dB in the direction of the *unburied* cable, values that are much smaller, and a pattern that is more symmetric in the plane of the cable, than for the 2.4 m antenna. Figures 39 and 42 illustrate the expected symmetric behavior about the vertical axis in the plane perpendicular to the cable in both cases. The plus sign symbol, polar plots in all six figures apply to the *buried* cable condition. These plots reveal that pattern distortions can be significantly reduced by burying the cable, even at the relatively shallow depth of 0.305 m (12 in). The figures indicate that, under representative sandy soil conditions, cable burial can reduce maximum directivity deviations, relative to the no-cable case, to quite acceptable values of about 1 dB and 0.5 dB, for the 2.4 m and 5.4 m monopoles, respectively, at the elevation angles of interest below 30° to 40° .

4.4.2.2 Phase Effects at 5MHz

The rectangular plots of figures 44 and 45 illustrate the corresponding azimuthal variations in the phase of the E_θ radiation field, at constant range, at the two elevation angles of 10° and 30° , for the 2.4 m monopole, under unburied, buried, and no cable conditions; while figures 46 and 47 illustrate similar but smaller phase variations for the 5.4 m reference monopole in the presence of the same 221 m feed cable. The solid horizontal line indicates the constant phase omnidirectional behavior of the no cable condition. In the presence of the cable, departures in phase angle from omnidirectional behavior are modest for the 2.4 m monopole. The departures range from approximately +14 electrical degrees to -7 electrical degrees, at an elevation angle of 30° in the vicinity of peak directivity, for the *unburied* cable, to a slightly worse condition of +16 electrical degrees to -13 electrical degrees, for the *buried* cable. For the 5.4 m reference monopole, the situation becomes much more favorable, with

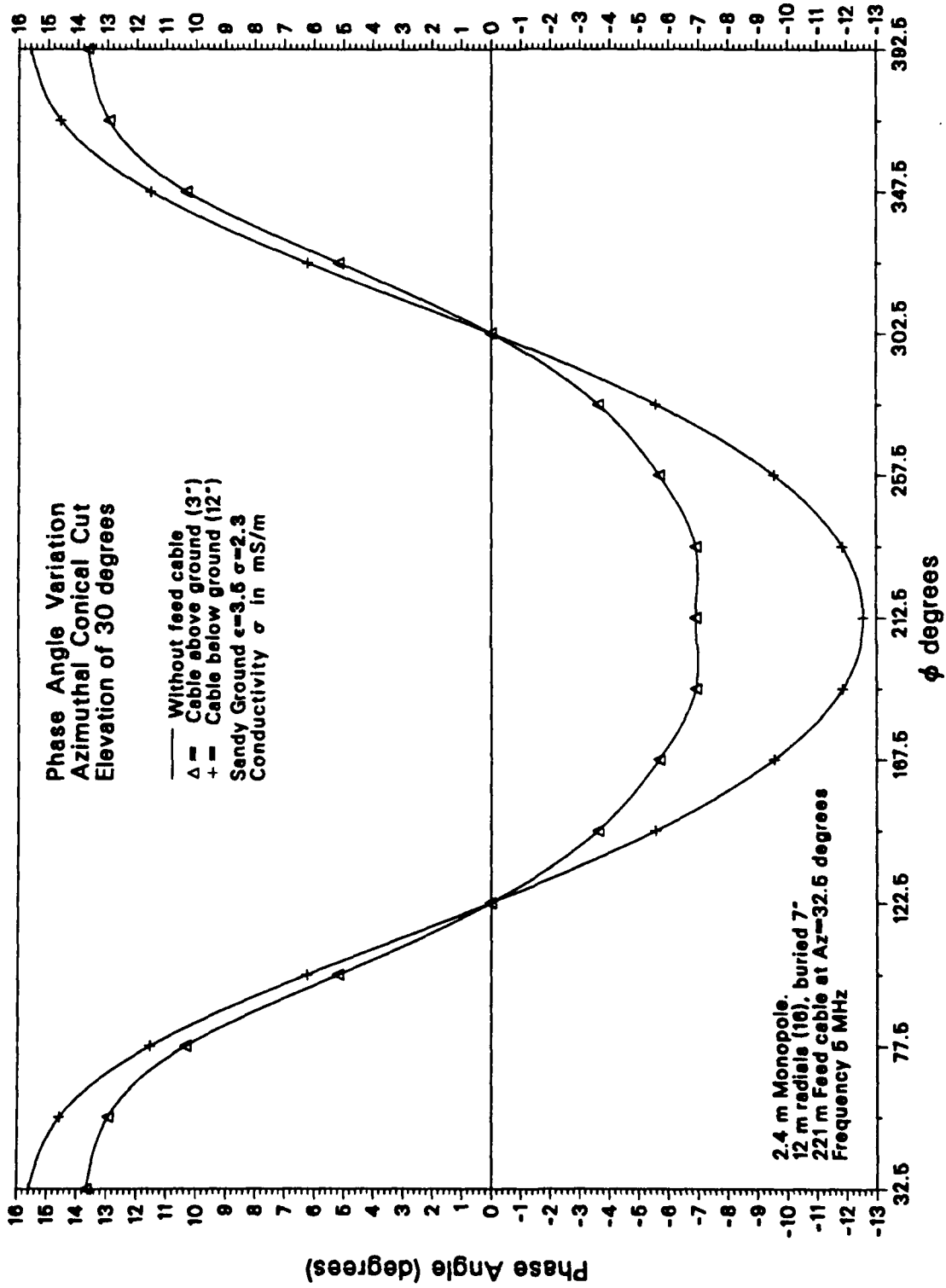


Figure 44. Azimuthal Variation of Cable Effects on Radiation Field Phase at 30° Elevation, for 2.4 Meter Monopole on Sandy Soil

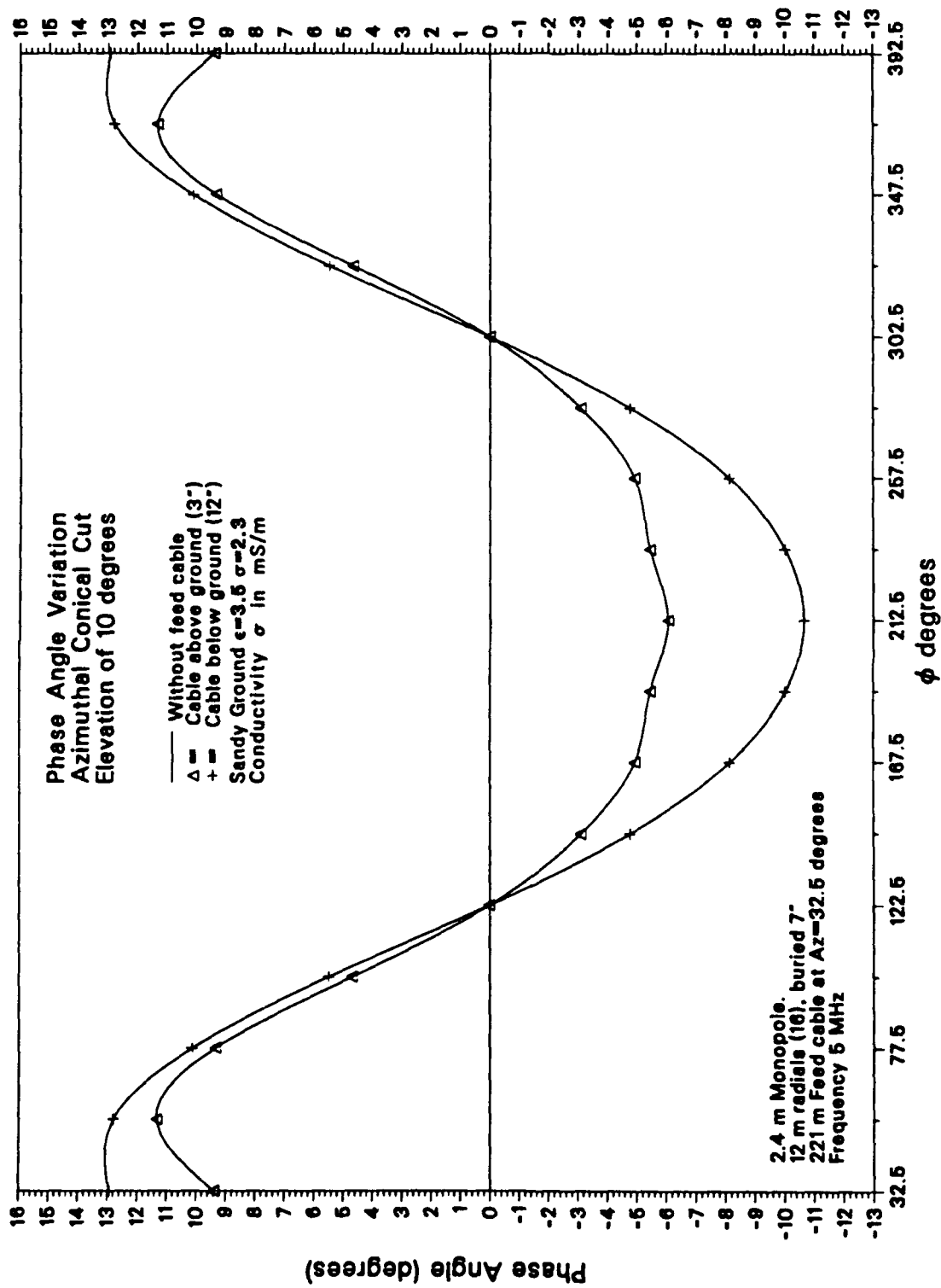


Figure 45. Azimuthal Variation of Cable Effects on Radiation Field Phase at 10° Elevation, for 2.4 Meter Monopole on Sandy Soil

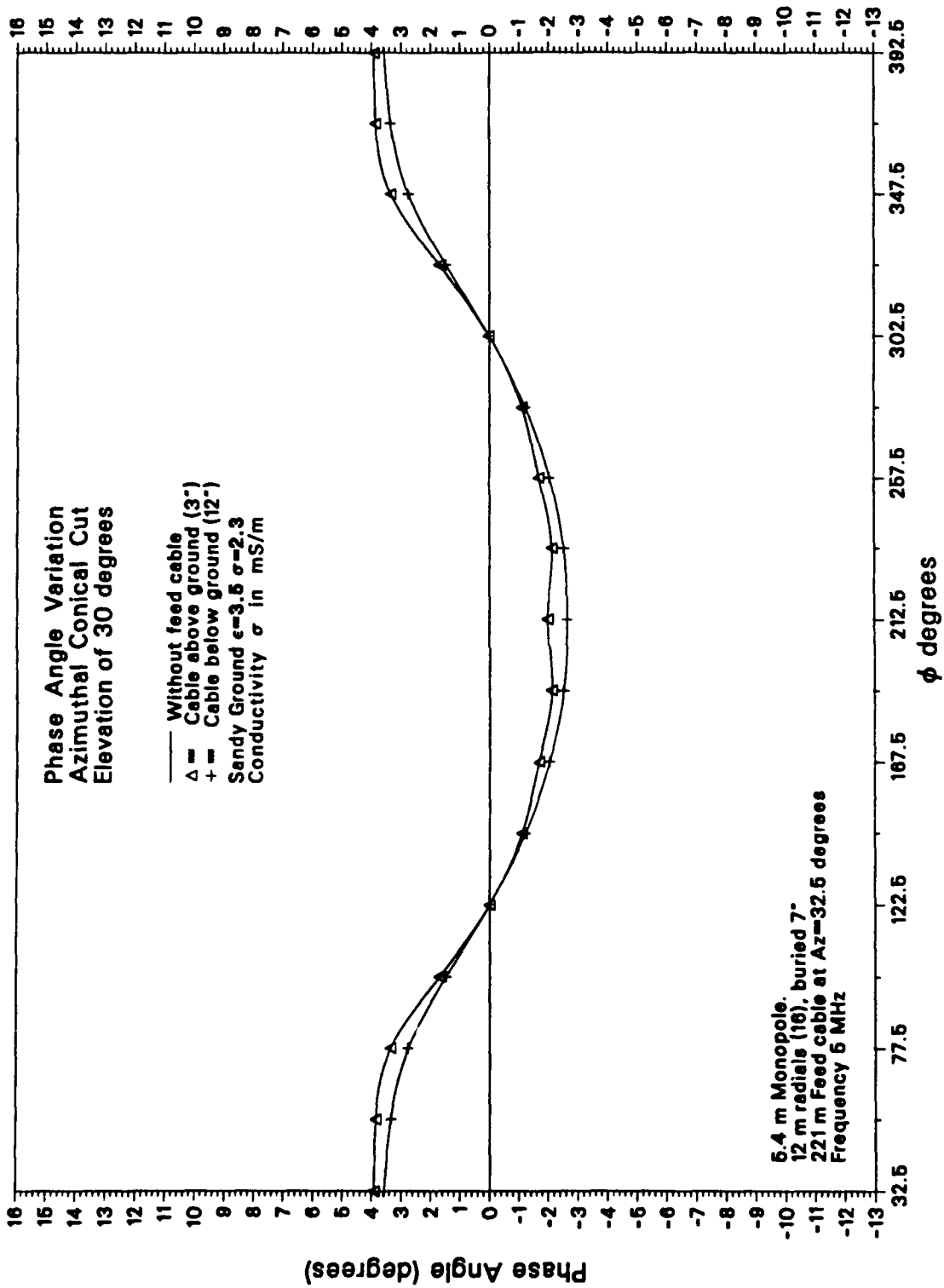


Figure 46. Azimuthal Variation of Cable Effects on Radiation Field Phase at 30° Elevation, for 5.4 Meter Monopole on Sandy Soil

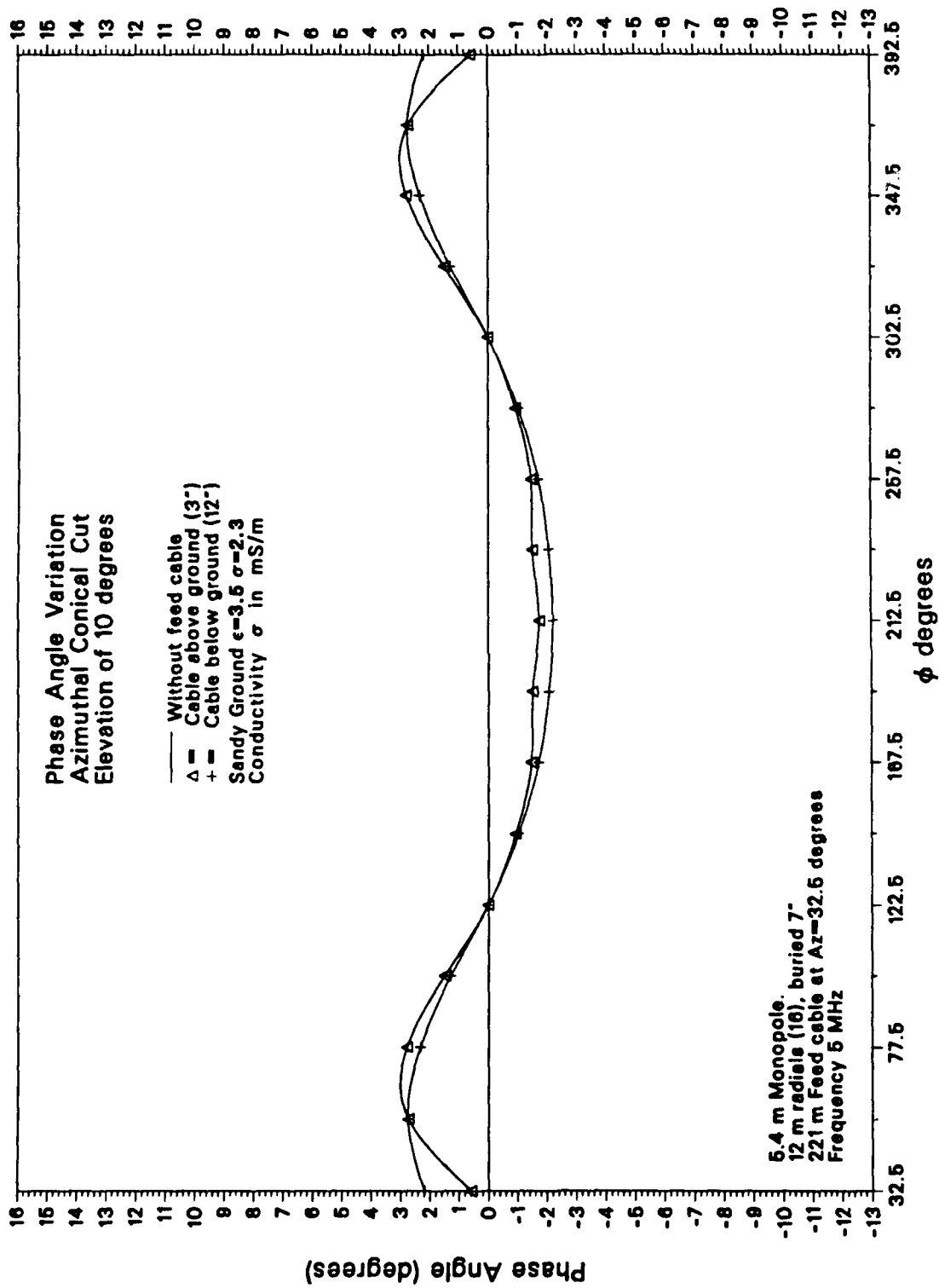


Figure 47. Azimuthal Variation of Cable Effects on Radiation Field Phase at 10° Elevation, for 5.4 Meter Monopole on Sandy Soil

only negligible departures in phase angle of approximately +4 electrical degrees to -2.5 electrical degrees from omnidirectional constant phase behavior, at 30° elevation, for both the unburied and buried cable conditions. These phase variations, in effect, translate the antenna phase center slightly away from the monopole and along the cable direction. For 5.4 m and taller monopoles, the amount of phase center shift is negligibly small.

4.4.2.3 Directivity and Phase Effects versus Frequency

The variations in directivity and radiation phase can also be expressed in terms of front-to-back and front-to-side differences in directivity (dB) and radiation field phase (degrees), at various elevation angles, to note the degree of departure from the omnidirectional azimuth behavior of an isolated monopole. These directivity and phase differences, for both 2.4 m and 5.4 m monopoles and unburied and buried cable conditions, are tabulated in tables 18 and 19, respectively, together with absolute directivity values at three HF band frequencies: 5 MHz, 15 MHz, and 25 MHz, and two elevation angles: 30° and 10°. Examination of the tables reveals that the directivity pattern distortion effects become less pronounced at higher frequencies, and can be reduced at all frequencies by burying the cable and increasing the height of the monopole. Phase variations also become less pronounced at higher frequencies, but may even increase slightly with cable burial. However, phase variations can also be reduced to insignificant levels at all frequencies by increasing the monopole height to values such as 5.4 m or higher. The right-most section of table 19 for the 5.4 m monopole also illustrates that the directivity and phase effects are relatively insensitive to burial depth for practical burial depths.

4.4.2.4 Effects of Miscellaneous Parameters

Analyses were also conducted on the effects of cable length, cable depth, presence of insulating jacket, number of ground screen radials, soil electrical properties, and the amount of cable left unburied.

Cable Length: It was found that the pattern effects quickly become independent of cable length. Therefore, cable sections closest to the antenna count the most, since they are the major contributors to the pattern asymmetries. This can be readily illustrated by observing the buried (dashed) and unburied (solid) cable current behavior at 5 MHz in figures 48 and 49 for the 2.4 m and 5.4 m monopoles, respectively. The figures show that, for representative sandy soil conditions, the undesired current on the buried cable is attenuated by more than 20 dB within the first 20 m to 30 m from the antenna. In fact, even the current on the unburied cable is attenuated by greater than 20 dB within the first 80 m to 100 m from the antenna. The observed oscillatory current behavior at the end of the unburied cable is due to the standing wave generated by the "open circuit," unterminated end of the insulated wire that was used to model the unburied cable. The rapid current attenuation behavior also helps to explain why significant pattern asymmetries, similar in magnitude to those expected for a *totally unburied* cable, have been observed experimentally (and analytically) for the 2.4 m monopole when as little as 15 m to 23 m (50 to 75 ft) of the 221 m (725 ft) feed cable were left unburied at the antenna end of the cable [18].

Representative plots of the currents flowing in the 12 meter long radial wires have also been included in figures 48 and 49, for convenient reference. They represent the currents flowing

IL3125-1

Table 18. Directivity and Phase Variation for 2.4m Monopole with Buried and Unburied Feed Cable versus Frequency for Sandy Soil Condition ($\epsilon_r = 3.5, \sigma = 2.3$ millisiemens/m)

Freq (MHz)	Elev Angle (°)	Without Cable D (dB)	Unburied 221m Feed Cable 0.075m (3in) Above Ground						Buried 221m Feed Cable 0.305m (12in) Deep					
			D(dB)			$\Delta\phi$ (°)			D(dB)			$\Delta\phi$ (°)		
			F	F-B	F-S	F-B	F-S	F	F-B	F-S	F-B	F-S	F	F-B
5	30	5.0	7.3	3.4	3.3	-20.6	-13.7	5.8	1.0	1.4	-28.2	-15.6		
	10	1.3	4.1	3.9	3.7	-15.5	-9.4	2.0	1.1	1.4	-23.6	-12.9		
15	30	5.1	5.9	1.2	1.3	-4.5	-2.9	5.2	0.1	0.2	-4.7	-3.3		
	10	0.5	2.3	1.9	2.1	-0.9	-0.6	0.8	0.3	0.4	-4.1	-3.2		
25	30	5.3	6.6	1.7	1.6	-0.8	0.7	5.7	0.5	0.5	-2.3	-1.9		
	10	1.4	3.4	2.4	2.4	2.9	3.8	1.8	0.6	0.6	-2.1	-2.0		

F = Front Value (In Azimuth Direction of Cable)
 B = Back Value (At 180° to Azimuth of Cable)
 S = Side Value (At 90° to Azimuth of Cable)

For 2.4m High Monopole with 12m Radius Ground Screen of 16 Radials and 221m Feed Cable of Radius 7 mm with 1 mm Thick Jacket

Table 19. Directivity and Phase Variation for 5.4m Monopole with Buried and Unburied Feed Cable versus Frequency for Sandy Soil Condition ($\epsilon_r = 3.5, \sigma = 2.3$ millisiemens/m)

Freq (MHz)	Elev Angle (°)	5.4m Monopole No Cable D (dB)	Unburied 221m Feed Cable 0.075m (3in) Above Ground					Buried 221m Feed Cable 0.305m (12in) Deep					Buried 221m Feed Cable 0.457m (18in) Deep							
			D(dB)		ΔD(dB)		Δφ (°)		D(dB)		ΔD(dB)		Δφ (°)		D(dB)		ΔD(dB)		Δφ (°)	
			F	F-B	F-S	F-B	F-S	F-B	F-S	F	F-B	F-S	F-B	F-S	F	F-B	F-S	F-B	F-S	
5	30	5.1	6.2	1.6	1.6	-5.9	-4.9	5.4	0.6	0.6	-6.2	-3.6	5.4	0.5	0.5	-5.6	-3.3			
	10	1.4	2.8	1.9	1.8	-2.3	-0.6	1.8	0.6	0.6	-4.4	-2.2	1.8	0.6	0.6	-4.0	-2.1			
15	30	5.1	6.0	1.0	1.0	-2.0	-1.5	5.4	0.4	0.4	-1.2	-1.2	5.3	0.3	0.3	-1.3	-1.4			
	10	1.1	2.6	1.6	1.7	0.8	1.1	1.5	0.6	0.5	-1.0	-1.1	1.5	0.5	0.4	-1.4	-1.5			
25	30	5.5	6.2	0.9	0.9	-4.2	-3.6	5.7	0.3	0.3	-2.6	-2.7	5.6	0.2	0.1	-2.4	-2.5			
	20	5.9	6.9	1.2	1.2	-3.2	-2.9	6.1	0.4	0.3	-2.4	-2.5	6.0	0.2	0.2	-2.3	-2.5			
	10	3.3	4.7	1.5	1.5	-1.8	-1.7	3.6	0.5	0.4	-2.4	-2.5	3.5	0.3	0.3	-2.5	-2.6			

F = Front Value (In Azimuth Direction of Cable)
 B = Back Value (At 180° to Azimuth of Cable)
 S = Side Value (At 90° to Azimuth of Cable)

For 5.4m High Monopole with 12m Radius Ground Screen of 16 Radials and 221m Feed Cable of Radius 7 mm with 1 mm Thick Jacket

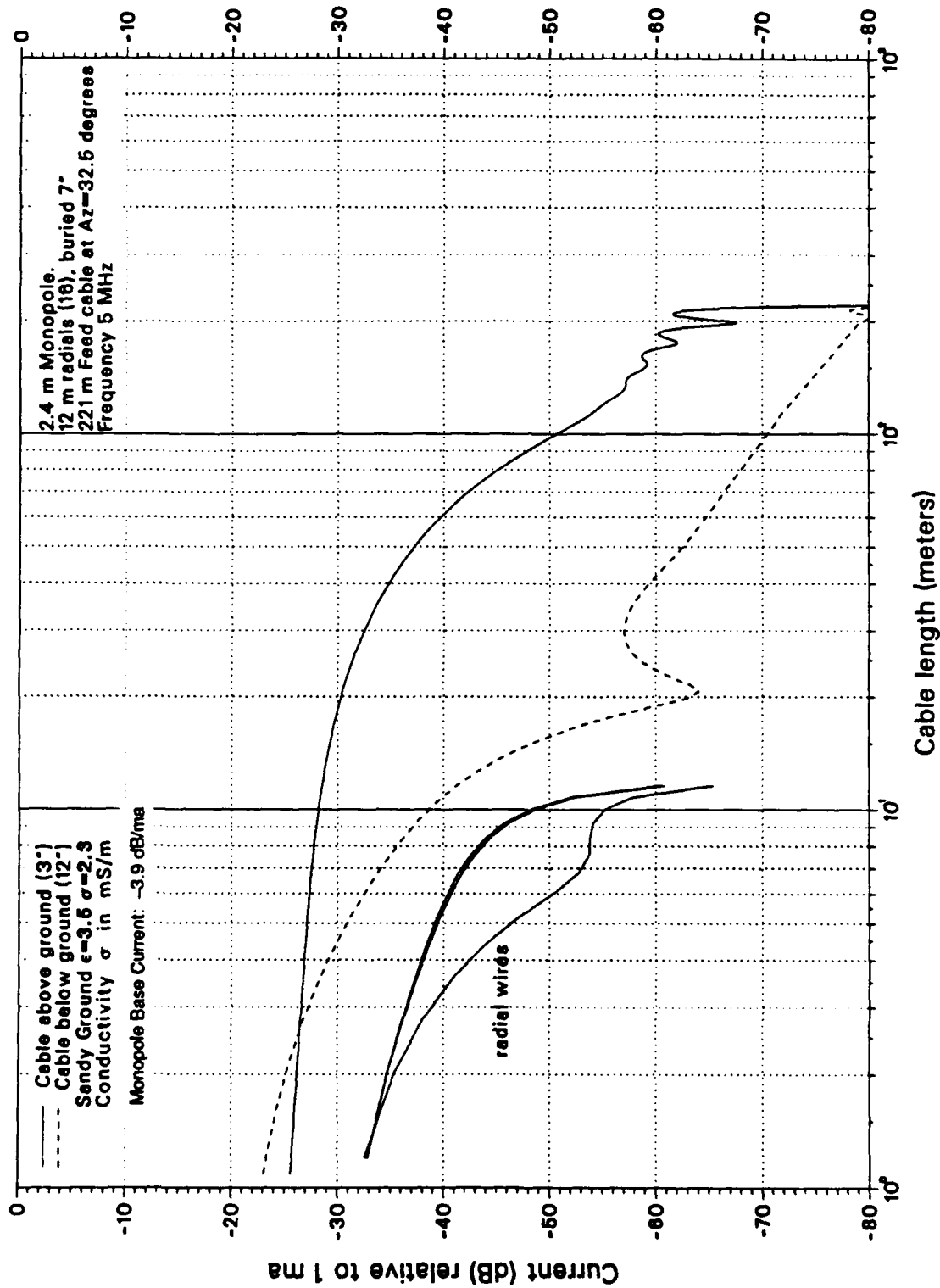


Figure 48. Cable External Current versus Distance from Antenna, for Buried and Unburied Cable Feeding 2.4 Meter Monopole on Sandy Soil at 5 MHz

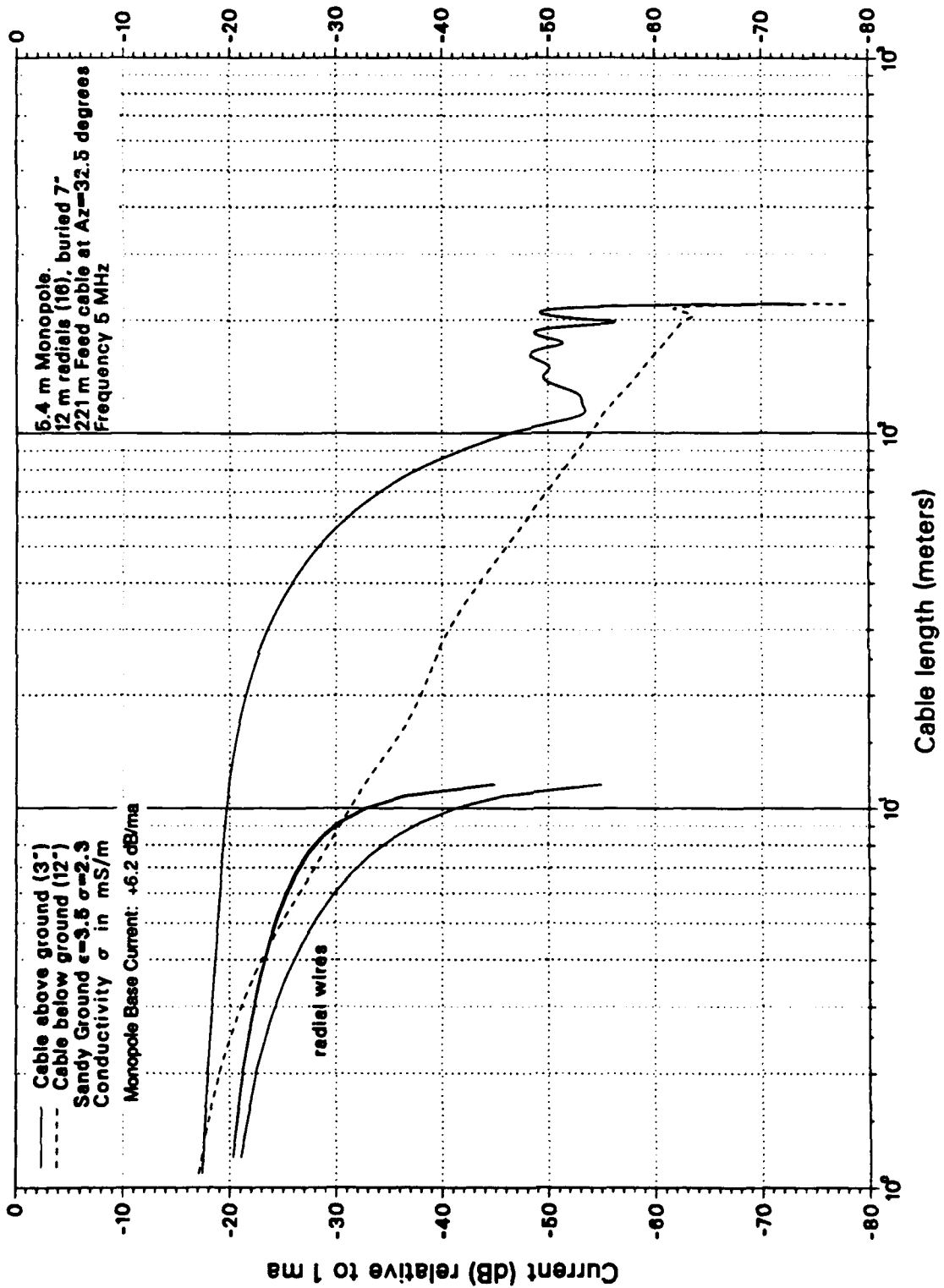


Figure 49. Cable External Current versus Distance from Antenna, for Buried and Unburied Cable Feeding 5.4 Meter Monopole on Sandy Soil at 5 MHz

in the radial closest to the cable (22.5°), the radial approximately perpendicular to the cable (112.5°), and in the one nearly opposite in direction to the cable (202.5°); for the unburied (above ground) cable case. The current deficit in the closest (22.5°) radial is due to the influence of the cable. The ground radial currents for the buried (below ground) cable case are nearly identical to those for the unburied cable, with the exception that the current deficit in the closest radial is markedly decreased.

Cable Depth: The attenuation rates of the external current on buried cables, and the associated radiation pattern effects, were found to be essentially independent of cable depth for the 0.178 m (7 in) to 0.457 m (18 in) burial depths examined; thereby indicating that significant current attenuation benefits can be achieved by just burying the cable at shallow depths significantly less than a skin depth in the ground. In the HF band, the external cable currents "bleed off" into the surrounding conducting ground over a relatively short length of cable, whether the cable has a thin insulating jacket around it or it is kept bare. This occurs because the jacket presents a low impedance path to ground at HF, as opposed to the high impedance path it becomes at low frequency (LF) and very low frequency (VLF), where jacketing is purposely used to maintain high current levels on long wire buried antennas.

Soil Electrical Properties: As the soil degenerates to an extremely dry condition, its conductivity can decrease significantly below the representative sandy soil value of 2.3 millisiemens/m, so that the soil will eventually become a low loss, low permittivity dielectric. In this case, the pattern distortion effects should approach those of either an unburied cable or a cable in free space. Analyses to date indicate that undesired adverse behavior for a buried cable will first become apparent at the low end of the frequency band around 5 MHz. The increase in undesirable effects for buried cables, should not occur until the ground becomes dry enough that the conductivity decreases at least to values approaching $\sigma = 0.15$ millisiemens/m, for the very dry ground condition, and lower.

For the very dry ground, soil condition and a frequency of 5 MHz, attenuation of the external currents on buried cable becomes less severe, thereby causing variations in directivity to increase somewhat. Table 20 reveals that the front-to-back variation in directivity, for the 5.4 m high monopole with a buried cable, increases to -2.3 dB and -1.6 dB at 30° and 10° elevation, respectively, versus the single value of +0.6 dB at both angles for the sandy soil condition ($\sigma = 2.3$ millisiemens/m). Furthermore, the negative sign of the variation indicates that the "bulge" distortion in the directivity pattern is no longer centered on the azimuth direction of the cable, as in section 4.4.2.1, but becomes centered around 180° to the cable azimuth direction, for the low conductivity, very dry ground condition. Table 21 shows that the taller 6.3 m final design monopole produces lower variation levels of -1.6 dB and -1.0 dB at 30° and 10° elevation, respectively.

It can also be seen from tables 20 and 21 that burying the cables in very dry soil does not produce appreciably different behavior at 5 MHz from that obtained for an unburied cable. However, these values of directivity variation are still acceptably small for the pseudo-random phased array Texas application. The associated phase variations in the radiation field are more critical, since they affect the beamforming ability of a phased array. Examination of tables 20 and 21 reveals that these phase variations also remain negligibly small for both the 5.4 m and 6.3 m monopoles.

HL3123-1

Table 20. Directivity and Phase Variation for 5.4m Monopole with Buried and Unburied Feed Cable versus Frequency for Very Dry Ground Condition ($\epsilon_r = 4, \sigma = 0.15$ millisiemens/m)

Freq (MHz)	Elev Angle (°)	5.4m Monopole No Cable D (dB)	Unburied Cable 0.075m (3in) Above Ground						Buried Cable 0.305m (12in) Deep						Buried Cable 0.457m (18in) Deep					
			D(dB)		$\Delta\phi$ (°)		D(dB)		$\Delta\phi$ (°)		D(dB)		$\Delta\phi$ (°)		D(dB)		$\Delta\phi$ (°)			
			F	F-B	F-S	F-S	F	F-B	F-S	F-S	F	F-B	F-S	F-S	F	F-B	F-S	F-S		
5	30	5.1	3.7	-2.3	-1.3	-10.6°	-10.6°	3.7	-2.3	-1.3	-6.6°	-7.2°	3.9	-2.0	-1.1	-5.6°	-5.9°			
	10	0.9	0.2	-1.4	-0.6	-9.5°	-9.7°	0.0	-1.6	-0.8	-5.9°	-6.5°	0.2	-1.4	-0.7	-5.1°	-5.4°			
15	30	5.3	6.2	0.9	1.2	-5.1°	-4.2°	5.5	0.3	0.3	-0.8°	-2.0°	5.5	0.3	0.3	-0.8°	-2.1°			
	10	2.0	3.4	1.5	1.8	-3.9°	-3.6°	2.2	0.5	0.4	-1.3°	-2.4°	2.1	0.5	0.4	-1.5°	-2.6°			
25	30	5.3	5.9	0.6	0.7	-4.5°	-4.1°	5.5	0.2	0.2	-3.6°	-3.6°	5.3	0.0	0.0	-3.3°	-3.4°			
	20	5.9	6.7	0.9	1.0	-3.9°	-4.0°	6.1	0.3	0.2	-3.4°	-3.5°	5.9	0.1	0.1	-3.3°	-3.4°			
	10	3.4	4.6	1.2	1.3	-3.4°	-3.6°	3.7	0.4	0.3	-3.5°	-3.6°	3.6	0.2	0.1	-3.6°	-3.6°			

F = Front Value (In Azimuth Direction of Cable)
 B = Back Value (At 180° to Azimuth of Cable)
 S = Side Value (At 90° to Azimuth of Cable)

For 5.4m High Monopole with 12m Radius Ground Screen of 16 Radials and 221m Feed
 Cable of Radius 7 mm with 1 mm Thick Jacket

IL3122-1

Table 21. Directivity and Phase Variation for 6.3m Monopole with Buried and Unburied Feed Cable versus Frequency for Very Dry Ground Condition ($\epsilon_r = 4, \sigma = 0.15$ millisiemens/m)

Freq (MHz)	Elev Angle (°)	6.3m Monopole No Cable D (dB)	Unburied Cable 0.075m (3in) Above Ground						Buried Cable 0.305m (12in) Deep						Buried Cable 0.457m (18in) Deep					
			D(dB)		ΔD(dB)		Δφ (°)		D(dB)		ΔD(dB)		Δφ (°)		D(dB)		ΔD(dB)		Δφ (°)	
			F	F-B	F-S	F-B	F-S	F-S	F	F-B	F-S	F-B	F-S	F-S	F	F-B	F-S	F-B	F-S	F-S
5	30	5.1	4.1	-1.7	-1.0	-8.6°	8.9°	4.2	-1.6	-0.8	-5.6°	-6.1°	4.3	-1.4	-0.8	-5.3°	-5.2°			
	10	0.9	0.6	-0.9	-0.3	-8.0°	-8.2°	0.4	-1.0	-0.4	-4.9°	-5.3°	0.5	-0.9	-0.4	-4.4°	-4.7°			
15	25	5.5	6.3	0.9	1.2	-5.3°	-4.5°	5.7	0.4	0.4	-1.1°	-2.2°	5.6	0.4	0.3	-1.0°	-2.2°			
	10	2.3	3.6	1.5	1.7	-4.2°	-3.9°	2.5	0.5	0.5	-1.5°	-2.5°	2.4	0.5	0.4	-1.6°	-2.7°			
25	30	5.0	5.1	0.1	0.1	-4.8°	-4.8°	4.9	-0.1	-0.1	-2.8°	-2.8°	4.8	-0.2	-0.2	-2.2°	-2.2°			
	20	6.0	6.5	0.4	0.4	4.7°	-5.0°	6.1	0.0	0.0	-2.9°	-3.0°	6.0	-0.1	-0.1	-2.6°	-2.6°			
	10	4.0	4.8	0.8	0.8	4.5°	4.8°	4.1	0.1	0.1	-3.1°	-3.2°	4.0	0.0	0.0	-3.0°	-3.0°			

F = Front Value (In Azimuth Direction of Cable)
 B = Back Value (At 180° to Azimuth of Cable)
 S = Side Value (At 90° to Azimuth of Cable)

For 6.3m High Monopole with 12m Radius Ground Screen of 16 Radials and 221m Feed Cable of Radius 7 mm with 1 mm Thick Jacket

Additional Current Suppression: The above predicted small increases in directivity and phase variation, as the soil conductivity decreases, can be even less severe in practice. Namely, laboratory measurements have shown that the lossy spirally wound steel armor of the selected, coaxial feed cable will introduce an additional attenuation rate, ranging from about 0.5 to 1 dB/100 ft, to the undesired external cable currents, from 5 to 30 MHz, respectively. Further suppression of the external cable currents could be achieved, if required, at some moderate expense and inconvenience, by periodically loading the higher current section of the feed cable, located within approximately 100 meters of the antenna, with closely spaced ferrite toroidal cores, as done on some antenna pattern ranges to reduce the undesired effects of stray cable currents.

Number of Radials: Pattern distortions were also found to increase substantially as the number of ground radials was reduced from 16 to 6. This result is not surprising because, as the number of ground radials is reduced, a greater fraction of the ground screen current will be allowed to flow along the extended feed cable. Thus, a ground screen of 16 radials appears to provide satisfactory performance from the standpoints of system internal noise figure, directivity, and cable-based pattern distortion.

Lightning Protection Ground Rods: Each monopole antenna will also be equipped with four buried 10-foot, vertical ground rods (one per quadrant, connected to, but installed 10 feet from the monopole base) for lightning protection. Therefore, an additional NEC-3I run was made for the case of the 5.4 m thin monopole with its 12 meter radius, 16 radial ground screen, and 221 m feed cable, but also equipped with the selected configuration of four ground rods. The results verify that the effect of these ground rods on antenna HF performance is negligible.

4.4.3 Summary of Cable Effects

Radiation pattern effects caused by the presence of a coaxial feed cable have been investigated theoretically as a function of frequency, cable length, burial condition and jacketing, monopole height, and electrical properties of the soil. Adverse effects on radiation pattern directivity and phase increase if the cable is left unburied, or if the antenna becomes shorter, the radials fewer, and the frequency lower, in the HF band. Such effects are independent of typical cable-insulating jackets, weakly dependent on cable lengths beyond about 25 to 50 meters long, and weakly dependent upon burial depth and soil conductivity for most soils. Undesired pattern effects can become modestly more pronounced, even for buried cables, if the soil becomes so dry that the soil electrical conductivity decreases to around 0.15 millisiemens/m and lower. However, even these effects typically fall within acceptable bounds for the pseudo-random array application.

Overall, the investigation results indicate that the expected, undesirable pattern effects for the final antenna/cable design configuration, (consisting of a 6.3 m high, monopole tower, with its 12 meter radius ground screen of 16 buried radials and long coaxial feed cable buried at a depth of 0.305 to 0.457 m (12 to 18 inches)) in *sandy soil*, will be small, acceptable, and not adversely affect array performance. If the soil should, on occasion, approach a *very dry ground* condition or worse, the front to back variations in directivity are predicted to increase somewhat, but remain within acceptable limits, even at the worst frequency of 5 MHz; while the phase variations, which are more critical, are predicted to remain negligibly small. An additional external current attenuation of about 0.5 to 1 dB/100 ft introduced by the spirally

wound, lossy, steel armor of the selected feed cable, will moderate any increase in undesired directivity effects under such unfavorably dry soil conditions. Some concerns have also been expressed regarding potential parasitic pattern effects caused by cables feeding other monopole antennas. These effects are considered negligible, since cables directly connected to monopoles produce only acceptably small effects, and the nearest adjacent cables have been constrained to be greater than 100 meters from any monopole.

4.5 ELECTRONICS SHELTER EFFECTS ON RADIATION PATTERN

As stated in section 2.2.2, metal objects, such as the 20x8x8 ft electronics shelters located at each of the three nodes, will scatter energy radiated by or incident upon the antennas. Thus, shelters may introduce asymmetrical modifications to the directivity and phase patterns of the antennas, depending on the relative size of the shelters and distance from the antennas. The potential seriousness of any such shelter effects was evaluated by using NEC-3 computer software to model a monopole antenna having a radial-wire ground plane, both with and without the presence of a nearby electronics shelter. Computer runs were undertaken for both broadside and endfire orientations of the shelter, for several operating frequencies and representative distances of the shelter from the antenna. The associated gains and phases of the radiation patterns were compared with values for the monopole antenna in the absence of the shelter.

4.5.1 Geometry, Parameters, and NEC-3 Model

Figure 50 presents the coordinate geometry for the monopole antenna, its radial ground screen, and an electronics shelter. The asymmetric geometry of the antenna and shelter combination requires the use of NEC-3, rather than NEC-GS software. As in the feed cable analysis, the constraint concerning the wire segment length-to-diameter ratio, discussed in 3.3, requires that the triangular cross-section antenna tower of figure 2 be approximated by a thinner, solid monopole element of height, h , with reduced radius, b , and a short vertical excitation segment at its base. Use of this reduced monopole radius does not detract from the assessment of shelter effects on the monopole radiation pattern.

As indicated in figure 50, the thin monopole is placed above a ground screen consisting of $M = 6$, equally spaced, radial wires of length, a , and radius, b_w , which are located at a depth, z_0 , below a flat earth surface. To account for the currents induced on the conducting surface of the shelter, and estimate their corresponding effects on the antenna radiation pattern, the shelter surface is modeled as a wire structure consisting of a number K of identical concentric wire rectangles, displaced from the monopole by a distance, D , along the y -axis. Figure 50 depicts the broadside orientation of the shelter, where the length dimension of the shelter is perpendicular to, and bisected by, the y -axis. The endfire orientation (not shown) of the shelter has the long dimension aligned parallel to the y -axis, with the y -axis bisecting the shelter width dimension. To account for the shelter's footing on the ground, the shelter base has been placed 0.05 m (2in) beneath the surface of the ground.

IL3062-1

6 Radials, 12 Meters Long, Buried 0.78m (7in) Deep

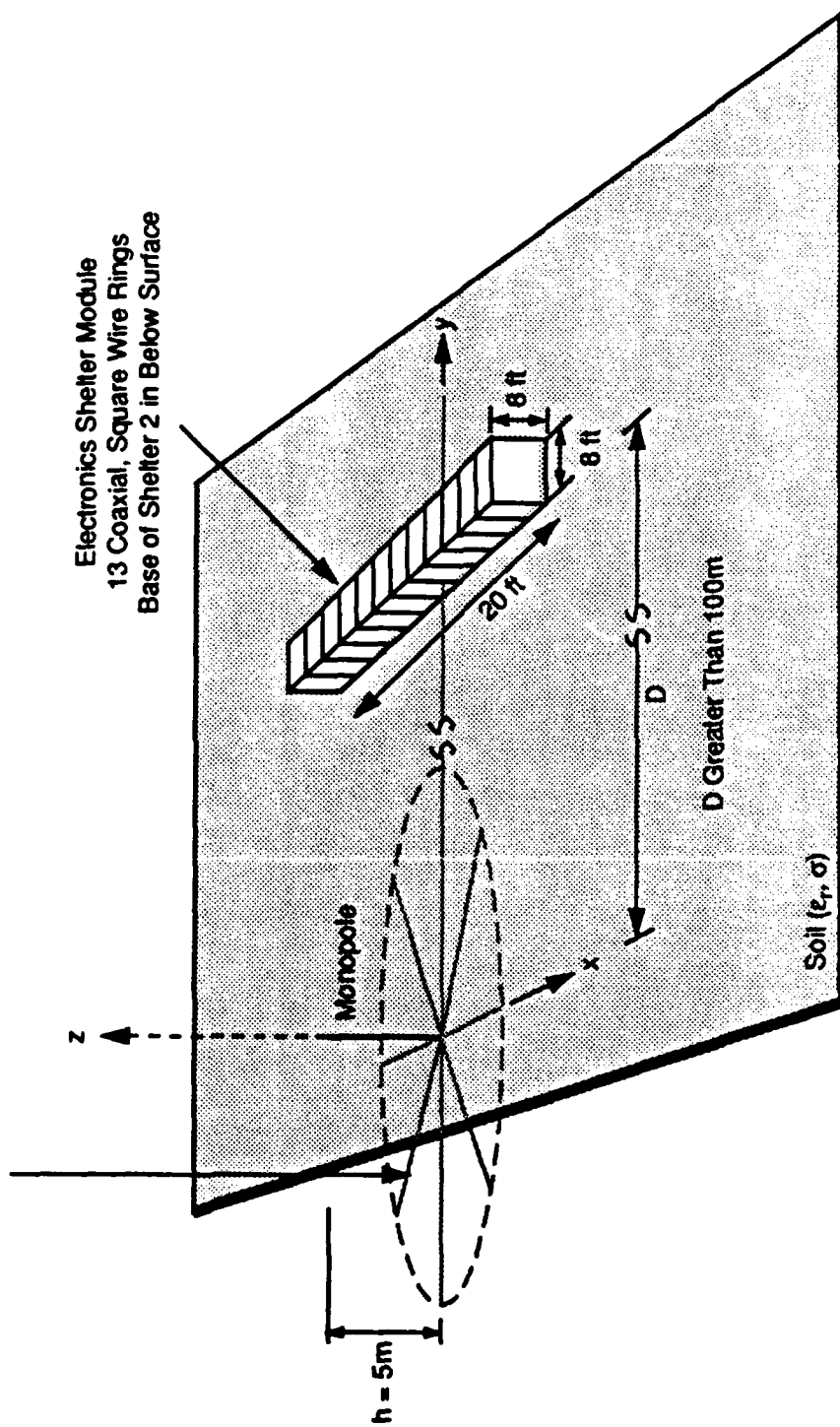


Figure 50. Coordinate Geometry for Investigation of Antenna Pattern Effects Due to Presence of Electronics Shelters at Nodes

The monopole is vertical, so the vertical component of the incident electric field is of primary interest; therefore, the concentric wire rectangles of the NEC-3 model are vertically oriented in planes parallel to the y - z plane. Figure 50 shows the broadside configuration of 13, $2.5\text{ m} \times 2.55\text{ m}$, vertical wire rectangles spaced 0.5 m apart. The 0.5 m spacing, and the predominant 0.5 m wire segment length, are both less than one-tenth wavelength at the highest operating frequency. NEC-3 runs for the broadside configuration confirmed the expectation of negligibly small differences in results between shelter models that connected all the wire rectangles, by means of horizontal wires passing through the rectangle corners, and ones that completely omitted the connecting wires. Therefore, subsequent analyses for both broadside and endfire shelter configurations were conducted without connecting wires.

The earth or ground material is characterized, as before, by the conductivity, σ , in millisiemens/m and relative dielectric constant, ϵ_r . The quantities x , y , z , and r , θ , ϕ are the conventional Cartesian and spherical coordinates, respectively, and ψ is the elevation angle measured from the horizon. The monopole element, radial wire conductors, and wire structure representing the shelter, are all constrained to have infinite conductivity.

The specific NEC-3 wire geometry used to model the thin monopole, its radial wire ground screen, and the shelter is described below. The monopole consists of a vertical wire section of height, h , and radius, b . As in the feed cable analysis, the vertical wire section for the thin monopole is centered on the z -axis, not displaced from it. Only six radials were used for this model, to simplify the geometry and conserve the total number of segments and computation time. Each of the six radials consists of a mostly horizontal wire section of radius, b_w , which begins at the base of the monopole wire section with a short downward-sloping transition section, and continues horizontally to a radial distance, a , at a depth, z_0 , beneath the surface.

The shelter is modelled by concentric wire rectangles each consisting of six wire sections, each of wire radius b_c . The broadside configuration in figure 50 consists of 13 rectangles parallel to the y - z plane, each having four 2.5 m wire sections. One of the two horizontal 2.5 m sections is a buried wire connected at each end to two short vertical wire sections 0.05 m long that connect to the two vertical 2.5 m sections at the ground surface. The endfire configuration consists of six rectangles parallel to the y - z plane, each having two horizontal wire sections 6 m long, one of which is a buried wire connected at each end to two short vertical wire sections 0.05 m long that connect to the two vertical 2.5 m wire sections of the rectangle at the ground surface. Each of the wire sections of the antenna, ground radials, and shelter is, as before, suitably divided into wires and subdivided into wire segments, N_i , according to the guidelines in section 3.3 where i denotes the i -th wire. As in the NEC-3I cable analysis, NEC-3 requires that each of the six individual ground radial wires, with their associated coordinates and numbers of wire segments, must be individually specified. All shelter wire segments were constrained to be 0.5 m long, with the exception of the short 0.05 m vertical buried segments. The structure is modelled in NEC-3 by specifying one of the rectangles, which is then repeated K times with 0.5 m spacing via translation, and then translating the whole wire structure, defined originally as centered on the origin, along the y -axis by the desired separation distance D . The associated wire model coordinates and parameters are presented in table 22.

IL3120-1

Table 22. NEC-3 Wire Model and Parameters for Shelter Effects Analysis**a) Wire Model Dimensions**

Monopole Height (h)	5.0m	(16.4ft)
Monopole Wire Filament Radius (b)	0.01m	(0.39in)
Excitation (Feed) Section Length (l_c)	0.5m	(19.7in)
Ground Wire Radial Extent (a)	12.0m	(39.4ft)
Ground Wire Radius (b_w)	0.01m	(0.39in)
Ground Wire Burial Depth (z_o)	-0.05m	(-2.0in)
Number of Radials (M)	6	6
Shelter Vertical Height (h_s)	2.5m	(8.2ft)
Shelter Length (L_s)	6.0m	(19.7ft)
Shelter Width (W_s)	2.5	(8.2ft)
Shelter Base Depth Below Surface (z_s)	-0.05m	(-2.0in)
Shelter Wire Filaments Radii (b_s)	0.01m	(0.39in)
Shelter Distance from Monopole (D)	100, 200m	(328, 656ft)
Shelter Orientation – Broadside	Centered on and Perpendicular to y-axis	
– Endfire	Centered on and Parallel to y-axis	

b) Soil Characteristics Sandy Soil; $\epsilon_r = 3.5$, $\sigma = 2.3$ millisiemens/m

c) Frequencies 5, 15, 25 MHz

IL3121-1

**Table 22. NEC-3 Wire Model and Parameters for Shelter Effects Analysis
(Concluded)**

d) Wire Model Coordinates (meters) and Wire Segmentation

Monopole – 5.0m high, 0.01m radius

Vertical Wire – Section 1 $x_1 = 0.0, y_1 = 0.0, z_1 = 0.0; x_2 = 0.0, y_2 = 0.0, z_2 = 5.0; N = 10; l = 0.5$
(Includes Excitation Segment at Base)

Ground Screen – 6 Radials, 12m in length, 0.01m radius, -0.05m depth

Radial Wire 1 – Section 1 $x_1 = 0.0, y_1 = 0.0, z_1 = 0.0; x_2 = 0.8, y_2 = 0.0, z_2 = -0.178; N = 1, l = 0.8$
– Section 2 $x_2 = 0.8, y_2 = 0.0, z_2 = -0.178; x_3 = 12.0, y_3 = 0.0, z_3 = -0.178, N = 14, l = 0.8$

Radial Wires 2 through 16 – Repeat radial wire 1 geometry around monopole, one every 60° with corresponding coordinates

Shelter – 6.0 x 2.5 x 2.55m, Broadside Case – 13 Concentric Wire Rectangles: 2.5 x 2.55m
Endfire Case – 6 Concentric Wire Rectangles: 6.0 x 2.55m

Representative Wire Rectangles

Broadside Case Wires – This 2.5 x 2.55 rectangle is then repeated 12 times by translating it in the -x direction in 0.5m steps. Then the whole structure is translated in the +y direction to the desired distance D from the monopole.

- Section 1 $x_1 = 3.0, y_1 = 1.25, z_1 = 0.0; x_2 = 3.0, y_2 = 1.25, z_2 = 2.5; N = 5, l = 0.5$
- Section 2 $x_1 = 3.0, y_1 = 1.25, z_1 = 2.5; x_2 = 3.0, y_2 = -1.25, z_2 = 2.5; N = 5, l = 0.5$
- Section 3 $x_1 = 3.0, y_1 = -1.25, z_1 = 2.5; x_2 = 3.0, y_2 = -1.25, z_2 = 0; N = 5, l = 0.5$
- Section 4 $x_1 = 3.0, y_1 = -1.25, z_1 = 0; x_2 = -3.0, y_2 = -1.25, z_2 = -0.05; N = 1, l = 0.05$
- Section 5 $x_1 = 3.0, y_1 = -1.25, z_1 = -0.05; x_2 = 3.0, y_2 = 1.25, z_2 = -0.05; N = 5, l = 0.5$
- Section 6 $x_1 = 3.0, y_1 = 1.25, z_1 = -0.05; x_2 = 3.0, y_2 = 1.25, z_2 = 0; N = 1, l = 0.05$

Endfire Case Wires – This 6.0 x 2.55 rectangle is then repeated 5 times by translating it in the -y direction in 0.5m steps. Then the whole structure is rotated 90° and translated in the +y direction to the desired distance D from the monopole.

- Section 1 $x_1 = 3.0, y_1 = 1.25, z_1 = 0.0; x_2 = 3.0, y_2 = 1.25, z_2 = 2.5; N = 5, l = 0.5$
- Section 2 $x_1 = 3.0, y_1 = 1.25, z_1 = 2.5; x_2 = -3.0, y_2 = 1.25, z_2 = 2.5; N = 12, l = 0.5$
- Section 3 $x_1 = -3.0, y_1 = 1.25, z_1 = 2.5; x_2 = -3.0, y_2 = 1.25, z_2 = 0.0; N = 5, l = 0.5$
- Section 4 $x_1 = -3.0, y_1 = 1.25, z_1 = 0.0; x_2 = -3.0, y_2 = 1.25, z_2 = -0.05; N = 1, l = 0.05$
- Section 5 $x_1 = -3.0, y_1 = 1.25, z_1 = -0.05; x_2 = 3.0, y_2 = 1.25, z_2 = -0.05; N = 12, l = 0.5$
- Section 6 $x_1 = 3.0, y_1 = 1.25, z_1 = -0.05; x_2 = 3.0, y_2 = 1.25, z_2 = 0.0; N = 1, l = 0.05$

4.5.2 Radiation Patterns

Several NEC-3 computer runs were conducted to examine the behavior of the monopole antenna radiation pattern in the presence of a shelter located at a representative distance, D , from the monopole, and in the absence of the shelter. Both broadside and endfire shelter orientations were examined, for representative sandy soil ($\epsilon_r = 3.5$, $\sigma = 2.3$ millisiemens/m) ground conditions, at three representative frequencies, 5, 15, and 25 MHz.

An assessment of the influence of the shelter was performed by comparing the shelter versus no shelter radiation pattern results, specifically, by comparisons of the variations in power gain and phase for the radiated fields, as a function of polar and azimuth angles, frequency, and shelter distance from the monopole, with its 6 radial, 12 meter radius ground screen. Representative results are tabulated in tables 23-25, for the cases of no shelter, broadside shelter at 100 m and 200 m, and endfire shelter at 100 m, at 5, 15, and 25 MHz, respectively.

The tabulated results are for the principal ($\phi = 0^\circ$) y-z elevation plane, containing the monopole and bisecting the shelter, the plane in which adverse pattern effects will be most pronounced, if present at all. Examination of these results reveals that shelter-based pattern effects are negligibly small in all cases, even for the 100 m distance, which is less than half the minimum monopole-to-shelter distance anticipated for the Texas array.

IL3115-1

Table 23. Shelter Effects at 5 MHz on Radiation Pattern Power Gain and Phase, in Principal Elevation Plane Containing 5 Meter Monopole and Bisecting Shelter, versus Frequency, Distance, and Polar Angle

For 5 meter Monopole with 6 Radials 12m Long

Frequency (MHz)	Polar Angle (°)	Azimuth Angle (°)	No Shelter		Endfire Shelter at 100m		Broadside Shelter at 100m		Broadside Shelter at 200m (Expanded Polar Angle Scale)			
			Power Gain (dB)	E _θ Phase (°)	Power Gain (dB)	E _θ Phase (°)	Power Gain (dB)	E _θ Phase (°)	Polar Angle (°)	Azimuth Angle (°)	Power Gain (dB)	E _θ Phase (°)
5	0.00	90.00	-999.99	-105.14	-60.75	56.23	-68.56	58.36	75.00	90.00	-9.21	171.61
	5.00	90.00	-25.78	-178.56	-25.73	-179.44	-25.76	-178.86	76.00	90.00	-9.51	171.10
	10.00	90.00	-19.81	-178.64	-19.75	-178.77	-19.79	-178.65	77.00	90.00	-9.84	170.55
	15.00	90.00	-16.37	-178.77	-16.34	-178.62	-16.37	-178.72	78.00	90.00	-10.22	169.97
	20.00	90.00	-14.00	-178.95	-14.00	-178.78	-14.00	-178.93	79.00	90.00	-10.66	169.35
	25.00	90.00	-12.22	-179.19	-12.24	-179.11	-12.22	-179.22	80.00	90.00	-11.16	168.68
	30.00	90.00	-10.84	-179.50	-10.86	-179.51	-10.84	-179.53	81.00	90.00	-11.75	167.97
	35.00	90.00	-9.76	-179.87	-9.77	-179.93	-9.76	-179.87	82.00	90.00	-12.44	167.20
	40.00	90.00	-8.91	-179.68	-8.91	-179.63	-8.91	-179.71	83.00	90.00	-13.26	166.37
	45.00	90.00	-8.27	-179.13	-8.26	-179.11	-8.27	-179.18	84.00	90.00	-14.25	165.48
	50.00	90.00	-7.81	-178.46	-7.81	-178.47	-7.82	-178.51	85.00	90.00	-15.47	164.51
	55.00	90.00	-7.55	-177.65	-7.55	-177.67	-7.56	-177.67	86.00	90.00	-17.05	163.47
	60.00	90.00	-7.49	-176.65	-7.49	-176.67	-7.50	-176.64	87.00	90.00	-19.18	162.33
	65.00	90.00	-7.67	-175.38	-7.68	-175.40	-7.68	-175.35	88.00	90.00	-22.32	161.09
	70.00	90.00	-8.19	-173.76	-8.19	-173.77	-8.19	-173.71	89.00	90.00	-27.96	159.74
	75.00	90.00	-9.21	-171.62	-9.21	-171.62	-9.21	-171.56	90.00	90.00	-999.99	0.00
80.00	90.00	-11.16	-168.70	-11.16	-168.69	-11.16	-168.64	Only bold values comparable with 100m shelter cases				
85.00	90.00	-15.47	-164.53	-15.47	-164.52	-15.47	164.47					
90.00	90.00	-999.99	0.00	-999.99	0.00	-999.99	0.00					

Table 24. Shelter Effects at 15 MHz on Radiation Pattern Power Gain and Phase, in Principal Elevation Plane Containing 5 Meter Monopole and Bisecting Shelter, versus Frequency, Distance, and Polar Angle

For 5 meter Monopole with 6 Radials 12m Long

Frequency (MHz)	Polar Angle (°)	Azimuth Angle (°)	No Shelter		Endfire Shelter at 100m		Broadside Shelter at 100m		Broadside Shelter at 200m (Expanded Polar Angle Scale)			
			Power Gain (dB)	E _θ Phase (°)	Power Gain (dB)	E _θ Phase (°)	Power Gain (dB)	E _θ Phase (°)	Polar Angle (°)	Azimuth Angle (°)	Power Gain (dB)	E _θ Phase (°)
15	0.00	90.00	-999.99	-151.39	-48.40	147.39	-54.45	176.02	75.00	90.00	-4.67	67.48
	5.00	90.00	-21.52	60.16	-21.66	57.86	-21.49	59.03	76.00	90.00	-4.99	67.32
	10.00	90.00	-15.54	60.57	-15.41	61.37	-15.53	61.07	77.00	90.00	-5.35	67.14
	15.00	90.00	-12.09	61.22	-12.20	61.00	-12.11	60.95	78.00	90.00	-5.76	66.95
	20.00	90.00	-9.70	62.06	-9.62	61.95	-9.67	62.20	79.00	90.00	-6.23	66.73
	25.00	90.00	-7.89	63.02	-7.93	63.30	-7.91	62.97	80.00	90.00	-6.77	66.50
	30.00	90.00	-6.47	64.04	-6.47	63.75	-6.45	64.03	81.00	90.00	-7.39	66.24
	35.00	90.00	-5.34	65.06	-5.32	65.22	-5.35	65.14	82.00	90.00	-8.12	65.96
	40.00	90.00	-4.44	66.00	-4.46	66.03	-4.44	65.89	83.00	90.00	-8.98	65.66
	45.00	90.00	-3.74	66.82	-3.73	66.69	-3.72	66.89	84.00	90.00	-10.01	65.33
	50.00	90.00	-3.23	67.49	-3.21	67.54	-3.24	67.54	85.00	90.00	-11.29	64.97
	55.00	90.00	-2.92	67.96	-2.92	68.03	-2.92	67.86	86.00	90.00	-12.91	64.58
	60.00	90.00	-2.83	68.22	-2.84	68.19	-2.81	68.18	87.00	90.00	-15.10	64.16
	65.00	90.00	-3.02	68.25	-3.01	68.20	-3.01	68.34	88.00	90.00	-18.29	63.70
	70.00	90.00	-3.57	68.01	-3.56	68.00	-3.57	68.11	89.00	90.00	-23.99	63.20
	75.00	90.00	-4.67	67.45	-4.67	67.46	-4.69	67.48	90.00	90.00	-999.99	0.00
80.00	90.00	-6.76	66.49	-6.76	66.51	-6.78	66.46	Only bold values comparable with 100m shelter cases				
85.00	90.00	-11.28	64.98	-11.28	65.01	-11.30	64.91					
90.00	90.00	-999.99	0.00	-999.99	0.00	-999.99	0.00					

IL3117-1

Table 25. Shelter Effects at 25 MHz on Radiation Pattern Power Gain and Phase, in Principal Elevation Plane Containing 5 Meter Monopole and Bisecting Shelter, versus Frequency, Distance, and Polar Angle

For 5 meter Monopole with 6 Radials 12m Long

Frequency (MHz)	Polar Angle (°)	Azimuth Angle (°)	No Shelter		Endfire Shelter at 100m		Broadside Shelter at 100m		Broadside Shelter at 200m (Expanded Polar Angle Scale)			
			Power Gain (dB)	E _θ Phase (°)	Power Gain (dB)	E _θ Phase (°)	Power Gain (dB)	E _θ Phase (°)	Polar Angle (°)	Azimuth Angle (°)	Power Gain (dB)	E _θ Phase (°)
25	0.00	90.00	-999.99	-164.29	-46.92	-14.65	-49.05	27.58	75.00	90.00	-2.20	37.04
	5.00	90.00	-25.89	82.79	-26.67	84.30	-26.38	80.75	76.00	90.00	-2.47	36.86
	10.00	90.00	-19.85	79.47	-19.70	81.77	-19.98	81.00	77.00	90.00	-2.79	36.68
	15.00	90.00	-16.24	74.39	-16.04	73.55	-16.10	74.85	78.00	90.00	-3.17	36.49
	20.00	90.00	-13.52	68.28	-13.64	67.51	-13.48	67.60	79.00	90.00	-3.60	36.30
	25.00	90.00	-11.20	61.99	-11.23	62.72	-11.27	61.96	80.00	90.00	-4.11	36.09
	30.00	90.00	-9.11	56.28	-9.03	56.15	-9.09	56.64	81.00	90.00	-4.71	35.88
	35.00	90.00	-7.23	51.54	-7.28	51.36	-7.21	51.31	82.00	90.00	-5.41	35.66
	40.00	90.00	-5.57	47.83	-5.55	48.04	-5.60	47.89	83.00	90.00	-6.25	35.43
	45.00	90.00	-4.14	45.02	-4.15	44.86	-4.11	45.06	84.00	90.00	-7.27	35.20
	50.00	90.00	-2.95	42.90	-2.94	43.00	-2.98	42.85	85.00	90.00	-8.53	34.95
	55.00	90.00	-2.04	41.28	-2.06	41.25	-2.02	41.30	86.00	90.00	-10.14	34.70
	60.00	90.00	-1.44	39.99	-1.43	39.95	-1.46	40.05	87.00	90.00	-12.32	34.43
	65.00	90.00	-1.18	38.92	-1.18	38.97	-1.18	38.79	88.00	90.00	-15.51	34.14
	70.00	90.00	-1.38	37.96	-1.39	37.99	-1.36	38.02	89.00	90.00	-21.20	33.84
	75.00	90.00	-2.21	37.03	-2.21	36.99	-2.21	37.15	90.00	90.00	-999.99	0.00
80.00	90.00	-4.11	36.07	-4.11	36.00	-4.13	36.09					
85.00	90.00	-8.52	34.96	-8.52	34.90	-8.54	34.91					
90.00	90.00	-999.99	0.00	-999.99	0.00	-999.99	0.00					

Only bold values comparable with 100m shelter cases

LIST OF REFERENCES

1. Weiner, M. M., July 1985, *Effect of Antenna Impedance Mismatch on the Signal-to-Noise Ratio of a Radio Receiving System*, ESD-TR-85-136, NTIS AD A159070, Electronic Systems Division, AFSC, Hanscom AFB, MA and March 1984, MTR-9221, The MITRE Corporation, Bedford, MA.
2. Weiner, M. M., March 1988, "Noise Factor of Receiving System with Arbitrary Antenna Impedance Mismatch," *IEEE Trans. Aerospace and Electronic Systems*, Vol. AES-24, No. 2, pp. 133-140,
3. Weiner, M. M., August 1990, *Noise Factor and Antenna Gain in the Signal/Noise Equation for Over-the-Horizon Radar*, MTR-10989, The MITRE Corporation, Bedford, MA NTIS AD-A231203.
4. Weiner, M. M., November 1991, "Noise Factor and Antenna Gains in the Signal/Noise Equation for Over-the-Horizon Radar," *IEEE Transactions on Aerospace and Electronics Systems*, Vol. AES-27, No. 6, pp. 886-890.
5. Weiner, M. M., September 1991, *Validation of the Numerical Electromagnetic Code (NEC) for Antenna Wire Elements in Proximity to Earth*, MTR-11278, The MITRE Corporation, Bedford, MA.
6. Burke, G. J., and A. J. Poggio, January 1981, *Numerical Electromagnetics Code (NEC) — Method of Moments*, Rept. UCID-18834, Lawrence Livermore National Laboratory, Livermore, CA.
7. Burke, G. J., 1983, *Numerical Electromagnetics Code — Method of Moments, User's Guide Supplement for NEC-3 for Modeling Buried Wires*, Rept. UCID-19918, Lawrence Livermore National Laboratory, Livermore, CA.
8. Burke, G. J., and A. J. Poggio, 1990, *Numerical Electromagnetics Code — Method of Moments, Users Guide Supplement for NEC-GS*, Rept. UCRL-MA-107572, June 1991, Lawrence Livermore National Laboratory, Livermore, CA.
9. Burke, G. J., January 1988, *A Model for Insulated Wires in the Method of Moments Code NEC*, Rept. UCID-21301, Lawrence Livermore National Laboratory, Livermore, CA.
10. Burke, G. J., 1989, *Validation of NEC for Antennas Near Ground*, Rept. UCRL-101190, NTIS DE89-D16502, Lawrence Livermore National Laboratory, Livermore, CA.
11. Burke, G. J., and E. K. Miller, June 1989, *Numerical Modeling of Monopole on Radial-Wire Ground Screens*, 1989 IEEE AP-S International Symposium, Vol. I, San Jose, CA.
12. Burke, G. J., March 1989, *Recent Advances to NEC: Applications and Validation*, Rept. UCRL-100651 Preprint, Lawrence Livermore National Laboratory, Livermore, CA.

13. Haus, H. A., et al, January 1960, "IRE Standards on Methods of Measuring Noise in Linear Two-Ports," *1959 Proceedings of the IRE*, Vol. 48, pp. 61-68.
14. Haus, H. A., et al, January 1960, "Representation of Noise in Linear Two-Ports," *Proceedings of the IRE*, Vol. 48, pp. 69-74.
15. CCIR (1963), 1964, *World Distribution and Characteristics of Atmospheric Radio Noise*, Report 322, 10th Plenary Assembly, Geneva (1963), Int. Radio Consultative Committee, Int. Telecommunication Union, Geneva, Switzerland.
16. CCIR (1983), 1986, *Characteristics and Applications of Atmospheric Radio Noise Data*, Report 322-3, 16th Plenary Assembly, Dubrovnik (1983) Int. Radio Consultative Committee, Int. Telecommunication Union, Geneva, Switzerland.
17. CCIR (1983), 1986, *Man-Made Radio Noise*, Report 258-4, 16th Plenary Assembly, Dubrovnik (1983), Int. Radio Consultative Committee, Int. Telecommunication Union, Geneva, Switzerland.
18. Spaulding, A. D., and R. T. Disney, June 1974, *Man-Made Radio Noise, Part 1: Estimates for Business, Residential, and Rural Areas*, OT Report 74-28, Dept. of Commerce, Boulder, CO, Available from the U. S. Government Printing Office, Washington D. C.
19. Weiner, M. M., September 1991, *Performance of Ground-Based High Frequency Receiving Arrays with Electrically-Small Ground Planes*, MTR-11277, The MITRE Corporation, Bedford, MA.
20. Hagn, G. H., 1992, "Receive Antenna Assumptions for Short-Wave Broadcast Coverage Models," Accepted for publication in *IEEE Trans. Antennas and Propagation*, figure 4.

GLOSSARY

CCIR	International Radio Consultative Committee
cm	centimeter
dB	decibel
EM	electromagnetic
ETWK	extended thin wire kernel
HF	high frequency
Hz	hertz
km	kilometer
LF	low frequency
LLNL	Lawrence Livermore National Laboratory
m	meter
MHz	megahertz
NEC	numerical electromagnetic code
NEC-GS	numerical electromagnetic code-ground screen
NEC-3I	numerical electromagnetic code-3 insulated wire
OTH	over-the-horizon
OTH-B	over-the-horizon backscatter
TWK	thin wire kernel
VLF	very low frequency